UC Berkeley
UC Berkeley Electronic Theses and Dissertations

Title
Cortical representation of social communication in Egyptian fruit bats

Permalink
https://escholarship.org/uc/item/8019v7mn

Author
Rose, Maimon C

Publication Date
2021

Peer reviewed|Thesis/dissertation

eScholarship.org Powered by the California Digital Library
University of California

Cortical representation of social communication in Egyptian fruit bats

By

Maimon C. Rose

A dissertation submitted in partial satisfaction of the

requirements for the degree of

Doctor of Philosophy

in

Neuroscience

in the

Graduate Division

of the

University of California, Berkeley

Committee in charge:

Professor Michael Yartsev, Chair
Professor Michael DeWeese
Professor Kristofer Bouchard
Professor Frederic Theunissen

Fall 2021

Abstract

Cortical representation of social communication in Egyptian fruit bats

by

Maimon C. Rose

Doctor of Philosophy in Neuroscience

University of California, Berkeley

Professor Michael Yartsev, Chair

Social interactions often occur in group settings and are mediated by communication signals that are exchanged between individuals, frequently utilizing vocalizations. The neural representation of group social communication remains largely unexplored. Here, we conducted simultaneous wireless electrophysiological recordings from the frontal cortices of groups of Egyptian fruit bats engaged in both spontaneous and task-induced vocal interactions. We found that the activity of single neurons distinguished between vocalizations produced by self and others, as well as among specific individuals. Coordinated neural activity among group members exhibited stable bidirectional inter-brain correlation patterns specific to spontaneous communicative interactions. Tracking social and spatial arrangements within a group revealed a relationship between social preferences and intra- and inter-brain activity patterns. We also present preliminary results relating to the neural correlates of social-vocal interactions in juvenile bats. Combined, these findings reveal a dedicated neural repertoire for group social communication within and across the brains of freely communicating groups of bats.

Dedication

To my wife and friend, Leah Hirschfeld, whose support I couldn't have done this without and who taught me about love and hash maps.

Table of Contents

CHAPTER 1: INTRODUCTION 1

1.1 MOTIVATION 1
1.2 THE NEUROETHOLOGICAL APPROACH TO SOCIAL INTERACTIONS 2
1.3 SOCIAL-VOCAL INTERACTION IN EGYPTIAN FRUIT BATS 2

CHAPTER 2: CORTICAL REPRESENTATION OF GROUP SOCIAL COMMUNICATION IN BATS 5

2.1 INTRODUCTION 5
2.2 SINGLE NEURON ACTIVITY DISTINGUISHES BETWEEN VOCALIZATIONS PRODUCED BY SELF AND OTHERS 6
2.3 SELF AND OTHER RESPONSIVE NEURONS ARE NOT MODULATED BY SPECIFIC ACOUSTIC FEATURES, PLAYBACK OR ECHOLOCATION PRODUCTION 6
2.4 SINGLE NEURON ACTIVITY EXHIBITS SELECTIVITY FOR CALLS PRODUCED BY SPECIFIC INDIVIDUALS 7
2.5 VOCAL INTERACTIONS ELICIT STABLE CORRELATED NEURAL ACTIVITY ACROSS THE BRAINS OF GROUP MEMBERS 9
2.6 INTRA AND INTER-BRAIN ACTIVITY PATTERNS ARE RESTRUCTURED OUTSIDE THE GROUP SOCIAL CONTEXT BETWEEN SPONTANEOUS AND TRAINED VOCAL BEHAVIOR 12
2.7 INTER-BRAIN CORRELATION AND IDENTITY SELECTIVITY VARY WITH SOCIAL PREFERENCES OF GROUP MEMBERS 15
2.8 DISCUSSION 18
2.9 MATERIALS AND METHODS SUMMARY 19

CHAPTER 3: NEURAL ACTIVITY IN THE FRONTAL CORTEX OF JUVENILE BATS DURING VOCAL INTERACTIONS 20

3.1 MOTIVATION 20
3.2 EXPERIMENTAL DESIGN 21
3.3 RESULTS 21
3.4 DISCUSSION 24

CHAPTER 4: CONCLUSION 25

CHAPTER 5: SUPPLEMENTARY METHODS 27

CHAPTER 6: SUPPLEMENTARY FIGURES 56

CHAPTER 7: REFERENCES 97

List of Figures

Figure 1 Neural correlates of social-vocal interactions during free group vocal communication. 8

Figure 2 Group inter-brain activity patterns around social vocalizations produced during free group vocal interactions..... 11

Figure 3 Restructuring of neural activity during task-induced vocal behavior..... 14

Figure 4 Social-spatial patterns are related to both intra- and inter-brain neural activity during group communication. 17

Figure 5 Neural correlates of social-vocal interactions in juveniles..... 23

Acknowledgements

Thank you to Dr. Michael Yartsev for his indomitable optimism in the pursuit of science. I've learned a great deal as a graduate student and was able to pursue many interesting questions. That would not have been possible without the effort and support Michael provided to keep me going along with his willingness to take the time to think and talk about experiments, results, careers, or whatever else came up. Thank you for providing such a rich environment for pursuing science over these years. I'd also like to thank the Yartsev lab as a whole for being an excellent group of researchers and friends, where ideas are freely exchanged, collaborations are natural, and everyone is willing to lend a helping hand. In particular, I'd like to thank Boaz Styr for our close collaboration and conversations over coffee and cookies; Tobias Schmid for growing together as graduate students; Wujie Zhang and Will Liberti for their sage advice and excellent critical feedback; and Yuka Minton for making it look easy to manage such a dynamic group of people. Thanks also to the members of my thesis committee, who provided their time to improve my work and to the Helen Wills Neuroscience Institute at large for creating a vibrant community of researchers. I am also deeply grateful to Drs. Ronald Cohen and David Freedman, two of my early mentors who introduced me to scientific research and provided me with the spark to pursue this degree.

I'd also like to thank my parents and siblings for creating a loving family and for all their support and care over the years. Thank you as well to my in-laws who have lovingly adopted me as one of their own. A special thanks to all my friends over the years from Silver Spring to Chicago to the Bay Area who made this such an enjoyable experience and provided laughter and a chosen family. Finally, I'd like to acknowledge all the bats who made all of this science possible.

Chapter 1: Introduction

1.1 Motivation

From the mundane to the most meaningful, it is easy to take for granted how the brain allows us to navigate social interactions. However, when one considers the massive amount of information that needs to be processed, stored, recalled, and manipulated on very short time scales while at the same time paying attention, perceiving, and actively communicating with other individuals, this feat can be appreciated for its complexity. One must be able to recall long-term memories, ranging from the recent past to one's earliest memories. One must also be able to empathize and understand another's feelings and intentions, frequently through a combination of direct as well as indirect cues. Complicating the task even further is the requirement to be able to "step into another's shoes" and see the world through their eyes in order to predict and respond to what they might do or say. Maintaining these mentals models of other individuals requires a vast amount of information especially when considering nested models wherein one models how another individual would model a third separate individual. Indeed, while artificial intelligence has made great strides in other realms hitherto considered the exclusive domain of the human brain such as chess, facial recognition, and language generation, we are still far removed from realizing a convincing artificial intelligence that replicates the social skills of a young child. Clearly the ease with which many of us are able to interact with others belies a deep complexity. This complexity in turn suggests that the brain may have evolved specific circuits and mechanisms to enable successful social interactions despite their large cognitive demands.

The large cognitive demands imposed by social interactions as well as their vital importance to a fulfilling life can also be appreciated by considering the decreased ability to socially interact in a wide range of psychiatric disorders. Social deficits are a defining symptom of autism spectrum disorder (*1*) and are also frequently found in most forms of mental illness from depression (*2*) to schizophrenia (*3*) to attention hyperactive deficit disorder (*4*). The etiology of these social deficits varies across diseases as well as across individuals. This variety in etiology illustrates the many intricate cognitive processes that must function individually as well as fit together as a whole in order to successfully interact with others.

Despite the great complexity of the cognitive processes underlying social interactions, it is of vital importance to better understand the neural underpinning of these processes, both because it is an intrinsic part of our humanity and day-to-day life, but also because an improved understanding may lead to better treatment of social deficit disorders. When social cognitive processes fail to function correctly social impairment can be devastating and exact a great toll on

one's life and well-being. These impairments are prevalent across society, and even incremental improvements in our understanding and ability to treat them would result in improved well-being for many.

1.2 The neuroethological approach to social interactions

Considering the great need for a better understanding of the neural underpinnings of social interactions along with its inherent complexity, multiple different complementary approaches are necessary to achieve that goal. Of course, the primary approach to understanding human social cognition is to study human neuroscience. However, to probe and manipulate neural activity at fine resolution in order to determine its role in neural computations, one must make use of animal models that recapitulate certain aspects of social interactions (*5*). One such approach, which constitutes the vast majority of work in systems neuroscience, is to use the standard model organisms, such as mice. Because human social interactions are such a multifaceted and complicated behavior, inevitably, no single model system will mirror all relevant aspects (*6*). Frequently studies of mouse behavior rely on well-tested, but simplistic behavioral paradigms (*7–10*). Furthermore, until recently it has been technically challenging or impossible to perform neuroscience experiments on multiple interacting individuals simultaneously (*11*) which is an obvious reductionist deficit when studying a behavior that is intrinsically about the interactions between multiple individuals. Consequently, a gap exists in our ability to study the neural basis for group social interactions in a model organism that exhibits important aspects of social interactions.

We propose, therefore, to take a neuroethological approach to fill in these gaps. Neuroethology takes the position that because natural selection and evolution have endowed certain species with specific behaviors relevant to survival, researchers who wish to study the neural underpinnings of those behaviors should utilize the corresponding species for their investigations and should study their behaviors in a context where those selective pressures are relevant (*12*, *13*). By allowing the behavior of the animal to inform the neural investigation, we can be more certain that the neural findings will be more relevant to the behavior under study rather than to other spurious or unrelated behavioral phenomena.

1.3 Social-vocal interaction in Egyptian fruit bats

Vocal communication is a vital component of social interactions. Humans, and many other social organisms, use vocalizations to convey information and mediate social interactions. However, most neuroscientific studies of vocalizations have in the past focused on either production or perception, independent of a social interaction taking place (*14–21*). This has

allowed a deep understanding of the neural basis for vocal behavior such as the production and perception of learned birdsong in zebra finches (*22*, *23*) and the auditory processing of echolocation signals in bats (*24–27*). However, because these studies have primarily been conducted in single, isolated individuals, they have not been able to study social interactions per se.

In order to bridge the gap in our understanding of social-vocal interactions in group settings, I have studied groups of interacting Egyptian fruit bats (*Rousettus aegyptiacus*) while they freely engage in spontaneous social-vocal interactions. These bats offer a number of distinct behavioral advantages that make them well suited to studying these phenomena. First, like many bat species, they are a highly social species. They can live up to 25 years (*28*). During that extended lifespan they live in large colonies that consist of hundreds to thousands of individuals (*28*, *29*). They appear to engage in self-quarantine when exposed to pathogens (*30*). They form long-lasting social relationships based on past experiences (*31*, *32*). In particular, they exhibit stable producer-scrounger dynamics that persist over long periods of time (>16 months). Producer bats scavenge for food from trees and other resources, while scroungers take the food directly from the mouths of other bats (*31*). These dynamics show up in mating patterns as well, with female bats preferentially mating with male bats from whom they consistently scrounge food (*32*). Individual bats have also been shown to be able to distinguish familiar from unfamiliar bats within their colonies (*33*). This ability to identify individuals within a large colony may enable the non-random associations these bats form, which are not explained by genetic relatedness (*34*, *35*). These social dynamics indicate that long-term relationships must be remembered by individual bats within the larger colony and that those relationships impact their interactions.

These bats also exclusively use vocalizations as part of close-proximity social interactions (*36*, *37*). This has been demonstrated in previous work, and we have confirmed that in our experimental setup, this is indeed the case (Figure 3B). Furthermore, when placed in groups and allowed to freely interact, these bats will spontaneously engage in a large number of social-vocal interactions, and do not need to be trained or encouraged to vocalize. These vocalizations are not broadcast as in bird song or in territorial calls, rather they are directed at specific individuals during an interaction (*36*). Consistent with the directed nature of their vocalizations, *Rousettus* vocalizations have been shown to potentially contain context specific and individual specific information suggesting that they may mediate certain aspects of social interactions (*36*). To varying degrees of accuracy, it is possible to decode the emitter of the call, the addressee, the context of the vocal interaction and the behavioral response of the interacting bats (*36*). Vocalizations are primarily produced during interactions involving feeding, sleeping, aggression and mating (*36–38*). The frequent use, context and individual specific nature of their vocalizations suggest that these bats are using their vocalizations as a form directed inter-individual communication.

These vocalizations also develop and are plastic into adulthood in a feedback dependent manner, indicating the possibility of vocal learning or vocal usage learning. Juvenile bats produce

a unique call that is eliminated from their repertoire during development (*28*, *29*, *38–40*). Juvenile bats that have been isolated from other bats from birth and subsequently introduced to non-isolated bats produce calls more similar to their juvenile state than normally developing bats (*38*). Similarly, juvenile bats exposed to a frequency shifted acoustic input relative to the normal repertoire produce frequency shifted calls matched to the acoustic input (*38*, *40*). Furthermore, adult bats exposed to prolonged acoustic disturbances will make modifications to their vocalizations which persist even when the disturbance is removed, indicating adult vocal plasticity (*37*). These studies indicate that both juvenile and adult bats can learn certain aspects of their vocalization, making *Rousettus* a possible candidate for studying vocal learning in mammal. This is advantageous because very few mammalian species are vocal learners (*41*), and none are tractable model organisms for neuroscience research.

Because vocalizations are discreet events and only occur during social interactions, they can be used as an easily detectable index into the occurrence of social interaction events. Combined with their directed, communicative usage, social vocal interactions in this bat species present a tractable and relevant model for studying the neural basis of social interactions in freely behaving groups of individuals. We therefore developed the technology and techniques necessary for performing electrophysiological recordings in the brains of multiple bats simultaneously while also monitoring and characterizing their social vocal interactions. The results of those experiments constitute the bulk of this dissertation. Additionally, we piloted the study of neural correlates of vocal development in juvenile *Rousettus* and present the results of that work.

There are many aspects of neural activity during social-vocal interactions that can be studied simply by allowing groups of individuals to interact freely while recording neural activity. The experiments described below can be framed as an initial foray into describing the neural correlates of social-vocal interactions, but we hope they also serve as inspiration for future work. Furthermore, there are many potential regions in the brain that are likely involved during social-vocal interactions. We chose to study the frontal cortex (our reasoning can be found below), but the same techniques described here can be used to study other brain regions as well. The primary lines of research into neural activity during social-vocal interactions we performed can be grouped into four main categories: 1) The representation of individual identity and interaction status in single neuron activity in individual's brains; 2) The correlation between activity in different brains; 3) Comparing neural activity between spontaneous and trained vocal interactions; and 4) the influence of social status on intra- and inter-brain neural activity.

Following this work, I present the results of a preliminary investigation into neural activity in the frontal cortex of juvenile bats during social-vocal interactions. I describe our efforts developing the methodologies necessary for recording electrophysiological signals from juvenile bats during free behavior. I then describe our attempts at relating that activity to the process vocal development and possibly vocal learning. Although this effort did not ultimately succeed in its goal of describing the neural correlates of vocal learning in a mammal, we found that the neural activity between adults and juveniles in the same brain area are remarkably similar. I discuss

possible implications of these results and future directions that neural recording in juvenile bats could take. Finally, I discuss the implications of the results presented in this dissertation and suggest directions for future research.

Chapter 2: Cortical Representation of Group Social Communication in Bats

2.1 Introduction

For many animals, including humans, social interactions often occur in group settings. These interactions are commonly mediated by vocal communication signals that convey social information, such as participant identity, context and social preferences (*1–3*). Substantial progress has been made towards investigating the neural representation of sensory, motor and social aspects of vocalizations separately (*4–8*), but rarely have all aspects been examined together (*9*) or in a group setting where behavioral and neural activity were recorded from more than two animals simultaneously. This has limited our ability to connect behavior and neural activity to that occurring between individuals or pairs, rather than within groups. It has also limited exploration of the specific social and neural relationships that exist within a group (*10*). A combined approach will allow us to better understand how communication signals are represented within and across the brains of freely interacting group members.

We studied social-vocal communication in groups of Egyptian fruit bats (*Rousettus aegyptiacus*). Similar to other bats (*11*), this species lives in large colonies where individuals form long-term and persistent relationships (*12–14*) and communicate using vocalizations that contain socially relevant information, including individual identity and behavioral context (*3*). These vocalizations exclusively occur as part of close-range, direct interactions with conspecifics (*3*, *15*, *16*), providing a reliable indicator of social communication between group members. The social-vocal behavior of the Egyptian fruit bat thus presents an opportunity to investigate neural computations related to key aspects of group communication including: 1) representations of self versus others and individual identities 2) shared activity patterns across the brains of group members 3) influence of social context and 4) impact of social relationships between individuals.

To study social-vocal communication under group conditions, we allowed multiple bats to interact freely while monitoring their behavior in an enclosure in the dark ("free communication session"; Fig. 1A, group sizes of n = 4 and n = 5 male bats). Under these conditions the entire group is in close proximity and vocalizations only occur during social interactions (*3*, *15*, *16*). We therefore considered all interactions that included a spontaneously occurring vocalization to be a social-vocal interaction involving all bats in the group. These interactions occurred hundreds of times per session and were non-stereotyped (see supplementary methods for a list of defined

behavior types). Because video recordings alone are not sufficient to accurately and consistently assign the identity of the vocalizer (*3*, *15*, *16*), we developed an on-animal wireless vibration sensor that allows for unambiguous identity detection (Fig. 1B and fig. S1; development of this technology was done in close collaboration with Dr. Julie Elie). We found that vocalizations varied within and across bats in their spectral and temporal features (fig. S2 and Table S1) and that just 1% of vocalizations overlapped in time across bats, indicating that only one bat vocalized at a time during social interactions (Fig. 1B; fig. S1).

2.2 Single neuron activity distinguishes between vocalizations produced by self and others

We wirelessly recorded the activity of 1,153 single neurons and local field potential (LFP) activity from the frontal cortices of multiple bats simultaneously in each free communication session (fig. S3 and S4; Table S2; electrophysiological data from n = 7 total bats from two separate groups). Activity in this area has previously been shown to relate to social behaviors across a range of mammalian species (*17–21*), including bats (*22*). We began by looking for modulation of neural activity when an individual bat vocalized ("self") as well as when it listened to calls produced by other group members ("others"), in accordance with previous studies demonstrating vocalization related frontal cortical activity in multiple species (*23–26*). We found that single neurons modulated their firing rates around the time of vocalizations both in the bat vocalizing ("self-responsive neurons", 20.7% of neurons; see Tables S2 – 4 for subpopulations of neurons), and in the other bats in the group ("other-responsive neurons", 11.7% of neurons) (Fig. 1, C and D; fig. S4 and S5). These neuronal populations were primarily non-overlapping (fig. S5D; Table S2), indicating that the same area of frontal cortex contains distinct representations of self- and other-generated vocalizations. A complementary decoding analysis indicated that 26% of all neurons exhibited firing rates containing sufficient information to differentiate between calls made by self and others (Table S2). Firing rate modulation occurred at short latencies, specifically during vocalizations and followed the fast temporal dynamics of vocalization sequences (fig. S6). Furthermore, manual annotation of individual bats' behavior around vocalizations showed that bats engaged in interactive and variable behavior before and after the time of the vocalizations, but that the type of behavior did not significantly affect firing rates for most call responsive neurons (fig. S7).

2.3 Self and other responsive neurons are not modulated by specific acoustic features, playback or echolocation production

The neuronal responses we observed could potentially be related primarily to the sensorimotor rather than social aspects of the social-vocal interactions. However, we found that neither self- nor other-responsive neurons modulated their firing rates in relation to the acoustic features of the vocalizations that were produced or heard (fig. S8 and S9). In order to further dissociate the sensorimotor and social aspects of vocalizations, we conducted an additional set of experiments where bats heard or produced acoustic signals in isolation (fig. S10). In contrast to group social communication, we did not observe any neurons that responded when an isolated bat was exposed to playback of pre-recorded vocalizations (Fig. 1E; fig. S10 A and B; Table S2). Similarly, we found that solitary bats flying freely and producing tongue-click echolocation pulses (fig. S10 C and D), that recruit many of the same orofacial muscles as vocalizations (*27*, *28*), elicited few echolocation-responsive cells (5.9% of neurons) and importantly, no overlap between echolocation and self-responsive neurons (Fig. 1E; fig. S10E; Table S2). Collectively, the low responsivity rates to non-social acoustic production and auditory stimulation, as well as the lack of neuronal modulation in relation to acoustic details of vocalizations, indicate that the observed neuronal responses to vocalizations produced by self or others were specific to vocal behavior occurring in a social context.

2.4 Single neuron activity exhibits selectivity for calls produced by specific individuals

In addition to discriminating between self and others, the group setting of our experiments enabled us to test if neural activity in the frontal cortex contains a representation of individual identity, an important aspect of social interactions which has been shown to be behaviorally relevant during vocal communication in this species of bat (*3*, *13*, *14*). We found that a subset of neurons in listening bats responded selectively to vocalizations produced by specific individuals within the group (Fig. 1F). Using the firing rates of these "identity-selective" neurons, we could decode the identity of one bat vs. other bats present in the group specifically around the time of vocal interactions (9.3% of neurons; cross-validated and false discovery rate corrected $p < 0.05$, bootstrap test; Fig. 1, F and G; fig. S11A; Table S3 and S4). We found that for the majority of identity selective neurons acoustic features failed to provide significant classification of caller identity (Fig. 1H, 56% of identity-selective neurons), indicating that these results could not be accounted for solely by acoustic differences across individual bats. Similarly, we found that physical contact and participation in social-vocal interactions did not drive the identity selectivity of single neurons. In particular, single neuron identity decoding accuracy generally did not significantly decrease either when restricting our analyses to include only interactions where all bats were in close physical contact (fig. S11B) or when only including interactions not involving the bat from which the identity selective neuron was recorded (fig. S11C). These analyses do not rule out contributions of unconsidered sensory, social or multimodal factors which have been shown to modulate frontal cortical activity (*29*) but do indicate that identity selectivity was not

solely dependent on proximity, participation in the vocal interaction or acoustic details. Combined, these results indicate that frontal cortical activity contains sufficient information to distinguish vocalizations produced by self vs. others as well as between individual group members.

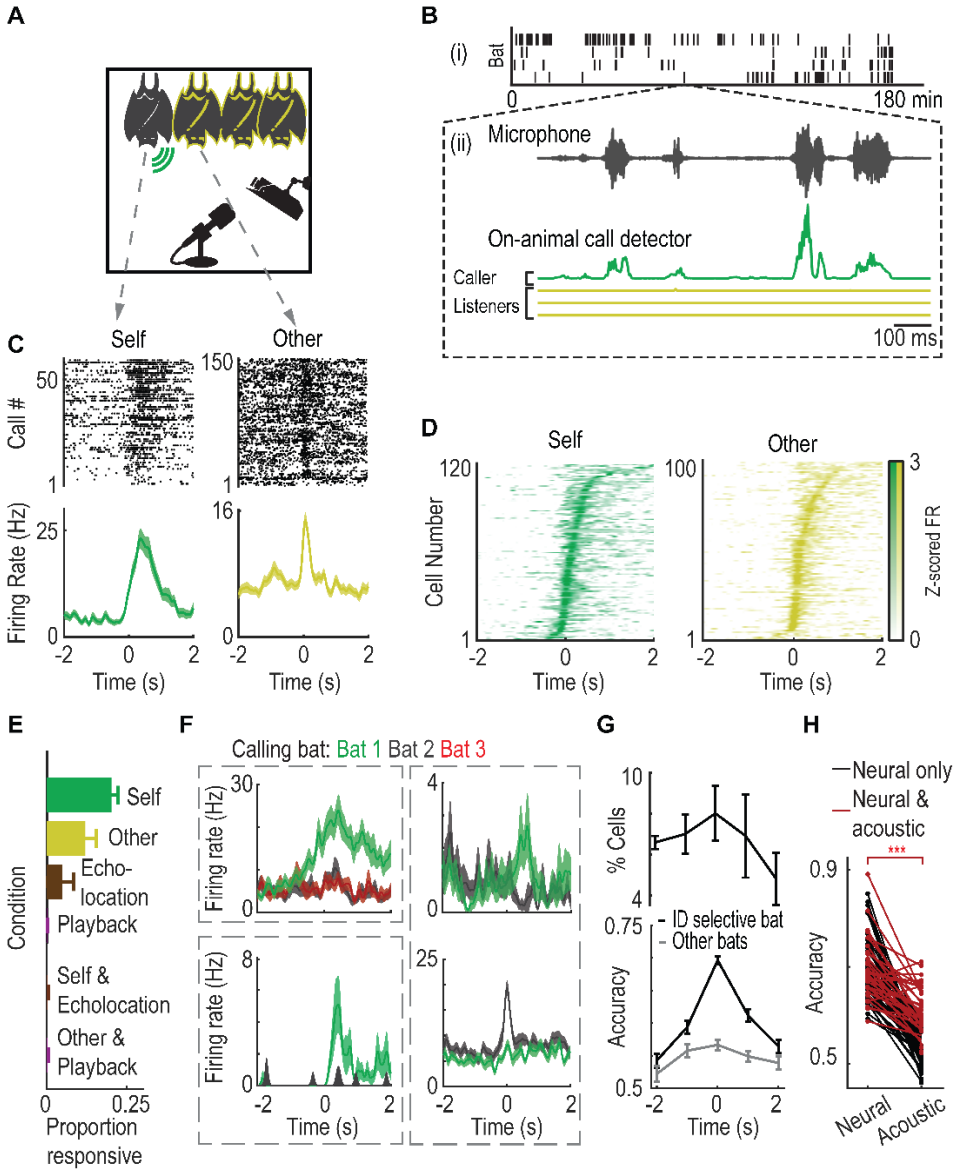

Figure 1 ***Neural correlates of social-vocal interactions during free group vocal communication.***

(A) *Experimental setup. Calling bat ("self") indicated by green symbol. Other bats are indicated by a yellow outline. Bats were monitored using cameras and a microphone.* ***(B)*** *(i) Ticks indicate vocalizations from different bats on each row (n = 4) during example session. (ii) Zoom-in on an example train of calls. Top: microphone recording of example calls. Bottom: corresponding filtered recordings from on-animal*

call detectors, colored according to (A). ***(C)*** *Example call-aligned raster (top) and peri-event time histograms (PETHs, bottom) of self and other-responsive neurons (in all following, calls start at '0').* ***(D)*** *Max normalized average firing rates of all responsive cells, sorted by time of maximum firing rate, for self- and other-responsive neurons.* ***(E)*** *Average fraction of responsive neurons per condition. SEM error bars (n = 7 bats).* ***(F)*** *Example identity-selective neurons modulating firing rates in response to one select bat's calls, but not for others (colored traces are one neuron's firing rates when listening to vocalizations from different bats). Right two examples are identity selective neurons recorded simultaneously from the same bat, each one selective for a different bat. Shaded areas indicate SEM.* ***(G)*** *Top: percent of all cells that are significantly identity selective, averaged across bats. Bottom: identity decoding accuracy over time averaged across all neurons that were identity selective at the moment of vocalizations. Plotted are decoding accuracies for the individual bat that drove identity selectivity (black) and for all other bats (gray). SEM error bars.* ***(H)*** *Decoding accuracy using neural data (left) and acoustic data (right). Shown are data only from neurons that exhibit significant neural identity selectivity. Instances with both significant neural and acoustic selectivity in red, instances with only significant neural selectivity in black. *** $p < 10^{-20}$, paired t-test.*

2.5 Vocal interactions elicit stable correlated neural activity across the brains of group members

Having considered the relationship between social-vocal communication and frontal cortical activity in the brains of individual bats, we next assessed the relationship in neural activity across the brains of group members during vocal interactions. Correlation in brain activity between pairs of individuals has been observed in studies in humans (*30*), duetting birds (*9*) and in dyads of socially, but not vocally, interacting rodents (*20*) and bats (*22*). Inter-brain correlation has further been shown to indicate, and possibly facilitate, successful vocal communication in humans (*31–34*). Previous findings in bats indicate that local field potential (LFP) activity was modulated on a long time scale (seconds to minutes) by non-vocal social interactions and was correlated across brains (*22*). We observed a strong, temporally precise modulation of LFP power on short time scales (milliseconds) around vocalizations in both low (<20Hz) and high (>70Hz) frequency bands (Fig. 2, A and B, and fig. S12). Moreover, we observed increased inter-brain correlation precisely around the time of vocalizations between pairs of calling and listening bats as well as between pairs of listening bats (Fig. 2C; fig. S13; n = 8,962 bat pairs and calls across two groups). Consistent with previous findings (*22*), pairwise inter-brain correlation was found to be most pronounced in high frequency LFP power (70 – 150 Hz; fig. S13). We therefore focused our subsequent analysis of inter-brain relationships on power in the high frequency LFP range.

The group setting of the experiment allowed us to measure directed inter-brain relationships simultaneously between multiple pairs of bats while also accounting for potential spurious correlations driven by common input from other group members using conditional Granger causality (GC) (Fig. 2D). We found that GC magnitude sharply increased around the time of vocal interactions across all calls (Fig. 2E, n = 995 calls and n = 4 bats; fig. S14, A-C, n = 827

calls and n = 3 bats), and also when separately considering the caller to listener and the listener to caller directions (Fig. 2F; n = 7 bats). This suggests a bidirectional inter-brain relationship during spontaneous social-vocal interactions between group members which may reflect vocal as well as other associated behavioral aspects of the interactions between the bats. These results do not, however, imply a causal relationship between the behaviors of individuals. The increase in GC was significantly greater than that observed in trial shuffled data, indicating a precise coordination in activity rather than simple co-activation (fig. S14D). Next, we assessed whether the variability in GC we observed across bats, and by listener and caller direction (fig. S14, E and F), reflected random association or a stable pattern of inter-brain activity. We found that the correlation in GC values throughout the experimental timeline was significantly higher than in data shuffled across bats (Fig. 2G) and GC values changed less than what would be expected by chance throughout the experimental timeline (Fig. 2H; fig. S14G). Lastly, we found that providing shared auditory input to two bats in separate, isolated chambers (Fig. 2I, n = 2 bats) did not elicit an increase in GC magnitude, indicating that social context was necessary for the existence of coordinated inter-brain activity between group members (Fig. 2I). To verify that these findings were not a result of our choice of parameters or the parametric assumptions of GC, using the same data we repeated the above GC analysis at different values of time lag and also calculated inter-brain relationships using the transfer entropy between pairs of bats. Using these measures, we observed similar results (fig. S15).

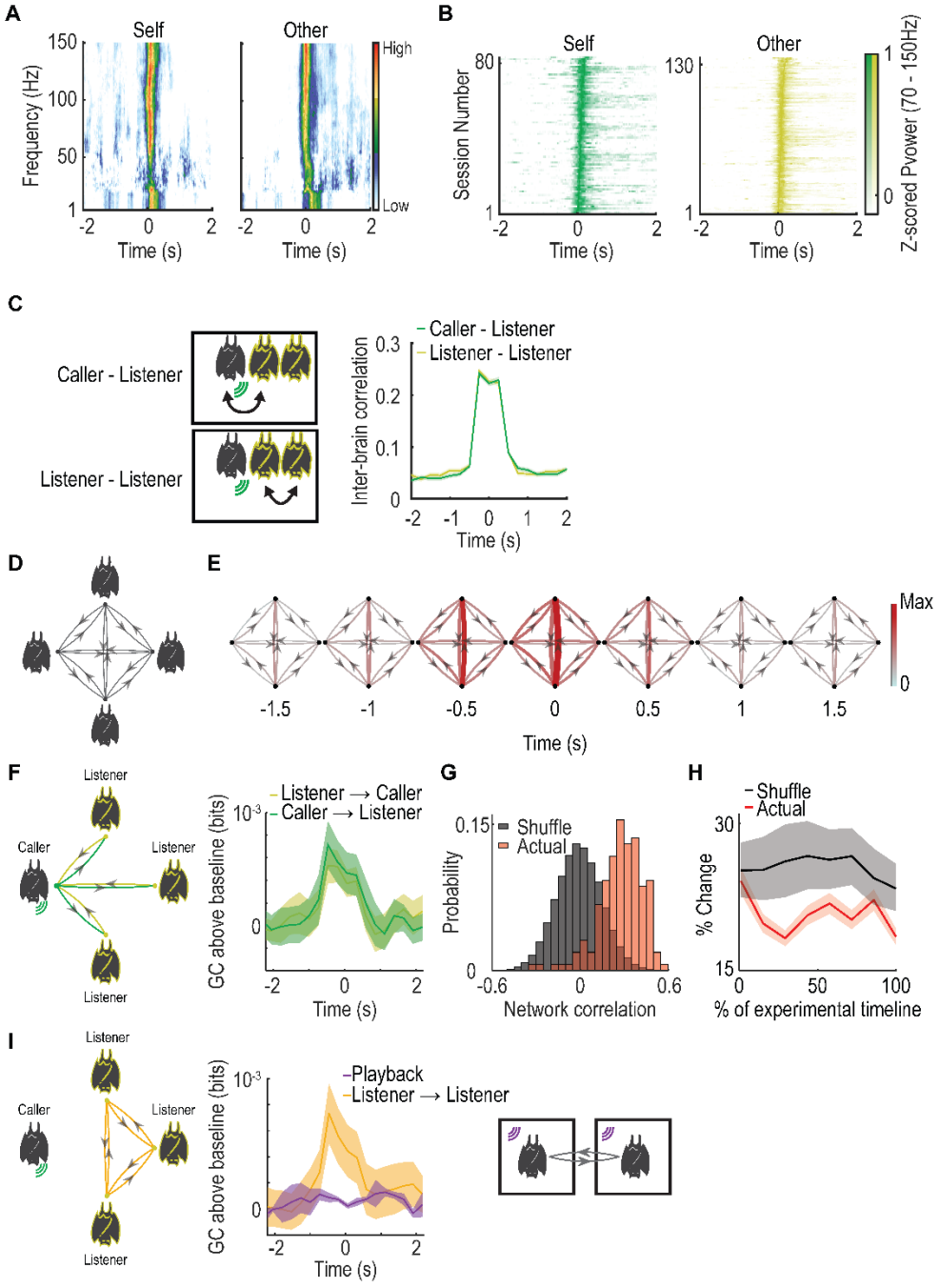

Figure 2 ***Group inter-brain activity patterns around social vocalizations produced during free group vocal interactions.***

(A) *Example average LFP spectrograms (normalized at each frequency bin) from one bat during one session.* ***(B)*** *Average power of high frequency LFP (70-150Hz) for all sessions, displayed as in (A).* ***(C)*** *Left, schematics of inter-brain correlation between bat pairs involving the calling bat (top) and involving only listening bats (bottom). Right, call aligned inter-brain Pearson correlation of high frequency (70-150Hz) LFP power averaged across all vocalizations and bat pairs. Throughout this figure shaded areas*

*are SEM. (**D**) Schematic illustrating all possible connections in a group of four bats. Nodes indicate bats, edges indicate inter-brain relationships, and arrows indicate directionality. (**E**) Group inter-brain GC graphs using all vocalizations (both calling and listening), calculated using a sliding window of 1s duration around call onset. GC magnitude are represented by both color and line width. (**F**) Left: illustration of the different directional relationships that exist when a given bat is vocalizing. Right: baseline-subtracted GC values aligned to call onset, calculated separately for vocalizations from each bat and averaged across bats. Data are shown according to the relationships delineated on the diagram to the left (colors). (**G**) Distribution of average correlation values between GC magnitudes calculated using vocalizations equally binned across all experimental days (red) compared to shuffled data (gray). High values indicate similarity over time. Actual values are significantly higher than shuffled ($p = 0.03$, Mantel test). (**H**) Bin-to-bin percent change in GC values over the duration of the experiment presented as percentage of experimental timeline and compared to shuffled values for the same bins. (**I**) Left: illustration of listener to listener relationships in the group setting. Right: simultaneous playback experiment. Middle: average baseline subtracted GC values during playback compared to listener-listener GC values during free communication.*

2.6 Intra and inter-brain activity patterns are restructured outside the group social context between spontaneous and trained vocal behavior

The results presented thus far show that social-vocal communication strongly modulated intra- and inter-brain neural activity in groups of freely interacting bats. We next sought to dissociate vocalizations from their typical social context in order to assess the impact of engaging in spontaneous, communication-driven vocal interactions. To that end, we developed an operant conditioning task wherein pairs of bats learned to produce vocalizations for reward in a context where they would not normally vocalize (this task was developed by Drs. Tobias Schmid and Julie Elie). This permitted testing the influence of social context on neural activity by comparing trained, reward-driven vocal interactions to spontaneous group vocal interactions.

In the operant conditioning task, a pair of bats was placed in a divided cage such that they were physically separated, but could still see, hear and smell each other and even interact in a limited way across the mesh divider (n = 4 bats; two pairs of trained bats; Table S3; Fig. 3A). Over the extensive course of training (fig. S16A) bats went from the naïve state of never calling in this context (Fig. 3B; Pre-training) to reliably producing hundreds of calls within a session (Fig. 3B; Trained). We found that under these conditions one bat in each pair spontaneously became the sole caller while the other became the listener, in clear contrast to the vocal behavior observed in the free-communication session (Fig. 3C and fig. S16B). Once conditioned, bats produced calls drawn from a similar vocal repertoire as in the free-communication session, but with less variability (Fig. 3D, and fig. S16 C and D). To enable a direct comparison of neural activity across contexts, we performed the operant session immediately prior to the free-communication session and recorded the same neural activity throughout (Tables S2 and S4). This comparison revealed marked

differences between the spontaneous and reward-driven contexts at both the intra- and inter-brain activity levels.

At the level of the single brain, certain neurons exhibited 'self' or 'other'-related response profiles during the operant session as in the free-communications session (compare fig. S17 and S18A with fig. S4 A – C). However, we also saw substantial differences between the two sessions (fig. S18). Specifically, during the operant session as compared to the free communication session we observed an increased variability in call related response latencies (Fig. S18E), decreased firing rate consistency when firing rates were aligned to vocalizations compared to aligning to reward (Fig. S18F), and an increase in neural activity modulation occurring during the reward period (Fig. S18 A and C). Most strikingly however, we observed a reorganization of the responsivity of single neurons between the free-communication and operant sessions. We found that 78% (50/64) of neurons responsive in either session were not similarly responsive in both sessions (Fig. 3E; fig. S18 G and H; Table S2), indicating that their responsivity was contextually dependent. This reorganization was evident across the population of responsive neurons which showed a systematic lack of firing rate consistency across sessions compared to within sessions (Fig. 3F). These differences were not driven primarily by acoustic differences between the calls produced in either session, as indicated by comparing acoustically similar calls across sessions and acoustically different calls within sessions (fig. S18I).

At the level of neural activity across brains, we compared inter-brain GC values across session types. We found that the bi-directional inter-brain relationship that we observed during communicative behavior breaks down during conditioned vocalizations. Instead of both caller and listener influencing one another (Fig. 2F), we observed no vocalization related change in GC in the listener to caller direction during the operant session (Fig. 3G). As in the single neuron activity, the observed differences in inter-brain correlation were not driven primarily by acoustic differences across session (fig. S18J). Combined, these results suggest that the neural activity shifted away from the communication-related representation seen during spontaneous group social communication to a task-related representation in the reward-driven context.

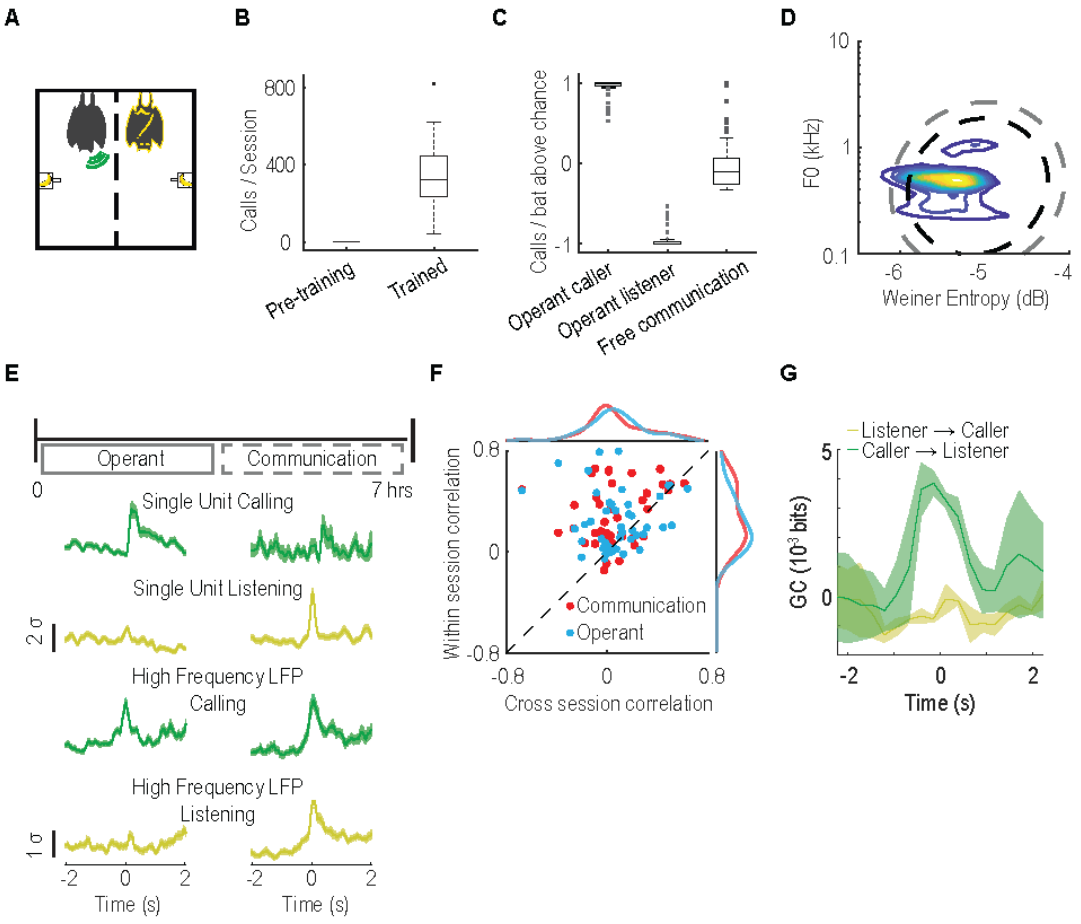

Figure 3 ***Restructuring of neural activity during task-induced vocal behavior.***

(A) *Operant session schematic. As above, green and yellow represent the calling and listening bat, respectively.* ***(B)*** *Number of vocalizations per session before (17 sessions, n = 4 bats) and after training (28 sessions, n = 4 bats). Box plot display showing median, interquartile range and ± 1.5 STD.* ***(C)*** *Average number of calls, compared to chance (assuming each bat is equally likely to call), produced by each bat and normalized by the number of bats in a given session. Calling and listening bats in the operant task separated to illustrate caller-listener dichotomy and to contrast with free communication where all bats vocalized at similar rates, on average. Displayed in box plot as in (B).* ***(D)*** *Contour plots representing the distribution of operant session vocalization by two acoustic features. Black and grey dashed lines correspond to areas encompassing 95% and 99% of a Gaussian distribution, respectively, fit to free communication session vocalizations.* ***(E)*** *Top: experimental timeline over the course of a day: operant and free communication sessions are performed in direct succession over the course of approximately seven hours. Bottom: normalized average firing rates from two example single units and normalized average high frequency LFP power from two example tetrode channels. Shown is activity aligned to vocalizations in the operant (left) and free communication (right) sessions. Shaded areas indicate SEM.* ***(F)*** *Cross- vs. within-session correlation of the PETHs of individual responsive neurons, colored according to session exhibiting responsivity (n = 64 neurons). Marginal distributions of cross- and within-session correlations are also shown. Note the deviation from unity due to high within- but not cross-session correlations.* ***(G)*** *Comparison of inter-brain GC values averaged across bats during the operant session. Shown for both possible directional relationships. SEM error bars.*

2.7 Inter-brain correlation and identity selectivity vary with social preferences of group members

Our findings thus far indicate that the neural activity patterns we identified during group communication depend on the social context at the group level. Next, we wanted to understand how these neural activity patterns vary according to social factors at the individual level. To do so, we utilized the fact that bats demonstrate robust spatial behavioral patterns that reflect social preferences of individuals within the group (*11*, *35*). We developed a system to precisely track the individual positions of a group of eight bats moving freely in a large enclosure (1.2 x 1.2 x 0.6 m [width, length, height]; Fig. 4 A and B; fig. S19) as part of a complementary experimental session (termed the "social-space" session) performed prior to each free communication session. This approach revealed stable social preferences of group members which were reflected in the neural activity during vocal interactions in the free communication session.

During the social-space session most bats spent the majority of the time, and exclusively vocalized, near other bats (Fig. 4B; fig. S19B and S20). However, individual bats differed in their proximity preferences relative to other group members, resulting in a bimodal distribution of inter-bat distances (Fig. 4C and fig. S21). Based on this bimodal distribution we derived a boundary to define distances between a pair of bats as either close together or far apart (Fig. 4C) and defined that pair's "social dwell time" as the percentage of a session spent close together. Using this metric, we found that the way individuals positioned themselves relative to each other was highly stable over weeks (Fig. 4D; fig. S22). Importantly, we observed two distinct social-spatial positioning preferences exhibited by different individuals: some bats consistently spent time far apart from other group members, while others spent the majority of time close together (example shown in Fig. 4E). We quantified these preferences for each individual (Fig. 4 F and G; fig. S23) and defined the "cluster status" of each bat as either "in-cluster" or "out-of-cluster" reflecting their social-spatial preferences with respect to other group members.

During the corresponding free communication sessions where all eight bats were close together, we recorded neural activity from the frontal cortex of four of the bats simultaneously. We found that the same neural activity patterns described in the previous smaller groups (n = 4 and n = 5 bats) were replicated in the larger group, including the representation of self vs. others, individual identity and inter-brain relationships (n = 8 bats; fig. S24 A and B and Table S3). We additionally performed a group playback session with all eight bats present to test if acoustic stimulation in a social context would drive other-responsive or identity-selective neurons. Consistent with our previous findings, we found that during group playback none of the other-responsive or identity-selective neurons significantly modulated their activity (Table S3), nor did we observe any increased inter-brain correlation (fig. S24C). Furthermore, using position tracking during the free communication session we found that individual bats' positions during calls could

not account for the observed identity selectivity in single neurons (fig. S25). Next, we asked whether the cluster status of individual bats inferred from the social-space session was related to the neural activity during vocal interactions in the free communication session. We focused our analysis on neural measures that intrinsically involve relationships between bats, namely the single neuron identity selectivity and inter-brain correlations.

We first examined whether the accuracy with which a calling bat could be decoded from the activity of identity selective single neurons was related to its cluster status. We found that neurons selective for in-cluster bats had 34% higher decoding accuracy on average compared to neurons selective for out-of-cluster bats (Fig. 4H; n = 68 neuron and bat pairs; p = 0.006, likelihood-ratio test; fig. S26). In- and out-of-cluster bats vocalized at similar rates across sessions (n = 14 sessions, p = 0.48, paired t-test) and produced calls that could not be discriminated using acoustic features (n = 15,061 calls, p = 0.15, bootstrap test) suggesting that differences in acoustic content between the groups alone did not account for the neural differences we observed.

Next, we asked whether vocalization related inter-brain correlation in the free communication session was related to the cluster status of the caller. Recent studies in humans have suggested that inter-brain synchrony can be modulated by differences across individuals in verbal communication (*32*, *34*, *36*) as well as social group affiliation (*37*, *38*). Consistent with these studies, we found that across all calls, inter-brain correlation was 43% higher between all pairs of bats when in-cluster bats vocalized compared to out-of-cluster bats (Fig. 4I; n = 5,758 bat pairs and calls; $p = 1.0 \times 10^{-10}$, likelihood-ratio test, controlling for bat pair and date of recording). This effect was persistent and stable over weeks and not driven by day-to-day variability (Fig. 4J). Furthermore, difference in pairwise inter-brain correlation according to the cluster status of the caller could not be accounted for by (i) the cluster status of the pair, (ii) whether the pair included the caller or (iii) the physical distance between the bats in the free communication session (fig. S27). Lastly, the difference in inter-brain correlation during calls produced by in- vs. out-of-cluster bats was greater than the difference in inter-brain correlation for 98.6% of all other possible subgroupings of this group of eight bats (n = 146 subgroups; Fig. 4K), supporting the notion that social-spatial preferences influenced inter-brain neural activity. Combined, these results indicate that intra- and inter-brain neural activity patterns during group social communication were modulated by the social-spatial preferences of individual group members.

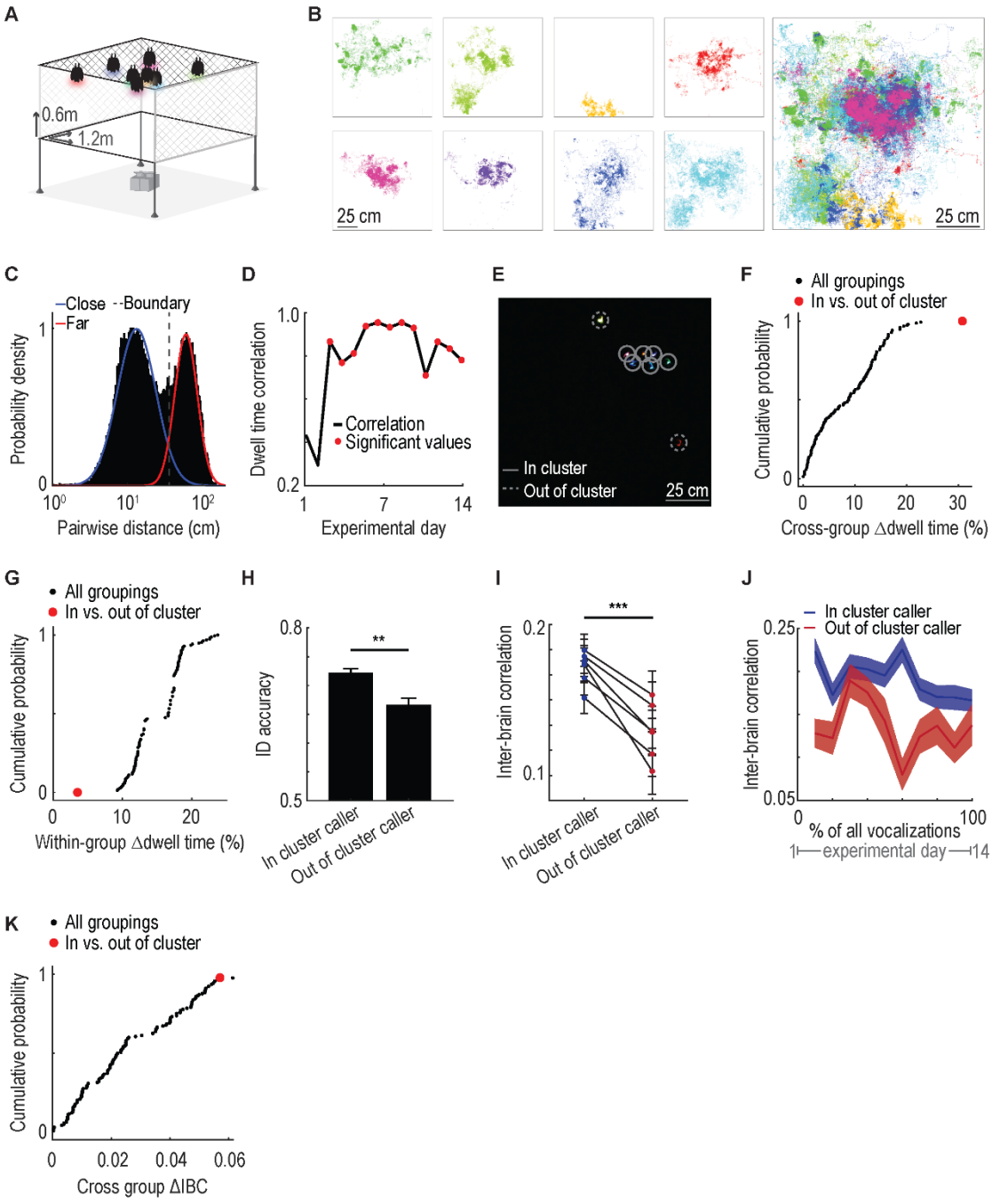

Figure 4 ***Social-spatial patterns are related to both intra- and inter-brain neural activity during group communication.***

*(**A**) Schematic of the "social-space" enclosure: a large environment (1.2 x 1.2 x 0.6 m) where bats could move freely (bats and cameras not to scale). Transparent plexiglass on two side and at the cage bottom allowed unobstructed video monitoring of all individuals (n = 8 bats). (**B**) Left, all tracked positions in an example session of each bat colored separately. Positions are shown on the XY plane corresponding to the enclosure ceiling where bats spent the majority of the time. Right, all bats' positions overlaid. (**C**) Histogram of all measured instantaneous distances between pairs of bats displayed on a logarithmic scale. Blue and red lines indicate a two-component Gaussian mixture model fit to these data. Dashed line*

*indicates the threshold for distances that were considered "close together" or "far apart". **(D)** Correlation between dwell times for all bat pairs on a given day and the median pairwise dwell time across all other days. Statistically significant correlation values are indicated with red dots ($p < 0.05$; Mantel test). **(E)** Still image from the color video camera positioned below the cage. Each bat has a different color LED. Individual bat positions indicated by circles. Lines are solid or dashed for in-cluster and out-of-cluster bats, respectively. **(F)** Cumulative probability distribution of the difference in mean dwell times between subgroups for all possible subgroupings of bats into two groups (n = 146 subgroupings). The in- and out-of-cluster subgrouping maximizes this value and is highlighted in red. **(G)** As in Panel F, showing the difference in mean dwell time within subgroups instead, which is minimized by the in- and out-of-cluster subgrouping. **(H)** Identity decoding accuracy of identity selective neurons when representing in-cluster vs. out-of-cluster bats (**, $p = 0.006$, likelihood-ratio test; n = 68 neurons and bat pairs). Bars indicate mean decoding accuracy across neurons; error bars indicate SEM. **(I)** Average IBC between bat pairs during vocalizations produced by in-cluster vs. out-of-cluster bats (***, $p = 1.0 \times 10^{-10}$, likelihood-ratio test, n = 5,758 calls and bat pairs). Each line indicates average IBC values for one bat pair; error bars indicate SEM. **(J)** Average IBC values separated as in panel I during all vocalizations across all free communication sessions, separated into equal sized bins over time. Shaded area indicates SEM. Note that IBC values during calls from in- vs out-of-cluster bats are higher at every time point considered, indicating persistence of effect across days. **(K)** Cumulative probability of absolute differences in mean IBC between subgroups for all possible subgroupings of bats into two groups. Red dot indicates difference in IBC between the in- and out-of-cluster bat groups. Note that only one other subgrouping has a larger difference in IBC.*

2.8 Discussion

In this study we recorded neural activity from the frontal cortex of groups of bats engaged in spontaneous social communication and studied neural processes both within and across the brains of individual group members. At the level of the individual brain, we found that frontal cortical neural activity distinguished not only between calls produced by self vs. others but also between individual identities. Furthermore, examining neural activity across the brains of group members revealed robust, bidirectional, stable inter-brain neural activity patterns that emerged only during spontaneous group vocal interactions.

Previous studies have demonstrated auditory responses in the frontal auditory field, an anatomically restricted region of the frontal cortex in microbats (*39–41*), even under anesthesia (*42*), whereas we did not observe neural responses to vocalization playback. This apparent discrepancy may be explained by our recordings being in an area outside of the frontal auditory fields, or possibly the lack of a frontal auditory field region in Egyptian fruit bats, especially considering the substantial neuroanatomical (*43–45*) and genomic (*46*) differences between micro- and megabats, as well as auditory functional specializations of the microbats (*47–49*). Future comparative studies will be crucial to further uncover the shared, as well as species-specific, neural circuits involved in vocal communicative behaviors. Yet collectively, our results are in line with findings in multiple species demonstrating the role of frontal cortex in processing cognitive or associative aspects of acoustic information in a contextually dependent manner (*50–53*).

By comparing neural activity during a highly trained, task-based vocal behavior to activity during a more ethologically relevant social-vocal behavior, we found that single neuron activity was highly contextually dependent and that inter-brain correlation was entirely absent in the task-based context. This breakdown in inter-brain correlation supports the hypotheses that bidirectional inter-brain activity patterns are a feature of socially interactive behaviors (*54*, *55*) and that shared inter-brain activity patterns may play an important role in social communication between group members (*19*, *31*, *33*, *34*, *54*). These findings also underscore the importance of incoporating components of ethologically relevant spontaneous behavior to complement the prevailing approach of less ethologically relevant, and often highly trained, experimental designs (*56*, *57*).

Consistent with the hypothesis that the repertoire of intra- and inter-brain activity patterns we observed reflects, or possibly serves as the basis for, social interactions, we found that bats that chose to spend more time together elicited a more accurate representation of identity at the single neuron level as well as higher levels of inter-brain correlation between the group members. It is possible that the reduced inter-brain correlation and identity accuracy elicited by out-of-cluster bats reflects differential communicative efficacy, as suggested by studies in humans (*34*, *36*). This, in turn, may relate to the abilities of individuals to negotiate a place within a group. Therefore, an important avenue for future studies will be to follow the co-evolution of neural and social dynamics during the formation and restructuring of social groups of varying compositions. Similarly, future studies that perturb neural activity during social interactions will be able to dissect the circuits supporting the social behaviors described here.

In addition to bats, a wide range of species naturally interact in groups and exhibit a diversity of social structures and forms of communication. Extending the approach taken here to other species in order to uncover similarities and differences in neural repertoires for social communication may provide important insight into the neural mechanisms that facilitate successful group living.

2.9 Materials and methods summary

To study social-vocal interactions under ethologically relevant group conditions, we allowed groups of bats to interact freely in a dark enclosure and spontaneously vocalize while recording audio, video and neural data. We used wireless tetrode-based electrophysiology to record single neuron activity and local field potentials from the frontal cortices of multiple Egyptian fruit bats (*Rousettus aegyptiacus*) simultaneously (these experiments were repeated in three separate groups of size n = 4, 5 and 8). The identity of the vocalizing bat was determined using a custom-made on-animal call detector device. For certain subsets of bats, we also performed the additional following experiments: (1) playback of vocalizations from a loudspeaker to either individual isolated bats or bats in the group setting; (2) production of echolocation signals by an individual bat while freely flying; (3) pairs of bats engaged in an operant vocalization production

task; and (4) tracking the position of individual bats in a larger enclosure to determine social-spatial preferences of members in the group. Single neuron firing rates were calculated and used to determine which neurons modulated their firing rates while producing a vocalization (self-responsive) or listening to other bats' vocalizations (other-responsive). Single neuron firing rates were also used to determine if responsive neurons encoded the acoustic features of vocalizations. Identity selectivity of single neurons was assessed by training classifiers to use firing rates around vocalizations in order to predict the identity of the vocalizer. The power in the high frequency band (70 – 150Hz) of the local field potential was calculated and used to determine the level of inter-brain correlation and Granger causality between the brains of individual bats around vocalizations. Responsivity of single neurons, identity selectivity of single neurons, and inter-brain correlation measures were compared between spontaneous and trained vocalizations. Elicited identity selectivity accuracy and inter-brain correlation measures were also compared between vocalizations produced by individual bats that exhibited one of two different modes of social-spatial preferences: (i) those preferring to position themselves close to other group members (in-cluster) or (ii) those preferring to remain further away from other group members (out-of-cluster). Further detailed description of the methods are provided in the online supplementary materials.

Chapter 3: Neural activity in the frontal cortex of juvenile bats during vocal interactions

3.1 Motivation

As described above, several studies have suggested that the development and plasticity of social vocalizations of *Rousettus* contains certain aspects of what is typically considered vocal learning. They can modify their vocalizations in response to acoustic feedback both as adults and as juveniles and they readily engage in social-vocal interactions in group settings. The number of vocally learning model organisms for neuroscience research is highly limited (*41*), and of those that are experimentally tractable, we are generally limited to songbirds. It would be very valuable, therefore, to develop a mammalian model of vocal learning considering the large evolutionary and anatomical differences between mammalian and avian brains (*38*, *41–45*). Toward this end, we piloted a study of electrophysiological recording in the frontal cortex of juvenile bats. Here I describe those efforts, providing both practical details as well as our results.

Prior to this study, no neural recordings had been reported in juvenile Egyptian fruit bats, so we had to develop the methodologies to enable this study. We successfully implanted tetrodes and recorded single unit neural activity in four juvenile bats (experiments for one bat took place in a different enclosure than the remainder of the juvenile bats and all the adult bats, and therefore excluded those data from analysis) ages 54-123 days in order to target the age range that has been

suggested to display maximal vocal variability during development. Juvenile bats are substantially more sensitive to anesthesia than adult bats, requiring careful dosing and monitoring during surgical procedures. They are also more sensitive to being kept under anesthesia for long periods of time, presumably due to their smaller energy reserves. This necessitates a quick surgical procedure and close post-surgical care. We found that subcutaneous injections of saline-ringer solution during anesthesia improved surgical outcomes. We also found that providing food and liquid to the recovering juvenile bat as quickly as possible resulted in more favorable post-procedure outcomes. Juvenile bats also possess a thinner skull than adults, requiring greater care during craniotomies and when placing anchor and ground screws. After tetrodes and micro-drives were successfully implanted, we found that after an adjustment period juvenile bats could still crawl and climb without apparent handicap, despite the greater implant to body weight ratio compared to adults. We did not test if juvenile bats could fly post implantation. In at least one of the implanted juveniles, we were able to successfully record neural activity at least 2 months post-surgery, despite the growth exhibited by the bat during this time period.

3.2 Experimental design

To assess the relationship between neural activity and vocalizations in juvenile bats, we performed a modified version of the free-communication experiment described above in adults, wherein recordings were made from multiple animals simultaneously in a group setting. With the juveniles, we only recorded one animal at a time and only ever with one additional non-implanted adult male bat. In this setting we observed that the juvenile will interact with the adult and vocalize, but the adult virtually never vocalizes itself (manual annotation of video from 849 calls from two juvenile/adult bat pairs showed 846 juvenile calls and 3 adult calls). We did not use the piezoelectric call detector device with the juveniles. For the one bat recorded in a smaller cage, video was recorded using a webcam unsynchronized with other systems. For the other three bats: for one bat we recorded continuous video throughout the experiment, for the other two we recorded sound triggered video clips attempting to isolated video around vocalizations alone. We recorded a total of 114 free communication sessions with the juvenile bats. During those sessions, we recorded a total of 711 well isolated single neurons and 7,476 vocalizations. Of those neurons, 463 were recorded on days with at least 15 calls produced allowing us to perform further analysis.

3.3 Results

The goal of this pilot study was initially to test if neural activity in frontal cortex tracked vocal development in the juvenile bats. However, we were ultimately unable to assess this relationship for several reasons. Primarily, we were unable to observe evidence of vocal development in the vocalizations we recorded from the juveniles implanted with tetrodes. The most prominent reported feature of vocal development in *Rousettus* is the development of the fundamental frequency of their vocalizations. To assess vocal development, we regressed

fundamental frequency (log values were used to account for the large range of frequency values measured) of all vocalizations on the age in days of the individual juvenile when it produced that vocalization. Over a range of 50 days of age across the three bats used for analysis a mixed effect linear model accounting for the identity of the bats resulted in null result (fixed effect of days of age, $p = 0.12$). Including the fourth bat for a range of 68 days similarly resulted in a null effect ($p = 0.054$). Considering the relatively small sample size of calls recorded (previous studies showing vocal learning in this species analyzed approximately 1,000,000 calls from 10 juveniles and adults over >6 months (*38*)), it is likely that we simply did not collect enough data to observe a reliable trend.

The secondary goal of this pilot study was to compare the neural responses observed in adults to those observed in juveniles in the same brain area (stereotactic coordinates for implants were calibrated for the different brain sizes of juveniles and adults, and coarse anatomy histologically compared post-hoc for similarity). Due to the complexity of the experiments at such a young age, only one implanted juvenile bat was placed in a chamber at a time with one adult bat and these were allowed to freely interact (Fig. 5a). These interactions also differed from adult-adult interactions under the same conditions. Only the juvenile bat produced social vocalizations with little to no vocal response from the adult, in agreement with previous reports of minimal vocal exchange between juvenile and adult bats of this species (*38*). The vocalizations the juvenile bats produced had higher average fundamental frequencies than adult calls (Fig. 5b). We observed a similar pattern of neuronal responses in juveniles during vocalizations to that found in the adult experiments. In detail, at both the levels of single unit and LFP responses, we found a substantial modulation of neural activity tightly locked to vocal communication (Fig. 5c, f) with nearly identical response latencies (Fig. 5d-g), proportions of responsive neurons (Fig. 5h; adult: 23%, juvenile: 26%; t-test $p = 0.72$) and a similar lack of correlation between firing rates and acoustic features of the produced vocalizations (Fig. 5i, j). Combined, these similarities between the neural representation in the frontal cortex of adult and juvenile bats suggests that the neural signatures related to the production of social calls are already present at very early stages of development in which both the acoustic content and nature of the social interaction differ greatly from adulthood.

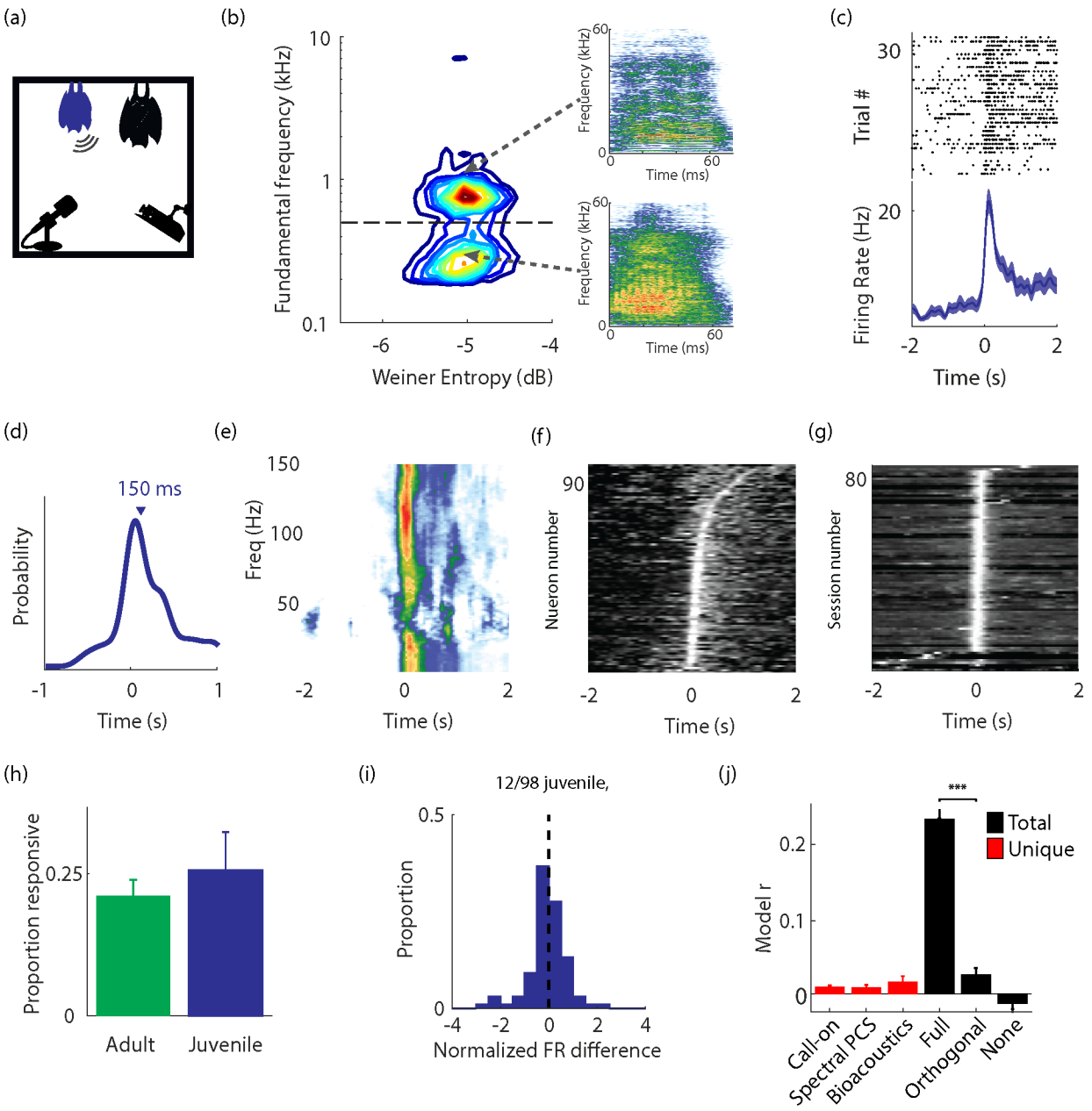

Figure 5 ***Neural correlates of social-vocal interactions in juveniles****.*

(a) Schematic of free communication session with a juvenile bat. (b) Distribution of juvenile vocalization acoustic features. (c) Example raster and PSTH for a juvenile production responsive cell. (d) Distribution of response latencies for all juvenile production responsive cells. (e) Example average frequency-normalized LFP spectrograms for production from one bat during one session. (f) Max-normalized average firing rates of all juvenile production responsive cells, sorted by time of max firing rate. (g) Power in high frequency LFP (70-150Hz) for all sessions, displayed as in (e). (h) Overall rates of responsive neurons, averaged across bats. Error bars represent SEM. (i) Distributions of normalized differences in firing rates between vocalizations with high and low F0. 12/98 juvenile production responsive cells have significantly different firing rates ($p < 0.05$; two-tailed Wilcoxon rank sum test). (j) Encoding model correlations as in Fig. 3d, e for juvenile production responsive neurons.

3.4 Discussion

Establishing a mammalian model of vocal learning remains an important goal for neuroscientific research. Being able to dissect the circuits implementing vocal learning and manipulate them in a mammalian brain could provide valuable insights into how humans can learn such a wide variety of vocalizations, in development and into adulthood. The Egyptian fruit bat similarly remains a promising model for achieving this goal; however, more work still must be done both from a behavioral and neuroscientific perspective. Behaviorally, the vocal repertoire needs to be much more thoroughly understood in terms of what calls are used in what context and what acoustic features are important to their use and learning, and what features are irrelevant. To accomplish this, one would need to create a highly detailed ethological catalog of vocalizations and behavior surrounding those vocalizations, delineate the different type of vocalizations (if discrete categories exist), and determine the association between behavioral context and vocalization. On top of this, it will be necessary to know how reliable those associations are in different contexts. Without this prior behavioral knowledge, one must simplify the analysis of vocal learning to certain pre-determined acoustic features which will almost surely lose a substantial amount of information, if not obscure any results whatsoever. With a defined repertoire of vocalizations, one can track the emergence and development of individual sounds, giving the ability to ask much more finely detailed questions about those changes. Our attempts at understanding vocal learning in these bats based solely on a limited number of vocalizations, without a deep ethological understanding of the vocal ontogeny resulted in our inability to determine if that learning was happening or not. That then translated into being unable to relate the behavior we were interested in (vocal learning) to the neural activity we observed.

Future studies of vocal learning in juvenile Egyptian fruit bats will require a more refined understanding of their vocal behavior in order to be able to analyze the changes over time. Studies of vocal learning could also proceed instead from adult vocal learning (training a bat to produce new sounds) or adult vocal usage learning (training a bat to produce existing sounds in new contexts). Given that we have already demonstrated that vocal usage learning is possible in the operant conditioning experiments presented above, one possible route forward would be to record neural activity during the vocal usage learning process. This process takes place over weeks to months of training, providing ample time to collect neural data and relate it to the changes taking place in vocal usage. This behavior is already well quantified and described, allowing for more detailed analysis. Determining the change in neural activity during usage learning, and where that change occurs in the brain would provide valuable information, as well as providing useful hypotheses for how vocal learning may occur during development.

Furthermore, having developed the methodologies to perform neural recordings in juvenile bats, we can now ask other questions in juvenile bats beyond vocal learning. One such example would be the inter-brain synchronization between juveniles and adults and, in particular, between

juveniles and their mothers. Recent work in humans has shown elevated inter-brain synchrony in prefrontal cortex between mother-child dyads, specifically during cooperation (*46*). While difficult to perform such experiments in humans, one could easily track inter-brain correlation between juvenile and mother bats over time and manipulate context and dyads to assess when and how mother-pup inter-brain synchrony occurs. This could provide valuable information about parent-child relationships and the developmental roots of inter-brain synchrony.

A recent study showed that juvenile bats passively learn navigational routes by being transported by their mothers to different sites (*47*), providing an intriguing behavior whose neural basis is unknown. One could record from both mother and pups during such transport flights and in later independent navigation by mother and pup individually. Doing so, one could assess how, e.g., the juvenile hippocampus represents space while being transported and learning new routes vs. flying those routes themselves or learning them themselves. One could also assess for the presence of inter-brain synchrony between mother and pups during such tutorial flights. One hypothesis that could be tested is that mother-pup dyads that exhibit higher synchrony transmit higher fidelity navigational information. To the best of our knowledge, inter-brain synchrony in the hippocampus of simultaneously recorded animals has never been studied and could yield valuable information about development and spatial learning.

Chapter 4: Conclusion

In this dissertation I have explored the neural basis of social-vocal interactions in group settings. I described a neural repertoire found in the frontal cortex specific to spontaneous social-vocal interactions that represents relevant social information about the vocalizing bats within individual brains. I also described an inter-brain activity pattern that is observed during spontaneous social interactions, but not during a trained vocalization task. Both of these intra- and inter-brain activity patterns are modulated by the social preferences of individual bats as reflected in social-spatial preferences. Finally, I described how neural activity in the same area of the juvenile brain is modulated in a manner similar to that in adult brains.

The representation of individual identity and role in vocal interactions is an important prerequisite for successfully navigating social interactions. Especially in a species with long term social relationships, knowing which individual is interacting and how is essential to properly respond. In a concurrent study of social interactions in groups of rhesus macaques Báez-Mendoza and colleagues found that single neurons represent the identity of individuals, their role in social interactions, and the history of those interactions as well (*48*). They hypothesize that these neurons could map group dynamics and form the basis for navigating short- and long-term social interactions. Both this study and the results presented above find that single neurons in the frontal cortex encode the identity of individual animals during social interactions and are modulated by social characteristics of those individuals. This is a remarkable result considering the considerable

differences between bat and monkey behavior, social structure, and neuroanatomy; however, it suggests that there are shared neural mechanisms for navigating social interactions across species. This is precisely the strength of the neuroethological approach which seeks to understand the neural underpinnings of natural behaviors in the appropriate context and then compare across species to find commonalities. We believe that the similarity in findings here indicates that the neural dynamics described truly reflect social dynamics and warrant future investigation.

The ability to record from multiple animals simultaneously while tracking their vocal behavior, spatial position, and neural activity opens the possibility for many possible future studies. One clear step forward would be to manipulate activity in the frontal cortex (and possibly other brain regions) during social interactions. The tendency for these bats to cluster tightly together provides a clear behavioral signal that can be observed relative to neural manipulation. Inhibiting activity either on medium- (e.g. DREADDs) or short-timescales (e.g. optogenetics) during social interactions and observing if individual bats change their social-spatial preferences in response to that manipulation would provide valuable information about the causal role of this area in social-spatial interactions. Similarly, one could transiently inhibit activity on-line selectively during social-vocal interactions and determine if those interactions resolve as they normally would, or if the outcomes change. In a similar vein, administering or blocking receptors for oxytocin in this area, or systemically, and observing the effect on the tendency to cluster could complement a large body of research on the role of oxytocin in social interactions. Because the tendency to cluster with other bats is so strong in this species and the observation that certain bats exhibit tendencies to cluster less, the ability induce or change these social-spatial tendencies could serve as a powerful platform for studying the neural mechanisms for social interactions beyond vocalizations.

Our investigation into the correlation between neural activity across brains was initially inspired by previous work by a different member of the Yartsev lab, Dr. Wujie Zhang, who showed that neural activity, especially high frequency local field potential power, is highly correlated between pairs of interacting bats and is not dependent on specific or shared behaviors (*49*). This accorded with two decades of work in humans has shown that inter-brain correlation is phenomenon observable in humans as well (*50–52*), and is modulated by relevant social factors such as teacher-student interactions (*53*), and inter-group conflict (*54*). Similar phenomena have also been observed in primates and mice (*55*, *56*). We then showed that inter-brain correlation exists in groups of multiple bats and is elevated specifically around the time of social-vocal interactions. We additionally found that vocalization related inter-brain correlation is specific to spontaneous vocal interactions and is modulated by the social-spatial preferences of the individual bats producing vocalizations. In particular, we found that bats that tend to spend less time in close proximity to other bats (which is atypical behavior in this species of bats, see e.g. (*30*)) elicit lower levels of inter-brain correlation than bats that spend more time within the cluster of other bats. As with the similar findings of identity related neurons in frontal cortex across bats and monkeys, the presence of inter-brain synchrony across a range of species indicates a fundamental phenomenon is being observed. Furthermore, our findings that social status modulates inter-brain correlation

concords well not only with an intuitive expectation of this phenomenon, but also with the observed relationship between inter-brain correlation and relevant social factors in humans.

Our findings of inter-brain correlation in groups of bats that is modulated by social preferences opens new possible lines of research for future studies. In particular, while measuring inter-brain synchrony is very feasible with non-invasive methodologies, using an animal model to perform invasive manipulations to determine what underlies this phenomenon could be highly useful. One study in humans showed that administering oxytocin intranasally enhanced inter-brain synchrony between pairs of interacting adult males (*57*). Similar studies could be carried out with more precise methods in bats and tracked over long periods of time. One could also carefully use behavioral manipulations which would be difficult to perform in humans, to assess what social relationships and behaviors contribute to inter-brain synchrony.

These findings in bats may also inform possible studies of inter-brain synchrony in humans. The difference between in- and out-of-cluster bats is reminiscent of humans with high or low social affinity. Determining the degree of social affinity in humans is not simple; however, there are disorders that manifest as decreased social functioning which may be studied using inter-brain synchrony as a tool. In particular, autism spectrum disorder (ASD) is characterized by difficulty in social communication and interaction. There has been very limited study of inter-brain synchrony in individuals with ASD; however, at least one study found that inter-brain synchrony and behavioral performance was modulated by severity of ASD symptoms (*58*). However, a different recent study found no significant difference in neural synchrony between pairs including typically developing children and children with ASD (*59*). More substantial and detailed research is needed to characterize the relationship between ASD and inter-brain synchrony. If such a relationship is found, however, it could be a valuable tool not only for diagnostic purposes, but also as a means to track treatment progress and possibly a component of novel treatment approaches.

The neuroethological approach to studying group social vocal interactions in Egyptian fruit bats enabled the discovery of neural activity patterns in and between individual brains that are specific to spontaneous, social interactions. By performing these experiments in a non-standard model organism, we were able to contribute to a cross-species evaluation of these neural phenomena and suggest that certain components of our findings reflect shared neural mechanisms across species. Developing the methodologies for studying freely behaving animals in group settings may enable future studies in bats, but also in other species. Our hope is that these findings will provide a framework for future studies and findings and possibly inspire new understandings of social interactions: both how the brain accomplishes such a complex task, but also how we might be able to help individuals who suffer from its dysfunction.

Chapter 5: Supplementary Methods

Supplementary materials and methods for Chapter 2:

Experimental model and subject details

Neural activity was recorded from a total of 11 adult male Egyptian fruit bats, *Rousettus aegyptiacus* (weight 141 - 165 g at implantation), across three experimental groups. 20 additional male bats were used to elicit interactions between the bats over the course of all experiments. The implanted bats consisted of N = 3 lab born (Group #1), N = 4 wild caught (Group #2), of N = 4 lab born animals (Group #3). The lab born bats, for which birth dates could be estimated, were 1 - 3 years of age at implantation. While the precise age of the wild caught bats could not be precisely estimated, all were greater than 4 years old. Prior to the start of experiments, bats were housed in a communal vivarium. After implantation, bats were initially single housed and subsequently, following recovery from surgery, were co-housed in cages with the other bats. The implanted bats from groups 1 and 2 were housed in standard housing cages. The implanted bats from group 3 were housed in the same cage used for the social-space session. All cages were kept in a humidity- and temperature-controlled room. The bats were kept on a 12-hour reversed light-dark cycle, and all experiments were conducted during the dark cycle. All experimental procedures were approved by the Institutional Animal Care and Use Committee of UC Berkeley.

Experimental design and details

Neural activity was recorded from a total of 11 bats. All 11 bats participated in free communication sessions. Three of the bats participated in the playback and echolocation sessions, but not operant sessions (group 1). Four bats participated in the operant sessions, but not playback or echolocation sessions (group 2). Four bats participated in the social space session and group playback session, but not operant or echolocation sessions (group 3) (Table S3). Unless otherwise stated, all analyses presented in and relating to Figures 1 – 3 and S1 – S18 use data only from groups 1 and 2 and all analyses presented in and relating to Figure 4, S19 – S23 and S25 – S27 use data only from group 3.

Experimental sessions

Free communication sessions

All free communication experiments were conducted inside a 40.6 x 33.7 x 52.1 cm (length, width, height) transparent plexiglass enclosure, which had netting on top that allowed bats to hang. For group 1 and group 2, enclosures were placed inside a 64.8 x 61 x 64.8 cm (length, width, height) chamber lined with anechoic foam and experiments were conducted in the dark (10^{-5} lux; corresponding to near complete darkness for this species of bat (59, 60)) with infrared (IR) lights to allow video recording. Illuminance levels were measured using ILT5000 Research/Lab Radiometer (International Light Technologies). Fans circulated air between the inside and outside of the chambers. Group 3 experiments were conducted in the same enclosure, but in this group the enclosure was not placed inside an intermediate chamber in order to allow for LED position tracking. Instead, the enclosure was in a large room lined with anechoic foam. Video was recorded throughout the experimental sessions using one (group 1) or two (group 2) high-speed IR-sensitive

cameras (Chameleon3, FLIR) at 100 frames/s. Video recording for group 3 used two IR-sensitive cameras (Chameleon3, FLIR) and two color cameras (Blackfly S, FLIR) at 20 frames/s (see social-space session below). Video recordings were made using StreamPix video recording software (StreamPix multi-camera version 7, NorPix Inc.). Ultrasonic microphones (USG Electret Ultrasound Microphone, Avisoft Bioacoustics; frequency range: 10-120 kHz) sampled at 250 kHz were used to record audio throughout the experimental sessions. Wireless piezoelectric vibration sensors ("call detectors") were placed on each animal. These were used to assign bat identity to vocalizations (see below and fig. S1 for further details). Transistor-transistor logic (TTL) pulses were sent via coaxial cables using a UltraSoundGate Player 216H (Avisoft Bioacoustics) simultaneously to: 1) the master transceiver that controls the neural recording devices and on-animal call detectors of all bats; 2) the audio recording system (UltraSoundGate 416H, Avisoft Bioacoustics); and 3) the data acquisition board of the computer controlling the video recording (USB-6525 Analog DAQ, National Instruments [groups 1 and 2]; mic-input port [group 3]). TTL pulses arriving simultaneously on all the above devices allowed us to synchronize these distinct recording systems. All experiments took place in an electromagnetically and acoustically shielded room (IAC Acoustics).

A total of 63 free communication sessions were conducted. Of those, 26 were conducted with three implanted bats and one interlocutor bat (group 1), 23 were conducted with four implanted bats and one interlocutor bat (group 2), and 14 were conducted with four implanted bats and four interlocutor bats (group 3) (Table S3). The non-implanted "interlocutor" bats were included in order to stimulate more vocal interactions. The interlocutor bats in groups 1 and 2 were selected daily and were not co-housed with the implanted bats. The interlocutor bats in group 3 were the same bats for all sessions in order to track the same group's social dynamics across days. One of the interlocutor bats was co-housed with the four implanted bats and the remaining three were housed separately. All free communication sessions lasted between 2-4 hours.

Audio playback sessions

Three types of playbacks sessions were performed: (1) single bat playback experiment (fig. S10A), (2) simultaneous pair playback experiment (Fig. 2I) and (3) playback experiments in the group social setting (Supplementary Table 3).

Single bat playback experiments were conducted using bats from group 1, always immediately prior to free communication session and in the same enclosure where the free communication session took place (fig. S10A). One of the three implanted bats was placed in this enclosure and between 8-14 pre-recorded vocalizations were played using ultrasound speakers (Vifa, Avisoft Bioacoustics; frequency range: 1-120 kHz). Bats never vocalized during the playback experiments. The pre-recorded vocalizations were from the same group of bats recorded during free communication sessions and the list of vocalizations played back was updated every 2-4 recording days. Vocalization recordings were compensated to account for the frequency response properties of both the recording microphone and the loudspeaker before being played back to ensure acoustic fidelity. Vocalizations were played in random order, with repetition, continuously throughout the

playback session, and with uniformly distributed intervals between vocalizations (1.5 - 3s interval range). The playback was designed to provide an auditory experience that is similar to the near-constant chatter of bat calls in a bat cave in the wild or in our bat colony room, as was done previously (*15*). Playback sessions lasted approximately 30 minutes in length. A total of 29 single bat playback sessions were conducted. On average, 267 ± 18 (median ± inter-quartile range) total vocalizations (including repeats) were played during a session.

Simultaneous pair playback experiments were performed seven times in the same manner as described above, but with two bats in two separate enclosures hearing the same playback simultaneously (Fig. 2I). These experiments were designed to test the influence of auditory input on the observed interbrain correlation between group members (Fig. 2). Because this phenomenon was primarily observed in the high-frequency LFP and because during these simultaneous playback sessions, our recording signal quality had degraded such that we no longer were able to reliably record single unit activity, we only analyzed LFP activity during these sessions.

Playback experiments in the group social setting were performed 14 times using bats from group 3, always immediately after the social-space session and before the free communication session. These experiments were meant to test if the responses of other-responsive and identity selective neurons were present even when the vocalizations of group members were broadcasted from a speaker instead of as part of ongoing social interactions. These experiments were identical to the single bat playback experiments with the following changes. Instead of a single bat present in the free communication enclosure, all eight bats were present, such that the social and environmental settings were similar to the free communication session, and neural activity was recorded from all four implanted bats simultaneously. Instead of selecting from a library of randomly chosen vocalizations, each day 10 pre-recorded vocalizations from each of the five most vocal bats were chosen at random and played back with uniformly distributed intervals between vocalizations (1.5 - 3s interval range) for 30 minutes.

Echolocation sessions

Echolocation experiments were conducted using the bats in group 1, always immediately after the free communication session. A single implanted bat was allowed to fly freely around a 2.5 x 3.3 x 2.4 m (length, width, height) room lined with anechoic foam (fig. S10C). Bats were familiarized with this room prior to experimentation by allowing them to fly freely in the same room. An experimenter was present in the room to encourage the bat to fly after it had landed and was equipped with an IR illuminator night vision goggle system (Edge GS, Pulsar). All lights were turned off in the room, aside from the IR illuminator used by the experimenter. Echolocation clicks were recorded using the same audio recording equipment as in the free communication session. Echolocation sessions lasted for approximately 15 minutes. Bats produced 427 ± 308 echolocation clicks (median ± inter-quartile range) per session. A total of 20 echolocation sessions were conducted.

Operant sessions

Operant session task design

Two separate pairs of implanted bats (N = 4 bats; group 2) were trained to voluntarily produce vocalizations during an automated reward-based conditioning task. This approach differed from a recent behavioral study of vocal plasticity in a different species of bats where individuals were conditioned to vocalize in isolation (*61*). The paired designed was important as it allowed studying neural activity in both calling and listening bats and hence facilitated direct comparison to the free communication session for the same individuals and neural activity. Operant sessions were conducted always immediately prior to the free communication session. Operant sessions lasted between 2-4 hours. A total of 47 operant sessions (one session per pair of bats) were conducted. Each pair of bats was placed in separate 30.4 x 20.3 x 20.3 cm (length, width, height) enclosure lined with plastic mesh netting. The composition of the bat pairs was always the same across all sessions. A mesh divider was present in the enclosure, dividing it in half lengthwise. The divider prevented bats from directly physically interacting, but they could still see, hear, and smell each other and could fit their digits between the spacing in the mesh. Each cage was placed inside a 64.8 x 61 x 64.8 cm (length, width, height) chamber lined with anechoic foam. Fans circulated air between the inside and outside of the chambers. The experiments were conducted with red LED lights illuminating the chambers. Video monitoring was done with webcams. Ultrasonic microphones (Earthworks, M50) were used in conjunction with an analog to digital convertor (MOTU, 896mk3) to record audio at a sampling rate of 192kHz throughout the session as well as detect task-relevant vocalizations online. Call detector devices were used to assign bat identity to vocalizations (fig. S1). We used a microcontroller (Arduino, Uno Rev3) in conjunction with IR beam-break sensors in the food ports to detect nose-pokes and to control a linear actuator (Actuonix, P16-200-256-12-S) which delivered a banana smoothie through a syringe tip in the food port when the bat successfully performed the task. LED's were also present to signal reward (green) or timeout (white). All task control and audio recordings were fully automated and controlled through a custom MATLAB program that was written in-house. This program recorded audio and processed it in real-time to detect vocalizations. Vocalization detection was performed as follows: we applied a low-pass filter (20kHz) and then binned the incoming signal in 20ms chunks and calculated the RMS of the signal within each bin. We set a threshold manually to discriminate between vocalizations and noise and kept that threshold constant throughout experimentation. During these sessions either bat from a pair could produce a vocalization loud enough to cross that threshold, at which point either of the two bats could break the IR beam in the food port to trigger delivery of a smoothie reward to both bats' food ports (see fig. S16A, right panel for schematic of operant chamber used during experimentation).

Operant session training

For each pair, two male bats were randomly selected from the colony at UC Berkeley and housed together for one week prior to starting training in order to collect baseline weights. Bats were motivated through food deprivation in their home cage while retaining their weight above 80-90% of normal baseline. The training was divided into three phases culminating in a 'trained' pair of

bats ready for experimentation (fig. S16A). The bats used for this experiment were trained and had been undergoing maintenance training for >24 months (non-consecutively) prior to experimentation.

During training and experimentation, bats were rewarded with a fruit smoothie for each correct trial. Each reward delivered a fixed amount of smoothie. The smoothie was made fresh daily with roughly equal parts of banana and cantaloupe melon, along with small amounts of apple juice, honey, and fruit bat supplemental powder.

Phase 1: Classical conditioning of reward cue light

The goal of the first phase of training (fig. S16A, left) was to teach the bats to associate the conditioned stimulus (green LED on) with performing a correct action. Each session of conditioning lasted about four hours. On the first day of training, two bats were introduced to the operant chamber and both bats could freely move around to access either side of the cage. Both bats had access to a single food port on the front side of the cage. The bats had to learn to poke their nose into the reward port to activate the conditioned stimulus followed by delivery of the reward.

As the training progressed, an additional IR beam break was placed on the side of the cage as a trigger for the conditioned stimulus. The bats freely moved around each day until they learned that when they crossed the beam break, a conditioned stimulus (green LED) was activated, after which they had 30 seconds to go to the food port to dispense the reward. As the conditioning procedure continued, the time they had to retrieve reward was continuously lowered until bats reached 80% success for retrieving the reward within five seconds after crossing the beam break.

Phase 2: Operant conditioning to vocalize for reward

During the second phase of conditioning, we aimed to reinforce vocalizations produced when the two bats interacted (fig. S16A, middle). We stopped the IR beam break activating the LED and set the activation of the LED and the delivery of the reward at the food port to be dependent on the production of any vocalization by the bats. The cage divider was open during this stage so bats could interact and there was still only one food port that both bats could access to retrieve reward. A trial started when either bat voluntarily produced a vocalization during a normal social interaction. These vocalizations occurred only with direct physical social contact between the two bats. When one bat vocalized, either bat could go to the food port to retrieve reward. Through this process, the bats learned to increase their call rate during this phase in order to receive more reward.

Phase 3: Operant conditioning to vocalize with a physical barrier

The goal of the final phase of training was to change the social context of vocal production by physically separating the bats into different sides of recording chamber and conditioning them to vocalize outside the spontaneous social context (fig. S16A, right). To do so, one bat was placed in the back half of the cage, the other in the front half, and the mesh divider was closed such that the

bats could not physically interact with each other as they normally would. The bats could still see, smell, and hear each other and even interact in a limited way across the mesh divider. Both the front and back sides of the cage had their own reward port. For each successful trial, reward was simultaneously delivered to both reward ports so that both bats had access to the reward at the same time. When either bat produced a vocalization, the conditioned stimulus (green LED) signaled a correct action and both bats had the opportunity to retrieve the reward from the reward port within 5s.

The bats learned to approach the divider and cooperate to activate the reward. The call rate increased through training and the bats began to produce more stereotyped calls to activate the reward. Interestingly, without shaping, the bats segregated roles in the task so that one bat became the 'caller' and the other bat became the silent 'listener' (Fig. 3C and fig. S16B). In all pairs of bats, the 'caller' learned to make high numbers of vocalizations on one side of the enclosure while the 'listener' bat passively listened and retrieved the reward on each trial. We continued to train the bats until they reliably segregated roles and produced sufficient numbers of vocalizations in this context.

Social-space session

Social-space experiments were conducted using the bats from group 3, always immediately prior to a group playback session followed by a free communication session. Social-space experiments were specifically designed to allow bats to move freely in a larger environment so that their precise location, and how individual bats chose to position themselves relative to others in the group (their social-spatial preferences), could be assessed. Thus, the sessions were conducted inside a 122 x 122 x 60 cm (length, width, height) enclosure. The enclosure had mesh netting on top and on two of the four sides to allow bats to hang upside down and move around freely (Fig 4A). The floor and two remaining sides of the enclosure were fitted with transparent Plexiglass, to allow for video recording from below and from the sides. The enclosure was placed on stands at a height of 60 cm above the floor, in a room (3 x 3 x 3 m) lined with anechoic foam. The experiments were conducted in the dark with infrared lights to allow for video monitoring. Video was recorded using two IR-sensitive cameras (Chameleon 3, FLIR) and two color cameras for color detection (Blackfly S, FLIR). Paired IR and color cameras were placed to the side of the cage pointing inward and also on the floor beneath the cage pointing upward. For both camera types, video was captured at 20 Hz. Video acquisition was made using StreamPix video recording software (StreamPix multi-camera version 7, NorPix Inc.). An ultrasonic microphone (USG Electret Ultrasound Microphone, Avisoft Bioacoustics; frequency range: 10-120 kHz) was used to record audio throughout the experimental sessions. Call detector devices were used to assign bat identity to vocalizations (fig. S1). LEDs onboard the call detectors were used to assign a specific color to each bat to allow for tracking of individual bats during the session.

14 social-space sessions were conducted. All social-space sessions and the group playback and free-communication sessions that followed were conducted with the same eight bats from group 3.

Surgery

Anesthesia and surgical procedures for the implantation of four tetrode microdrives generally followed those described previously in detail for Egyptian fruit bats (*22*). Anesthesia was induced using a subcutaneous injection of a cocktail of ketamine (22 mg/kgBW), dexamedetomidine (0.09 mg/kgBW) and midazolam (0.31 mg/kgBW). For the duration of surgeries, bats were placed in a stereotaxic apparatus (Kopf) and anesthesia was maintained throughout surgery by repeated injections (approximately once per hour) of an anesthesia maintenance cocktail of dexamedetomidine (0.125 mg/kgBW), midazolam (2.5 mg/kgBW) and fentanyl (0.025 mg/kgBW). The depth of anesthesia was assessed by regular testing for toe pinch reflexes and measuring the bat's breathing rate. The body temperature of the bat was kept constant at approximately 35-36°C, using a heating pad placed under the bat in conjunction with a rectal temperature probe (FHC).

Each bat was implanted with a lightweight four-tetrode microdrive (Harlan 4-Drive, Neuralynx; weight 2.1 g). Tetrodes (~45 um diameter) were constructed from four strands of platinum-iridium wire (17.8 um diameter, HML-insulated), twisted and bound by melting their insulation together. Each of the four tetrodes were kept in separated telescoped assemblies of polyimide tubes within the microdrive and could be moved independently. The tetrodes exited the microdrive through a guide cannula with ~300 um horizontal spacing between tetrodes. On the day before surgery, each tetrode's tip was cut flat using high-quality scissors (tungsten-carbide scissors ceramic coating, CeramaCut; FST) and plated with Platinum Black (Neuralynx) to reduce the impedance of individual wires to 0.3-0.8 MΩ (at 1 kHz).

During surgery, prior to placing the microdrive, the skull was scored to improve adhesion and mechanical stability. A circular craniotomy of 1.8 mm diameter was made in the skull over the left hemisphere. The center of craniotomy was positioned over the frontal cortex of the bat at 1.7 mm lateral to the midline and 12.19 mm anterior to the transverse sinus that runs between the posterior part of the cortex and the cerebellum (fig. S3A). These coordinates are identical to the coordinates used in a recent study in this bat species (*22*). After a durotomy, the microdrive was placed vertically such that the tip of the microdrive's guide tube was flush with the brain's surface. The remaining exposed craniotomy was then filled with a biocompatible elastomer (Kwik-Sil, World Precision Instruments) to protect the brain. A bone screw (FST) with a soldered stainless-steel wire was fixed to the skull in the frontal plate contralateral to the microdrive and served as a ground screw after its electrical connection with the brain was verified. An additional set of 3-5 bone screws were fixed to the skull to serve as anchor screws for maintaining mechanical stability of the implant. The exposed skull and the bases of the anchor screws were then covered with a thin layer of quick adhesive cement (C&B Metabond, Parkell) to provide a substrate for the adhesion of dental acrylic. Dental acrylic was then added to secure the entire microdrive to the screws and to the skull. At the end of the surgery, bats were given the analgesic Metacam and if needed the

anti-inflammatory drug dexamethasone. The bat was treated with antibiotics for one week and with pain medication for three days, post-operation.

Electrophysiological recording

Electrophysiological recordings were conducted using a wireless neural data logging device ("neurologgers"; MouseLog-16 (vertical version), Deuteron Technologies) that interfaced with the microdrive of each implanted animal. The neurologger amplified the voltage signals from the 16 channels of the four tetrodes referenced to the ground screw, performed analog-to-digital conversion at a sampling rate of 31.25 kHz, and stored the digitized data on an on-board 32GB SD card which can hold up to 9 hours of recording. The system has a bandwidth of 1 Hz - 7 kHz, records voltage with a fine resolution of 3.3 μv, and has a low level of noise generally close to the limit of Johnson noise from the impedance of a given source. The neurologger and its lithium-polymer battery were encapsulated in an in-house 3D-printed plastic casing to prevent damage to the electronics and weighed a total of only 9.9 g. The Egyptian fruit bats in our experiment weighed more than 140 g and could fly while equipped with the neurologgers with ease, as expected from previous experiments using wireless recording systems with heavier or comparable weights during free flight for over an hour and covering multiple kilometers (*62, 63*). The individual neurologgers (and audiologgers) were wirelessly controlled and synchronized by a single transceiver.

After all recording sessions were concluded for the day, we connected the tetrodes to a wired recording system (Digital Lynx, Neuralynx) to monitor the neural signals and advance the tetrodes. Tetrodes were moved downward once every one to two days (generally by 20-160 mm), in order to record single units and LFP at new sites.

Histology

Histology was done as described previously (*22*). Each bat was given a lethal overdose of sodium pentobarbital and, with tetrodes left in situ, was perfused transcardially using a flush of phosphate-buffered saline followed by fixative (4% formaldehyde + 0.1 M phosphate-buffered saline). Tetrodes were left in the brain for 30 minutes after perfusion and then the brain was removed and stored in fixative. Subsequently, a cryostat was used to cut 40 μm coronal sections of the brains. The sections were then Nissl-stained with cresyl violet. Slides were imaged using a light microscope and tetrode positions were determined by manually examining those images (fig. S3B).

Vocal and behavioral data analysis

Detection of vocalizations

All vocalizations were first automatically detected from the microphone recordings and then manually curated to eliminate noise and determine the vocalizer identity. Automatic detection was performed as follows: the envelope of the audio recording was calculated as the sliding RMS of the recording in 1ms long windows and then every time the amplitude of the envelope crossed a low threshold of 0.01 (set low to detect even very soft vocalizations) was considered a possible

call. All possible calls were then recursively merged if separated by <5ms. After merging, only possible calls longer than 15ms were considered. This resulted in a large number of possible calls, including many instances of noise. Each of these possible calls was then manually annotated as noise or as a call by listening to the microphone recordings and by visually examining the spectrograms of the on-animal call detector recordings on each animal.

On animal call detector device design

In order to reliably assign identity to bat vocalizations without the need for video annotation (*3, 15, 16*), we designed a wearable wireless piezoelectric accelerometer that detects laryngeal vibrations produced during vocalization ("call detector"; fig. S1A). Each bat wore a call detector throughout the group experiments (excluding echolocation and playback sessions). We used single-axis, low mass, piezo-ceramic accelerometers (BU-27135, Knowles Electronics) to detect laryngeal vibrations. These accelerometers have previously been used as bone-conduction microphones (*64*) and are sensitive in the 0-10kHz range which overlaps substantially with the acoustic frequency range of bat vocalizations. We attached these devices to a flexible rubber "necklace" sized for individual bats that is worn around the bat's neck. The necklace is fitted to maintain contact with the bat's throat, without restricting normal behavior. On the back side of the necklace we attached a wireless "audiologger" (AudioLog1 or AudioLog2, Deuteron Technologies) which records, digitizes, and saves the accelerometer recordings to a removable SD card. The audiologger and its lithium-polymer battery were encapsulated in an in-house 3D-printed plastic casing to prevent damage to the electronics (fig. S1A). All audiologgers were controlled by a single transceiver (the same transceiver also controlled the neural data loggers, see below). For these recordings, the accelerometers were sampled at 50 kHz and we focused our analysis on the 0-10 kHz frequency range where the accelerometers we used were most sensitive.

Vocalizer identity assignment

To assign individual caller identity, we needed to be able to discriminate between vocalizations made by the bat wearing a given call detector and vocalizations made by bats in close proximity to that bat. Both types of vocalizations elicit some response from the accelerometer; however, we empirically determined that on-animal and close proximity vocalizations can be easily and reliably distinguished by comparing power in the recorded accelerometer signal between the 1-3 kHz band (low) and the 5-10 kHz band (high). On-animal vocalizations have strong responses confined to the low band, while loud close proximity vocalizations have relatively weak responses confined to the high band (fig. S1, B and C). We compared the classification obtained with the call detectors with classification obtained using video annotation of two bats interacting. We found that classification using the ratio of low to high frequency power of the call detector signal during calls resulted in identical predictions of the vocalizing bat compared to classification using video annotation 98% of the time. We further verified this method by positioning a loudspeaker playing vocalizations at full volume 1cm from a call detector suspended in the air to mimic the input of a close proximity vocalization from another bat. We found that the same low vs. high frequency power comparison reliably distinguished the on-animal vocalizations from the close-range

playback (fig. S1B). For all vocalization experiments, we manually labeled individual bat identity by aligning spectrograms of all accelerometer recordings with the microphone recording and by comparing relative power in the relevant frequency bands (fig. S1, C and D). We manually annotated these data to ensure the highest degree of accuracy by eliminating misplaced identity due to non-vocal noise (fig. S1C) and to assess for the rare case of multiple bats vocalizing at the same time (fig. S1D). Individual identity was assigned to the call detector which showed the highest power in the low frequency range (~1-3kHz; fig. S1, B-D) and the most consistent dynamics with the microphone recording.

Call selection

We defined trains of vocalizations each separated by less than 1s as a call bout. In our recordings, 55% of calls occurred in a bout. For all subsequent analyses a minimum of 15 calls or bouts of calls was imposed (e.g. a given bat had to hear or produce at least 15 calls or bouts to assess cells recorded from that bat for listening or calling responsivity, respectively) unless otherwise noted. Calls and bouts of calls were only used if they met the following conditions: 1) separated by at least three seconds from a prior call such that there were no call of any kind present prior to call onset (time of zero corresponds to call onset) and 2) separated by at least three seconds from succeeding calls of a different type (e.g. for listening related analyses, no calls produced by the listening bat could occur 3s after call onset, and for calling related analyses, no calls produced by any bat other than the calling bat could occur 3s after call onset). This resulted in only using calls and call bouts containing vocalizations that a given bat heard or produced but not both. Because bats generally do not vocalize at the same time or exchange vocalizations in rapid succession (only 16% of recorded call bouts had a different bat produce a vocalization within 3s of the call bout starting), these restrictions did not result in excluding a large fraction of our data. It did, however, result in different size subpopulations of neural data used for different analyses (e.g. Table S2).

Bioacoustic feature calculations

All bioacoustic features are calculated as in (*15*). All recordings were compensated for the frequency response properties of the recording microphone. In brief, bioacoustic features for each call were calculated using a sliding window of 15ms with an overlap of 14ms across the call and then taking the average across those windows. The following features were calculated for each call: fundamental frequency (F0), aperiodicity, loudness (RMS), power spectral centroid (centroid), and Wiener entropy. Fundamental frequency and aperiodicity were calculated using the YIN algorithm (*65*). Inter-call intervals were calculated as the time between the end of a call and the beginning of the next call.

Calculation of acoustic discriminability

In order to determine the degree of discriminability between individual bats or between groups of bats we calculated the cross-validated classification accuracy of a logistic regression classifier with a uniform prior using the following bioacoustic features calculated for each individual call: fundamental frequency, call length, aperiodicity, and Wiener entropy. In order to calculate

discriminability of individual bats (fig. S16D, left), we tested how well this classifier could discriminate between the calls made by an individual bat and all the calls made by all the other bats in its respective group. To generate an estimate of the distribution of classification accuracies for each bat, we trained the classifier using 90% of the calls chosen at random and tested on the remaining 10%. This procedure was repeated 1,000 times. We used the same approach to calculate the discriminability of calls between groups (fig. S16D, right), but instead we calculated the classification accuracy between all calls made in the first group and all calls made in the second group. In order to test if calls made by in-cluster bats were significantly different from calls made by out-of-cluster bats we calculated the classification accuracy of a logistic regression classifier between the two groups of bats. To obtain a p-value for the significance of this accuracy we compared that accuracy to a bootstrapped distribution of accuracies obtained by randomly permuting the group labels and repeating 10,000 times.

Behavioral annotation

In order to describe the behavior that the bats engaged in and to control for behavior as a factor in determining neural responses (fig. S7), we manually annotated all vocal interactions in group 1 for which we had high quality, well illuminated, high speed video recordings from multiple cameras during the free communication sessions (n = 3 bats; 2,096 vocal interactions annotated). To do so, we examined the behavior that the bats engaged in during a ±1s window around the initiation of vocalization bouts. Based on our own empirical observations of the behaviors that these bats engage in when only male bats are present without food and not during sleep hours, in conjunction with previous detailed reports of this species' behavior (*3, 22*), we annotated for the following behaviors:

Aggression: Any behavioral interaction that involved directed aggressive behavior including biting, scratching, and striking.

Incidental contact: Any physical contact that was not made in a directed fashion. This includes wing flapping, climbing over other bats, and any ambulatory movement resulting in contact.

Spontaneous initiation: Any vocalization that was produced with no clear behavior preceding the vocalization, i.e. all other bats were motionless prior to vocalization.

Probing: One bat placing its snout close to another bat's head or body.

Grooming: A bat either licking itself or another bat or picking at its own claws with its teeth.

Non-social: Any vocalization that was produced by a bat not in close physical proximity or direct contact with other bats.

Other: Any other behavior that was not commonly observed.

The typical spatial arrangement that bats take on during vocalizations is one where all bats are tightly grouped together. As a result, in some cases, the cameras or illumination sources that we used were occluded by one or more of the bats in the chamber. In these cases, and others when the

camera's view was occluded or the bats were out of the camera's frame, the behavior could not be determined, and these behaviors were marked as 'unclear'.

We found that overall, two main behavioral modes accounted for the majority of annotated interactions: aggression and incidental contact (fig. S7). This is consistent with previous descriptions of this species' vocal behavior that reported that vocalizations primarily occur during sleep, mating, eating, and space negotiations (*3*). Considering that during these sessions bats: (i) were not sleeping in our chambers, as it was during their waking hours; (ii) were not mating, as there were no female bats present; and (iii) were not eating, as there was no food present, we found that the primary vocal behavior the bats engaged in consisted of negotiating perching position and personal space, which, under the above annotation scheme, are included under aggression and incidental contact. Therefore, in our analysis of neural responses according to behavioral mode, we focused on the differences in firing rates between those two main behavioral categories, as well as between those behaviors and all others to verify that other behaviors, especially when the behavior was unclear, did not have an outsized impact on firing rates (fig. S7C; modulation index is calculated as the difference in firing rates between categories divided by the sum of the firing rates).

We also quantified to what extent bats were in close physical proximity to one another during vocal interactions (fig. S11B). Previous reports and our observations indicate that bats only vocalize when in physical contact with one another (*3, 15, 16*). To quantify this, we also annotated vocal interactions for grouped or non-grouped interactions. We took a conservative approach and defined 'grouped interactions' as interactions when all bats in the chamber were in direct physical contact with one another (we observed zero vocal interactions where the vocalizing bat was not in physical contact with at least one other bat). We found that even using this conservative definition 71.6% of all annotated vocal interactions were grouped interactions.

Finally, we attempted to quantify the participants in vocal interactions (fig. S11C). We defined participants as 1) any bat that vocalized during the interaction 2) any bat that exhibited a change in behavior or movement patterns immediately prior to vocalization that appeared to elicit a vocalization or 3) any bat that exhibited a change in behavior or movement patterns immediately after vocalization that appeared to be due to the vocal interaction. This definition was intentionally broad to give us a conservative quantification of which bats were obviously not involved in an interaction, as our ability assign intention to behaviors is inherently limited.

Group positional data analysis

Automated location tracking in a group

To monitor the position preferences of individual group members during the social-space session and the corresponding set of free-communication sessions, we developed a new automated tracking system. This system allowed tracking the position and identity of all eight bats in Group 3 simultaneously with 2.5 cm spatial resolution and 50 msec temporal resolution. Summarized briefly (further detailed in the following sections), the location tracking was based on assigning a

unique color to each bat using the onboard LEDs on the call detectors. Color video was captured using the upward pointing floor camera. Video frames were segmented by light intensity and a classifier trained on manually annotated video recordings was used to assign location and bat identity based on average pixel color (fig. S19). Automated tracking results were tested against a subset of manually annotated data to determine detection performance. Location tracking was only used while bats were hanging from the ceiling and side cameras were used to assess the amount of time bats spent below ceiling level.

Assignment of LED colors

The "audiologgers" (AudioLog1 and AudioLog2, Deuteron Technologies) stored inside the call detector plastic protective casing (fig. S1) were equipped with three colored LEDs (red, green and blue). Each LED can be set to a specific intensity level (at 4-bit resolution), and additive color mixing can be used to produce unique colors. We choose a set of eight colors that were maximally separable in RGB color space. The additive colors used were the following (numbers represent % of maximal intensity of red, green and blue LEDs accordingly: Color #1, 'Red', (100, 0, 0). Color #2, 'Green', (0, 100, 0). Color #3, 'Orange' (100, 50, 0). Color #4, 'Spring green', (0, 100, 50). Color #5, 'Azure', (0, 50, 100). Color #6, 'Violet', (50, 0, 100). Color #7, 'Rose' (100, 0, 50). Color #8, 'Chartreuse', (50, 100, 0). To allow for better diffusion of color from all angles, we encased the 3 LEDs with a drop of translucent adhesive. In addition, call detector casing was 3D printed from translucent resin (Formlabs Clear Resin GPCL04), which was then sanded down to increase diffusion of the LED color and ensure a uniform appearance of the additive color mix from different angles. The spatial resolution imposed by the call detector for bat location is equal to the length of the long axis of the call detector casing, or 2.5 cm.

Color prediction model

To automatically identify the color for each detected bat, we trained a classifier to predict the color class from each individual segmented area. Video recordings were manually annotated using the MATLAB Image Labeler app. This resulted in an annotated data set consisting of 2,366 frames with the location and area of all visible LED lights and their respective color labels for each frame. Color values for each annotated color area were then converted from RGB to CIE L*a*b* (CIELAB) color space. This color space was chosen in order to assess the color hue independent of intensity which can vary with the bats' movements. Median *a*b* values measured for each annotated area clustered according to color (fig. S19A, third panel from the left). A linear support vector machine (SVM) classifier was trained on a portion of the manually annotated data set in order to predict the color of each LED light by its *a*b* color values. This classifier achieved a 5-fold holdout cross-validated color prediction accuracy of 99.7%.

Automatic detection of bat identity and location

As video recordings were done in the dark the location of the LEDs carried by the bats could be detected using a simple luminance threshold using the following procedure (fig S19A). First, a binary map of each frame was created using a luminance threshold (7% of maximum intensity).

Regions of connected components that constituted putative LED locations were identified based on pixels that crossed the luminance threshold. Small gaps in these regions were filled in using a flood fill algorithm. Next, region properties (size, bounding box, centroid location), were extracted. Regions with centroids closer than 15 pixels were recursively merged until all region centroids were at least 15 pixels apart. Remaining regions with areas less than 15 pixels after merging (e.g. faint reflections of light from the enclosure walls) were discarded. Regions with areas greater than 200 pixels were split using a watershed algorithm and reprocessed. Next, median *a*b* color values were calculated for each region which were used to predict each region's color using the color prediction model. When two or more regions were assigned the same color prediction (e.g. when an obstruction resulted in a single LED light source being split into two regions during the region detection step), the region with the highest posterior probability (as calculated by the SVM), was chosen, and the other regions with the same color prediction were discarded. This process was repeated for each frame independently. Predicted color was then converted to bat identity according to the unique color assigned to each bat. After all frames were processed, locations of each detected bat were extracted as the centroid of the corresponding regions. All detected locations that were outside the boundaries of the ceiling were discarded (see below). Each bat's location trace was then smoothed using a moving median with a window size of 250ms. To account for brief occlusions, gaps in location traces of less than 2 seconds were filled using linear interpolation. Finally, all distances were converted from pixel to cm using the conversion ratio of 1 cm to 4 pixels which was estimated from an image of a ruler taken prior to recording.

To assess the quality of tracking, location predictions were tested against an annotated data set. First, the accuracy of location predictions was assessed by measuring the Euclidean distance between the predicted and manually annotated locations. This location prediction error had a mean and standard deviation of 1.27 ± 0.17 cm across bats, less than the spatial resolution limit imposed by the size of the call detectors (2.5 cm). Second, we observed a false positive rate of $1.80 \pm 2.68\%$ (mean ± standard deviation across bats) referring to automatic detections that were not present in the manual annotation. Finally, to quantify the tracking coverage, the percentage of all frames across all session in which each bat was detected was calculated. On average each bat was detected 89.25 ± 4.33 % (mean ± standard deviation) of the total recorded time per session (range: max 94.36 %, min 83.60 %) and for 82% of all frames at least 7 bats detected.

Estimation of bat vertical movement

The size of the social-space enclosure allowed the bats to move freely in three dimensions. The bats could climb up and down along the two opposite mesh walls (60 cm vertically) and the larger volume of the enclosure (0.89 m^3) even allowed bats to perform short flights. However, during our recording sessions the bats spent the majority of their time hanging or moving along the enclosure's ceiling, with rare short excursions. To precisely measure the amount of time that bats ventured away from the enclosure ceiling, the vertical positions of bats during the social-space

session were recorded using the cameras placed to the side of the enclosure where a clear Plexiglas wall was fitted.

Bat size within Group 3 averaged approximately 20 cm along the cranial-caudal axis. Consequently, LEDs (placed on the neck of the bats near the head) were detected by the side cameras to be approximately 20 cm lower than the enclosure ceiling when bats were resting on the ceiling. A threshold of 25.6 cm below the ceiling (to account for movement while hanging) was set to quantify how much time bats spent not hanging on the ceiling. Bat vertical location were estimated using the same automated procedure described above. For each session the amount of time when at least one bat (out of the group of 8) was detected below the horizontal threshold was calculated. On average, all of the eight bats in the group were found above this threshold 96.5% of the time. Of the 3.5% of the time that any bat took an excursion away from the ceiling, 87% of these detected excursions consisted of only one bat out of the eight. Following these results, we focused our analysis on the 2D plane of the enclosure ceiling.

Correction of lens distortion

To capture the whole enclosure ceiling in the cameras' field of view, a 3.8 mm lens was used which introduced a slight distorting effect on the edges of the frame. Distortion correction was done using Camera Calibrator app in MATLAB. Specifically, we collected 58 images of a non-symmetric checkerboard pattern placed in varying positions on the enclosure ceiling. These images were used to create a model of the camera and lens that could be applied to correct the distortion. All images had a mean reprojection error of under 0.6 pixels (< 1.5 mm) individually, and the calibrated model using all images had a mean reprojection error of 0.41 pixels (1.0 mm). All position tracking in the social-space session was done after this correction.

Calculation of distance threshold and dwell time

In order to quantify the bimodality of the distribution of pairwise distances between bats, a two component Gaussian mixture model was fit to the distribution of all measured pairwise $\log_{10}$ distances between all bats (Fig. 4C). The distance threshold that defined when a bat pair was "close together" or "far apart" was calculated by extracting the mixing probability, p, of the short-distance component of the model and calculating the p-th quantile of the distance distribution, resulting in a value of 35.8cm. At all distances greater than that value, pairs of bats were considered far apart and at all distances below that value, pairs of bats were considered close together. Using this distance threshold, a "social dwell time" value was calculated for each bat pair for each session as the fraction of the time that the pair was close together out of the total time that both of the bats in that pair were tracked for that session (i.e. excluding time where one or both bats' LEDs could not be tracked) (fig. S22A; average distances between bat pairs for each session are shown in fig. S22B). Dwell time was used as the primary measure of bat social spatial preference as it captured the tendency of bats to associate with other bats or not while discarding variability due to potential large changes in distance that are beyond the distance threshold.

Calculation of spatial stability

To determine if the social-spatial preferences of pairs of bats were stable across days, dwell time matrices were constructed representing the social dwell times of each bat pair for each day (fig. S22). The Pearson correlation was then calculated between all unique values in each day's dwell time matrix with the median of the corresponding values across all other days' dwell time matrices (Fig. 4D). The significance of these correlation values was assessed using the Mantel test with 10,000 iterations which computes a *p*-value by comparing correlation values between matrices to a distribution obtained by randomly permuting the rows and columns of the matrices (MATLAB implementation from (*66*)). The same analysis was applied to distance matrices composed of the average distance between pairs of bats on each session (fig. S22C).

Determining individual bat cluster status

To determine which bats exhibited consistent preferences toward spending time close to other bats and which bats preferred to spend time far from other bats, we performed the following analysis. First, the metric used to capture these preferences was the average dwell time of each bat on each session which was calculated by averaging all the pairwise dwell times that involve that bat (each bat was involved in N – 1 = 7 pairwise distances). This quantity reflects how much time each bat spent in proximity to all other bats during each session. Next, all possible ways to split the group of eight bats in two ("subgrouping") were enumerated and searched for the subgrouping that best reflected the two social positioning patterns exhibited by the different bats. In order to decide which subgrouping to use, subgroups were ranked by average dwell times that were similar within groups, but different across groups. The cross-group difference in average dwell time for candidate subgrouping was calculated as the difference between the averaged mean dwell times of the members in both subgroups. The within-group difference in average dwell time for candidate subgrouping was calculated by taking the mean across subgroups of the average difference between each unique pair in both subgroups. One subgrouping both maximized the cross-group difference and minimized the within-group differences of average dwell time by a wide margin (Fig. 4 F and G). Membership in these subgroups thus defined the "cluster status" of each bat as either "in-cluster" or "out-of-cluster".

To test if cluster status was robust to different values of distance thresholds, the same analysis was performed to determine which bats were in- and out-of-cluster using different values of the distance threshold when calculating social dwell time. The same bats were classified as in- and out-of-cluster using distance thresholds 45% less or 20% greater than the empirically derived value of 35.8cm (fig. S23 B and C).

Electrophysiological data analysis

Preprocessing of electrophysiological data

To analyze local field potential (LFP) signals, we first low-pass filtered the raw voltage traces using a Kaiser window-based FIR filter with a low pass cutoff of 1 kHz and a stopband from 1 kHz to 1.2 kHz with 40 dB attenuation at 1.2 kHz and a 5% passband ripple. Filtering was done in the forward and reverse directions to eliminate phase delays. The voltage traces were then down-

sampled by a factor of 15, resulting in a sampling frequency of 2083.3 Hz. Power line noise was then filtered out using a 2nd order Butterworth band-stop filter with cut-off frequencies 59.5 Hz and 60.5 Hz, and another one with cut-off frequencies 119.5 Hz and 120.5 Hz. We only analyzed LFP data in windows of ± 4s around the start of vocalization bouts. We observed some transient artifacts in our recordings in the form of large amplitude, irregular voltage fluctuations that are visually distinct from normal LFP signals. To automatically detect and discard vocalizations during which these artifacts occurred we used a simple threshold crossing algorithm that we found worked well for our data. For each channel of each tetrode for a given bat on each recording day we assembled all vocalization-aligned LFP signals and calculated the mean and standard deviation of the LFP during a baseline period of 2-4s before vocalization onset. We then calculated the fraction of time from -2s to 4s after each vocalization onset that the LFP signal was above or below its baseline mean ± 5 standard deviations. Any channel that had >1% of its signal over threshold for a given vocalization was excluded from all further analyses. The average fraction of vocalizations that were excluded due to artifacts across all channels, bats, and sessions was 0.4 ± 0.29 % (mean ± standard deviation).

In order to extract spikes, we followed the same approach as described previously (*22*). First, we band-pass filtered (in both the forward and reverse directions) the raw voltage traces using a 6th-order Butterworth filter with cut-off frequencies of 600 Hz and 6000 Hz (fig. S4 B and F). For each recording channel and each session, a voltage threshold was set as the following quantity: the difference between the 75th percentile and the median of the voltage trace, divided by the 75th percentile of the standard normal distribution, and multiplied by a factor of three (*67*). Each time the voltage on one recording channel crossed its threshold, we found the sample having the peak voltage among the over-threshold samples and extracted 32 samples (1.02 ms) from each channel of the tetrode around the time of the peak sample: from the 7th sample before the peak sample to the 24th sample after. These extracted samples were then used for spike sorting. We performed spike sorting manually using SpikeSort3D (Neuralynx). Spike sorting was done using a combination of features including spike height and peak as well as principal components (fig. S4 C, D, G, and H). Sorted single units were further assessed for stability across the recording session(s). Time periods of stability were manually determined by visual inspection of cluster features for long lasting gaps in time of spikes or cessation of activity. Single units were then only analyzed during those periods of stability. For each tetrode on each session, after excluding spikes belonging to single units and after excluding artifacts based on waveform shape, all remaining spikes were grouped into multiunit activity.

Calculation of LFP spectrograms

For each vocalization we calculated the LFP spectrogram for each channel. Using sliding windows 192ms in length and 168ms of overlap, we calculated the LFP power spectrum in each window using the multitaper method with a time half bandwidth product of 4. We calculated power at integer frequencies between 5 and 150 Hz. We then separately z-scored the power in each frequency band for all further analyses. For assessing the relationship of neural activity between

brains, LFP spectrograms were reduced to power in high and low frequency bands (5-20 Hz and 70-150 Hz, respectively). These bands were used in order to reflect dynamics observed across many vocalizations. Figure 2A shows an example frequency-normalized, vocalization-averaged spectrogram where those bands are clearly present. The average power spectra around vocalization onset in shown in fig. S12, with two separate peaks visible within the defined low and high frequency bands. Similar frequency bands were found to be behaviorally relevant in a previous study of interbrain correlation in bats (*22*). We repeated the same analyses using the frequency bands defined in that study and observed similar results.

Calculation of firing rates

Firing rates were calculated by counting spikes in 5ms bins and smoothing with a Gaussian filter with a bandwidth of 50ms. For the purpose of determining responsive neurons, baseline firing rates were calculated as the average firing rate of each neuron in the range -3s to -2s relative to vocalization onset, averaged across all vocalization bouts.

Vocalization responsive neurons

In order to assess individual neurons as vocalization responsive we used a change point detection algorithm to determine if and when vocalization averaged firing rates changed substantially from baseline. We assessed for both self and other responsivity (as well as playback and echolocation responsivity). For self responsivity, we considered only calls produced by the bat from which the neuron under consideration was recorded from. For other responsivity, we considered only calls produced by other bats. Vocalization firing rates were calculated ±3s around call onset for all vocalizations separated by at least three seconds (see above for selection of used calls and call bouts) and then averaged across all of those instances. The algorithm we used to determine responsivity and response latency was the CUSUM method based on Poisson distribution of firing rates with multiplicative spike rate shift (*68*, *69*) which attempts to detect changes in firing rates compared to a baseline by recursively calculating a cumulative sum of residuals. We used this method because it makes few assumptions regarding the profile of response expected and is based only on the baseline firing rate. Considering the variety of response profiles we observed in our data, including both excitatory and inhibitory responses (Fig. 1C, fig. S5, S17, S18), this method provided qualitatively better results than other similar methods (e.g. simple threshold crossing). We calculate the CUSUM algorithm as follows: Let $\{y_1, \ldots, y_n\}$ represent data points in a time series of firing rates, i.e. the vocalization averaged firing rate and μ_0 is the baseline firing rate. Then:

$$S_0 = 0$$
$$S_t = \max(0, S_{t-1} + s_t)$$
$$\text{Where } s_t = y_t ln(\delta) + (1 - \delta)\mu_0$$

A neuron is considered responsive if any $S_t > \alpha$ and the response latency is calculated as the first time t that $S_t > \alpha$. S is calculated twice with δ set to δ or $\frac{1}{\delta}$ to assess for a positive or negative change in firing rate, respectively. If a given neuron is considered responsive for both a positive and negative change in firing rate, the response valence is considered the change with the greater difference from baseline. Further details and mathematical justification for this approach can be found in (*69*). Here, we set $\alpha = 20$ and $\delta = 2$ based on empirical observation and we consider the window ±1s around vocalization onset for responsivity.

Association of high firing rates with vocalization

To assess if the firing rates changes we observed around vocalizations can be explained by chance association, we compared the fraction of time that high firing episodes of responsive neurons occur around vocalizations to the overall fraction of time that vocalizations occur (fig. S6B). We did this as follows: for each responsive neuron we calculated the firing rate over the entire session, smoothed with a 2s wide Gaussian window and found the top 100 peaks in firing rate separated in time by at least 2s. Then, for each peak, we assessed if a vocalization occurred in a window ± 1s around that peak. We divided the number of times a vocalization was associated with a firing rate peak by 100 and compared with the total fraction of time spent vocalizing (calculated as the sum of the duration of all call bouts plus 2s for each bout). As shown in fig. S6B, nearly all responsive neurons fire much more frequently during vocalizations than would be expected by chance (the average probability of vocalization during the session), indicating that modulation in neural activity was specifically related to vocalization interactions.

Comparison of call to inter-call interval firing rates

To determine if firing rates of responsive neurons were modulated with the temporal dynamics of call bouts, we compared firing rates during the times when calls were being produced or heard to the inter-call intervals immediately surrounding those calls (fig. S6C). To do this, for each call bout we calculated 1) the call firing rates as the number of spikes that occurred during calls (defined as the time between call onset and offset padded by ±100ms to account for very short calls) divided by the total time spent calling, and 2) the inter-call interval firing rate as the number of spikes that occurred during the rest of the call bout (i.e. all time not during calls). For plotting purposes, the difference between call and inter-call firing rates were normalized for each neuron by the baseline firing rate standard deviation for that cell. For each cell we tested the significance of the difference in firing rates using a paired, two sided Wilcoxon signed rank test. As shown in fig. S6C, approximately 60% of responsive cells have significantly different firing rates between call and inter-call intervals, indicating a precise modulation of activity with the temporal dynamics of vocalizations.

Calculation of firing rate differences by bioacoustic features

The comparison of firing rates according to bioacoustic features (fig. S8) was performed as follows: for each feature the overall median value of that feature across all vocalizations was used to split vocalizations and their corresponding firing rates into high and low categories. Then for

each cell, if there were at least 10 calls in each category, the firing rate was calculated for each call in that category (± 100ms around each call) and the difference was calculated by subtracting the averages of all calls in either category. For plotting purposes, the difference between firing rates were normalized for each neuron by the baseline firing rate standard deviation for that cell. For each cell we tested the significance of the difference in firing rates using a two-sided Wilcoxon rank sum test (fig. S8C).

Linear encoding model

In order to systematically assess the contribution of different acoustic features to the encoding of individual neurons' firing rates, we built a linear encoding model (schematized in fig. S9A) with banded ridge regularization (*70*) inspired by a recent analysis of cortex wide activity in mice (*71*). Our model used various vocalization-derived features to predict the firing rate of a single neuron. In our case, we had three separate feature spaces: binary "call-on", principal components of call spectrograms, and bioacoustic features. Because these features inherently have very different distributions, we took advantage of banded ridge which allows for separate regularization of different feature spaces. Because we wanted to remain agnostic as to the temporal relationship between vocalization features and firing rates, we included as separate predictors time-shifted copies (in the positive and negative directions) of each vocalization derived feature. To prevent overfitting and accurately assess the predictive capacity of our model, we used a nested cross-validation scheme to simultaneously determine the ridge regularization parameter and fit our model. We then used the Pearson correlation coefficient between the predicted firing rate and the actual firing rate as a measure of the encoding capability of our model and compared between models with various features removed.

In detail, we considered only time around call bouts by reducing the entire session into a concatenation of all call bouts with ±2s padding. During the span of this concatenated time series, we calculated the firing rate of a given neuron by counting spikes in 5ms windows with 1ms step size and smoothing with a Gaussian window (20ms standard deviation). Nine total call features were calculated on the same time series. "Call on" was simply an indicator variable for if a call was occurring at a given time point. Bioacoustic features were calculated as above at 1ms resolution, here we used fundamental frequency, RMS, and Weiner entropy. Spectrograms principal components were calculated as follows: spectrograms were calculated as the power spectral density over time using a 1024-point short-time Fourier transform and a 150ms Kaiser window. Those spectrograms were then reduced using principle components analysis to their first five principal components to reduce dimensionality and maintain computational tractability. These nine call features were then copied and time shifted by 1ms for ± 200ms, and then smoothed by averaging every other 1ms for a design matrix with a total of 1,800 predictors. We then regressed the observed firing rates on this design matrix in the following way: we split the data into five even, contiguous cross-validation folds (each fold F_i consisted of a training set composed of 4/5ths of the data, and a test set with the remainder). For each fold, we considered five logarithmically spaced possible values for ridge regularization values $10^{\{3\ldots7\}}$. Within each fold we performed a

further five-fold nested cross-validation to determine the optimal regularization value. That is, for each fold F_i we split the training set into five further folds, then for each nested fold, F_{i_j}, we trained and tested 5^3 different models consisting of every possible combination of regularization parameters for each feature space. For each fold F_i separately, we then used the regularization parameters that resulted in the lowest average cross-validated mean squared error from the nested folds, $F_{i_{1-5}}$. Finally, for each fold F_i we measured the model fit by assessing the Pearson correlation coefficient between the predicted firing rates and the observed firing rates.

To assess the relative contribution of each feature type (call on, bioacoustics, spectral PCs) we calculate its unique encoding contribution by removing the feature from the model and assessing the decrease in model fit (fig. S9C "unique"). In order to maintain the same number of predictors so that we were comparing similar models, we randomly permuted the time series corresponding to that feature, thereby abolishing any relationship between that feature and the firing rate. We also wished to assess the contribution of just the binary predictor, "call on." However, because the other call-derived features are trivially highly correlated with the presence or absence of a call, we decided to perform the same analysis, but with "call on" regressed (because "call on" is a binary variable, regressing out "call on" from other variables consists simply of subtracting off the mean of each respective variable whenever a call occurred) out of all the other features to assess how well a model using only the residual information would fit (fig. S9C "orthogonal"). The values plotted in fig. S9 B and C are the average for all responsive neurons, where each neuron's value is the average across its cross-validation folds.

Within and across session firing rate correlation

To quantify the consistency of single neurons' firing rates around vocalizations within and across sessions (Fig. 3F and fig. S18F) we either split the calls in a given session into two groups of every other vocalization bout (within session) or one for each session (across sessions) and then calculated the average Pearson correlation coefficient for firing rates across all pairs of vocalization bouts (Fig. 3F). We assessed the significance of differences across contexts using the Wilcoxon rank sum test.

Comparing neural data between acoustically similar and distinct calls

To test if acoustic differences between calls produced in the free-communication sessions and the operant sessions drove the observed differences in intra- and inter-brain neural activity we classified calls as acoustically similar or distinct across sessions. This allowed comparing firing rates of all self and other responsive neurons and interbrain correlation across bat pairs during similar and distinct calls between the two sessions. To classify calls as acoustically similar or distinct between the free-communication and operant sessions (fig. S18 I and J) we took the following approach: using all calls from both sessions, we trained a binary classification decision tree to classify calls according to session type using the calls' bioacoustic features (fundamental frequency, call length, aperiodicity, and Wiener entropy). We limited the decision tree to a maximum of two splits in order to identify the most relevant features for classification. Those

features were aperiodicity and Weiner entropy. After fitting the classification tree, we extracted the values for those features at the two split points of the decision tree. We then defined acoustically "similar" calls as calls which had aperiodicity and Weiner entropy values within ±1 standard deviation of their respective split points. This resulted in selecting only those calls that were acoustically overlapping across sessions. Acoustically "distinct" calls were defined as all other calls, i.e. those calls that generally only occurred in one session or the other.

To calculate the difference in firing rates of responsive neurons within a given session between acoustically "distinct" and "similar" calls (fig. S18I, left) we performed the following analysis. First we calculated the average firing rates of each responsive cells in each session separately in the window ±500ms around the onset of each used calls and then calculated the difference between average firing rates during "distinct" calls and "similar" calls. Only cells for which we had at least 10 used calls of either type were used for this analysis (n = 146 neurons). Similarly, to calculate the difference in firing rates of responsive cells during acoustically "similar" calls, but across sessions (fig. S18I, right), we performed the following analysis. We first calculated the average firing rates of each cell that was used in both sessions and responsive in either session in the window ±500ms around the onset of each used calls in both sessions and then calculated the difference between average firing rates across sessions only during acoustically "similar" calls. Only cells which had at least 10 used calls of either type were used for this analysis (n = 51 neurons). To determine if the difference in interbrain correlation we observed across sessions was driven by acoustic differences, we used the same approach and calculate the average interbrain correlation during acoustically "similar" and "distinct" calls during each session (fig. S18J).

Pairwise interbrain correlation

To assess for pairwise interbrain correlation between bats as they vocally interacted, we took a similar approach to (*22*) and calculated the correlation between brains in different frequency bands of LFP power. However, here we compute the correlation around moments of social communication (vocalizations) and at a much finer time scale than done previously. In detail, we calculated the Pearson correlation coefficient of the power of the LFP spectrogram averaged in a given frequency band (5-20Hz and 70-150Hz) between pairs of bats. We did so using a sliding window of 0.5s and a step size of 0.25s in the range ± 2.5s around each vocalization separated in time by at least 3s. Correlation coefficients were calculated for each pair of bats, for each pair of 16 tetrode channels on each bat, for each vocalization, and for each time window. Correlation coefficients were then averaged across all pairs of tetrodes, resulting in one correlation coefficient per vocalization, bat pair, and time window. We did not include any vocalizations where artifacts in any LFP channel were detected.

For correlation in spiking data (single units and multi-unit activity), we performed the same analysis, but using the firing rates (calculated as described above) of the corresponding spiking signal instead.

Interbrain conditional Granger causality

We used the multivariate granger causality (MVGC) toolbox (*72*) to calculate Granger causality (GC) values around vocalizations in the high frequency (70-150Hz) power of the LFP which had an effective sampling rate of 41.6Hz (see above). We only used vocalizations where all tetrodes of all bats in a group were artifact free. We performed GC calculations in 1s long windows ±3s around call onset with a step size of 0.25s. Here we average LFP power across channels of each tetrode to maintain computational tractability such that each bat was characterized by four channels instead of 16. The MVGC toolbox calculates GC by modelling time series data as a vector autoregressive (VAR) process with a certain order, or lag, p. The Akaike information criterion was used to estimate the proper order of the VAR(p) model with a maximum lag of 20 samples (equivalent to 480ms). By windowing the data and using all vocalizations for each VAR estimate in so-called "vertical regression" we mitigate the strict stationarity requirements for GC analysis. In each window we calculated the GC value of each bat pair conditioned on the activity of the other bats present. Non-conditional GC, $F_{Y\to X}$, intuitively, measures the increase in predictability of a (potentially multivariate) time series X using past values of X and a separate time series Y beyond the predictability using only past values of X. Conditional GC, $F_{Y\to X|Z}$ includes the possibility that other separate variable(s) Z drive both X and Y. It measures the increase in predictability of X given X, Y, and Z beyond the predictability using just X and Z. This allowed us to measure the increase in predictability of a given bat's, Bat_1, neural activity using the neural activity of Bat_2 while simultaneously accounting for the activity of $Bat_{3\ldots N}$. Each bat's neural activity is a multivariate time series corresponding to the four time series obtained by averaging activity within each tetrode. By calculating this value for all bat pairs and in both directions, we obtain a connectivity matrix that represents the interbrain connectivity patterns across all bats in a group. This can be referred to as a "Granger causal graph" (*72*). Granger causal graphs can be displayed equivalently in graph or matrix form (Fig. 2E; fig S14, B, C and G). We used bits as the units for GC values reported here following the asymptotic equivalence between GC and transfer entropy (73). All GC calculations were done separately for each group and experimental session.

To compare GC values across conditions and bats we subtracted a baseline level calculated during the period >1.5s before the call (Fig. 2, F and I; fig. S14, E and F). In this way, we could directly compare the change in GC from a baseline level to values around vocal interactions.

To determine if the observed GC values were due to precisely coordinated activity rather than simple co-activation of LFP power across bats, we created a trial-shuffled distribution of GC values by bootstrap. For each bat pair we randomly shuffled the vocalization "trial" order of one of those bats LFP activity and recalculated the GC values 1,000 times (fig. S14D).

Because we used all vocalization to fit a given VAR model, we did not have the capability to estimate trial-by-trial variation in GC to obtain distribution estimates. For values averaged over bats (Fig. 2, F and I), error bars are estimated as the SEM across bats. For distribution estimates for individual bats, we used the MVGC toolbox routine *bootstrap_tsdata_to_mvgc* which randomly resamples the full VAR model residuals and adds those to the model predictions to form

surrogate time series. GC values were then calculated for those time series. This process was repeated 1,000 times and distributions were estimated based on the results (fig. S14E).

To assess the stability of interbrain connectivity patterns we sorted all vocalizations produced across all experimental days by time and grouped them into nine time bins such that each bin had the same number of vocalizations. Succeeding bins then represent steps in time, but each step is not necessarily uniform (due to the variable number of vocalizations produced each day). We then calculated Granger causal matrix for each bin and calculated the correlation of each bin's matrix with all other bins to estimate the degree of similarity across time (Fig. 2G). Bin-to-bin changes in connectivity matrices were also examined to validate the stability over time (Fig. 2H). We compared these values to a shuffled distribution using a Mantel test to assess for significance by using the same values in each bin's vector, but first randomly permuting the rows and columns of the corresponding Granger causal matrices, so that bin to bin values did not represent the same bat pair (Fig. 2, G and H).

Interbrain transfer entropy

Granger causality entails the assumption that the time series in question can be modeled by vector autoregressive process. This assumption may be violated by if the time series has long-term memory (i.e. autocorrelation does not decay exponentially) or if there exists a strong, slow moving average component (*72*). These assumptions may be violated by LFP data. We therefore performed a complementary analysis using transfer entropy (TE), an asymptotically equivalent measure to Granger causality (*73*). We used the neuroscience information theory toolbox (*74*) to calculate TE values around vocalizations in the high frequency (70-150Hz) power of the LFP which had an effective sampling rate of 41.6Hz (see above). We only used vocalizations where all tetrodes of all bats in a group were artifact free. As with the GC calculation described above, TE was calculated "vertically" across trials which mitigates the stationarity assumptions of TE generally. The values of the continuous LFP power data were binned (not in time) into 10 discrete states. Then, at each time point in the time series, $TE(X \rightarrow Y) = I(Y_{future}; X_{past}|Y_{past})$ was calculated where the past state occurs one time step before the future state (fig. S15B). Unlike GC analysis, TE does not as readily admit of incorporating multivariate (greater than 2) data.

Analysis of identity selectivity

Identity selectivity of single neurons

In order to quantify which single neurons were identity selective (Fig. 1 F-H and fig. S11), we looked at firing rates of neurons recorded in bats that were listening to vocalizations and asked if we could decode the identity of the vocalizing bat. This analysis was performed for each single neuron from bats that had heard at least 10 separate used calls from at least 2 other bats (N = 669 single neurons). For each neuron we trained one-vs-all logistic regression classification models to decode the identity of each other bat (if it produced at least 10 separate vocalization bouts) based on that neuron's firing rates during vocalizations. In detail, given bats $Bat_{1...B}$ and a single neuron from Bat_1 ("self-bat"), classifiers were trained to decode from that neuron's firing rate the identity

of Bat_2 ("target-bat") vs. $Bat_{3...B}$ ("non-target-bats"), then Bat_3 vs. $Bat_{2,4,...B}$, etc. We collected all vocalization bouts from the target-bat and all bout from non-target-bats and calculated the time-varying firing rates during each call in a window ±1s around the start of the bout in windows of 250ms. Next, we fitted a logistic regression classifier on the observed firing rates to predict if a vocalization came from the target-bat or non-target-bats and tested the classifier using five-fold cross-validation. The reported classification accuracy is the average classification accuracy across cross-validation folds. To test the statistical significance of the classification accuracy, we performed a permutation test with 10,000 repetitions by randomly permuting the labels of "target-bat" and "non-target-bat" and retraining the model in the same cross-validated manner as above. Because we tested up to N-1 one-vs-all classifiers, we used the Benjamini-Hochberg procedure to control the false discovery rate (FDR) at a level of 0.05 for each individual neuron. A neuron was considered "identity selective" if at least one of the classifiers had a significant classification accuracy.

Identity selectivity using acoustic features

We tested if vocalization acoustic features alone could reproduce the identity selectivity observed in single unit responses (Fig. 1H). We took the same approach used for each single neuron, but instead of firing rates we substituted a collection of call-averaged bioacoustic features (F0, Weiner entropy, RMS, call length, spectral centroid, and aperiodicity) for each call that occurred in the same window we used for calculating firing rates and kept all other parameters the same.

Identity selectivity using spatial position

We tested if the spatial positions of individual bats during the vocalizations produced in the free communication session alone could reproduce the identity selectivity observed in single unit responses (fig. S25). We took the same approach described above for each single neuron, but instead of firing rates we used either the position of the target-bat or the distance between the self-bat and the target-bat at the time of the vocalization.

Identity selectivity over time

To calculate decoding accuracy of single neurons over time we performed the same analysis on the same window size of 2s starting at 3s before the start of a call until 3 seconds after the call with a step size of 1s. For Fig. 1G we selected all significantly identity selective neurons at zero time-lag and found the average decoding accuracy of those neurons over time when decoding the identity of the bat(s) that they were selective for at zero time-lag. We also plot, for comparison, the decoding accuracy of the same neurons, but for the identity of the other bats present in the chamber for which that neuron was not selective.

Effect of proximity and participation on identity selectivity

In order to verify that the identity selectivity that we observed was not due to proximity or distance between bats (e.g. that one bat is consistently further away than all other bats), we used the behavioral annotation of spread and grouped interactions (see above; grouped interactions are

interactions where all bats were clearly in physical contact with one another) to exclude all non-grouped interactions and therefore guarantee relatively small distances between bats during these interactions. We then performed the same single unit analysis as above, this time only including interactions that were annotated as grouped. There were 1,501 such grouped interactions, which resulted in a total of N = 37 previously identified identity selective neurons that still met the criteria for a sufficient number of vocalizations using only grouped interactions (fig. S11B).

We took a similar approach in order to verify that the identity selectivity we observed was not due to participation or lack of participation in vocal interactions. As an example, if we recorded a neuron from self Bat_1 that was selective for target Bat_2 it could have been the case that target Bat_2 vocalizes primarily when it is interacting with the self-bat and that the self-bat was not involved in vocal interactions with other bats. In that case, the observed identity selectivity could have been because the self-bat was physically active when target Bat_2 called, but inactive during all the other bats' vocalizations. To control for this and other similar situations, we used the behavioral annotation of participants in vocal interactions to exclude all interactions that involved the self-bat. In this way, we limited the available interactions to those where the self-bat was effectively a bystander so that its behaviors during all such interactions were more similar. We performed the same single unit analysis as above, this time only including interactions not involving the self-bat. This resulted in a total of N = 19 previously identified identity selective neurons that still met the criteria for a sufficient number of vocalizations using interactions not involving the self-bat (fig. S11C).

For both controls for proximity and self-bat involvement we decreased the amount of available data according to a certain behavior and observed a decrease in decoding accuracy on average. To test if that decrease in accuracy is greater than what we would expect by randomly excluding trials, we estimated the expected change in accuracy when randomly subsampling the available calls to the same number of calls available for both above two analyses. We repeated this subsampling 1,000 times for each neuron and found the 95% confidence interval using that distribution. The average lower bound of that interval across identity selective neurons included in fig. S11, B and C is plotted. We found that for only 3/37 and 1/19 neurons in the proximity and self-bat controls, respectively, were lower than their individually calculated lower bounds, indicating that the decrease in accuracy that we observed could be due to chance and not due to proximity or self-bat interactions.

Self vs. other selectivity

In order to determine which single neurons were self vs. other selective (Table S2), we used the same decoding approach as when decoding individual bat identity. Here, the target-bat was the self-bat and the non-target-bats were all other bats.

Impact of caller cluster status on identity selectivity and interbrain correlations

In order to assess the impact of caller cluster status on neural activity in the free communication session, we asked whether a significant difference existed in single neuron identity decoding

accuracy and inter-brain correlation according to the cluster status of the caller. We used inter-brain correlation instead of Granger causality for this analysis because we could calculate inter-brain correlation on a call-by-call basis. Granger causality values were estimated using many calls at once and could therefore not be analyzed on a call-by-call basis.

To test if the cluster status of the calling bat had an effect on the accuracy with which pre-identified identity selective neurons could decode the identity of a target bat, we examined the cross-validated decoding accuracy values of all identity selective neurons. We used each accuracy value for all pairs of identity decoding neurons and target bats that had a bootstrap p-value less than 0.05 (n = 68 neuron-bat pairs). We then grouped identity decoding accuracy values according to the cluster status of the target-bat (Fig. 4H and fig. S26) and calculated the percent difference between the average values in either group. To test if this difference was significant, we fit a linear mixed-effects model to predict identity decoding accuracy values. In this model the only fixed effect was the cluster status of the target-bat. The other predictors, self-bat identity and recording date, were considered nuisance covariates and taken as random effects in order to control for them. We then performed a likelihood-ratio test between the model containing all predictors and the reduced model not containing the cluster status of the target-bat.

To test if a difference existed in the interbrain correlation between pairs of bats when an in-cluster bat vocalized compared to an out-of-cluster bat, we used the average interbrain correlation values in the window ±250ms around call onset (this window was chosen to capture to increase in inter-brain correlation observed around calls Fig. 2C) from all pairs of bats for all usable calls (excluding artifact contamination as described above; n = 5,758 calls and bat pairs composed of 1,569 calls and 6 bat pairs). Interbrain correlation values were then grouped according to the cluster status of the calling bat (Fig. 4I) and we calculated the percent difference between the average values in either group. To assess the effect of the calling bat's cluster status on the elicited interbrain correlation, we used a linear mixed-effect model with cluster status as the fixed effect and bat pair identity and recording date as the two random effects. Significance was assessed using a likelihood-ratio test comparing the full model to a reduced model without the cluster status of the caller. This test was repeated for different subsets of the data including only pairs of bats that were both listening (i.e. pairs not including the calling bat) (fig. S27A), only pairs of bats that included both one in-cluster bat and one out-of-cluster bat (fig. S27B), and only pairs of bats that included two in-cluster bats (fig. S27C). The final control we performed was to include the distance between each pair of bats during each vocalization in the free-communication session as an additional fixed co-variate in the model followed by performing the same test of significance (fig. S27D).

To assess if the difference in interbrain correlation was persistent across days, we sorted all vocalizations produced across all experimental days by time and binned them into nine bins such that each bin had equal number of vocalizations. Succeeding bins then represent steps in time, but each step is not necessarily uniform (due to the variable number of vocalizations produced each day). We then calculate the interbrain correlation during calls from bats with different cluster status in each bin (Fig. 4J).

To assess if the difference in interbrain correlation we observed was large relative to other possible subgroupings of bats aside from according to cluster status, we calculated the difference in interbrain correlation for all possible subgroupings of bats into two groups such that each group had at least 1,000 call and bat pair observations (n = 146 subgroupings; Fig. 4K).

Chapter 6: Supplementary Figures for chapter 2

Supplementary Figure 1 - Page 1

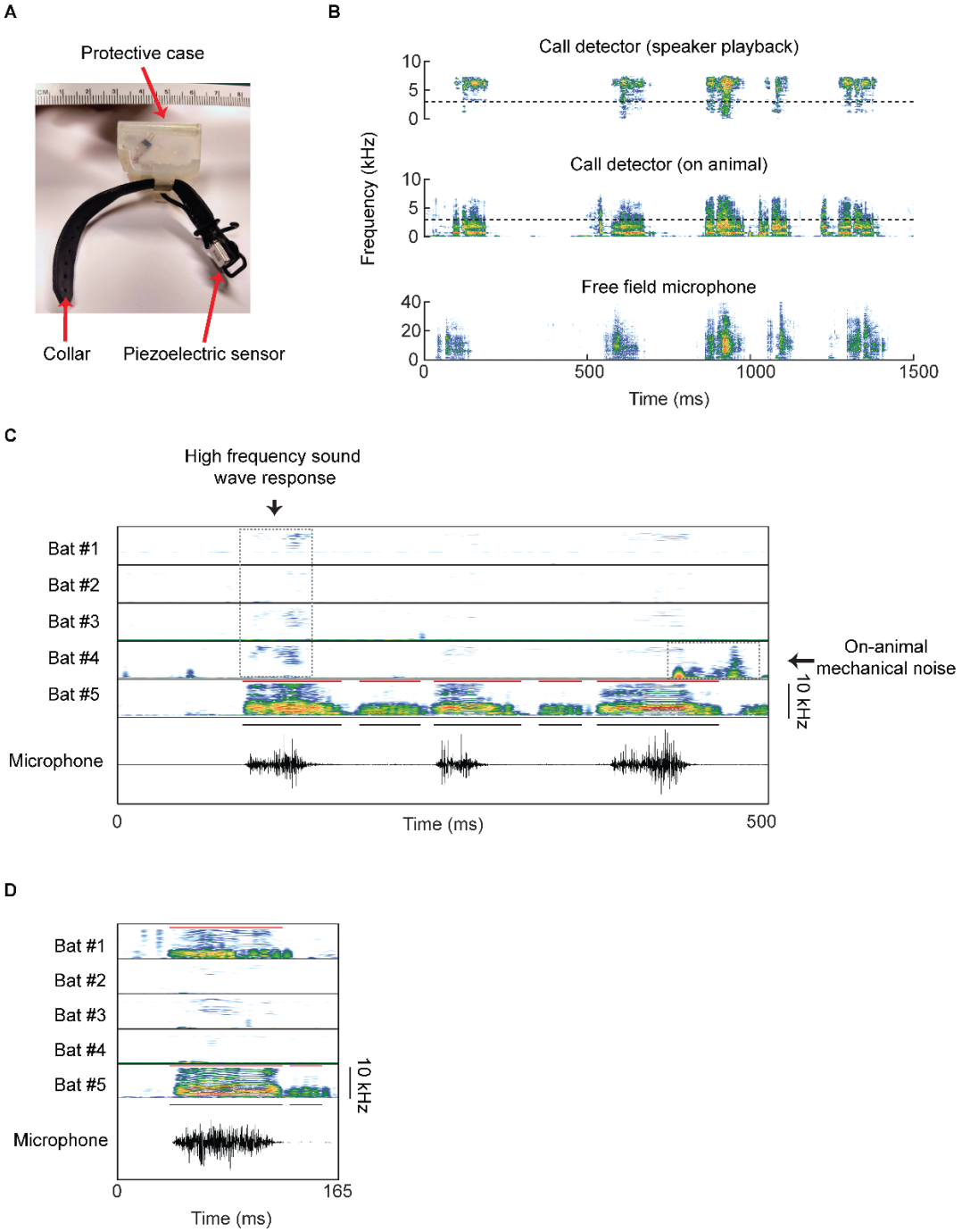

fig. S1. Wireless, on-animal call detector design and validation. **(A)** Call detector device – piezoelectric vibration sensor, collar, and protective case. **(B)** Comparison between spectrograms of a vocalization bout recorded on an animal wearing the call-detector (middle) to the same call bout recorded on a microphone (bottom). Top plot shows the same call bout played out of a loudspeaker and recorded on a call detector 1cm from the loudspeaker. Note the reduced power in low frequencies during playback (below dotted line, 3kHz). **(C)** Example call bout recorded on a microphone (bottom row) and five call detectors placed on five different bats (top 5 rows). Vocalizations were detected on one call detector ("bat #5") and assigned to that bat. Also highlighted is an example of the high frequency response on the call detectors on bats #1-4 due to the sound waves created by the loud vocalization produced by bat #5. Additionally, an example of on-animal mechanical noise (due to e.g. scratching of the collar) is highlighted on the call detector of bat #4 which is distinguished from signals due to vocalizations by both its spectral shape (e.g. lack of harmonics) and its lack of temporal alignment with the dynamics of the vocalization recorded on the microphone. Note that some of the calls visible on the call detector are less visible on the microphone but were detected based on the thresholds we used. Red lines above the calls of bat #5 indicate the detected calls on that bat's call detector. Black lines above the microphone recording indicate the calls detected on the microphone. **(D)** As in (C), showing a rare case when two bats vocalize at the same time (bats 1 and 5).

Supplementary Figure 2

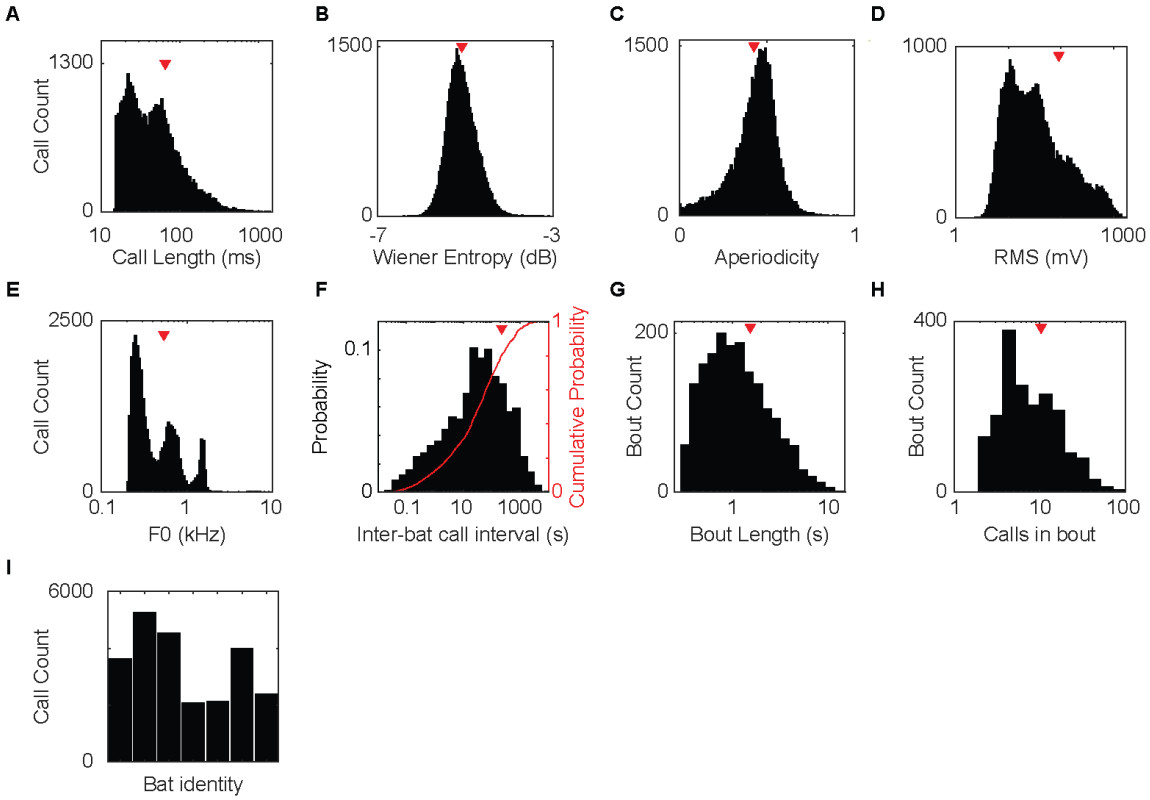

fig. S2. Bio-acoustic features of bat social vocalizations. **(A-H)** Distributions of bio-acoustic measures averaged within calls; red triangles represent mean value. **(I)** Number of calls produced by each implanted bat.

Supplementary Figure 3

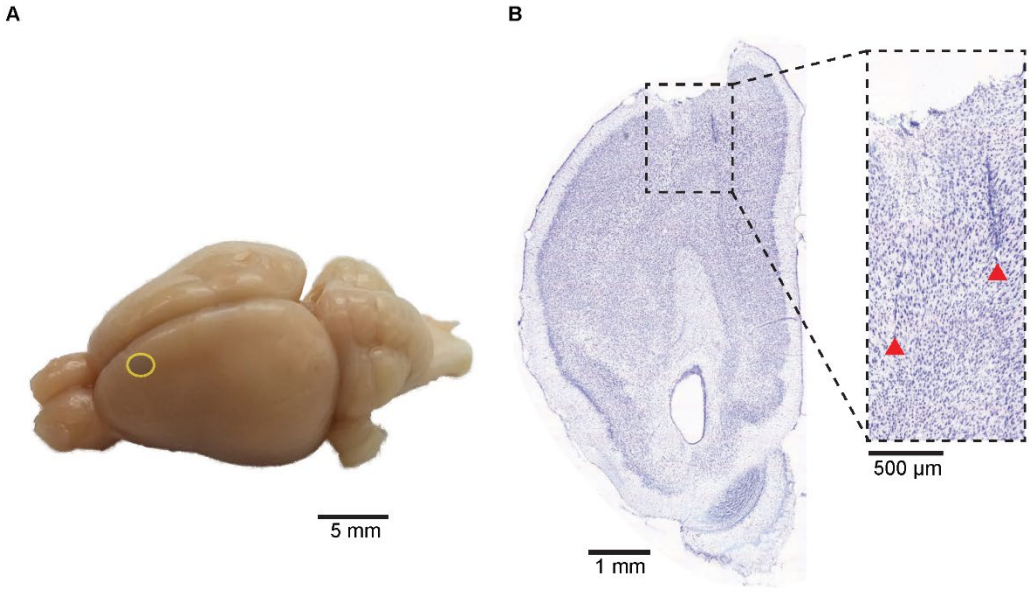

fig. S3. Recording site and tetrode track identification. (A) Egyptian fruit bat brain with estimated recording area highlighted by a yellow circle. **(B)** Nissl stain of a coronal brain slice at the plane of recording location. Red arrows indicate identified tetrode tracks. Scale bar is shown below each figure.

Supplementary Figure 4 - Page 1

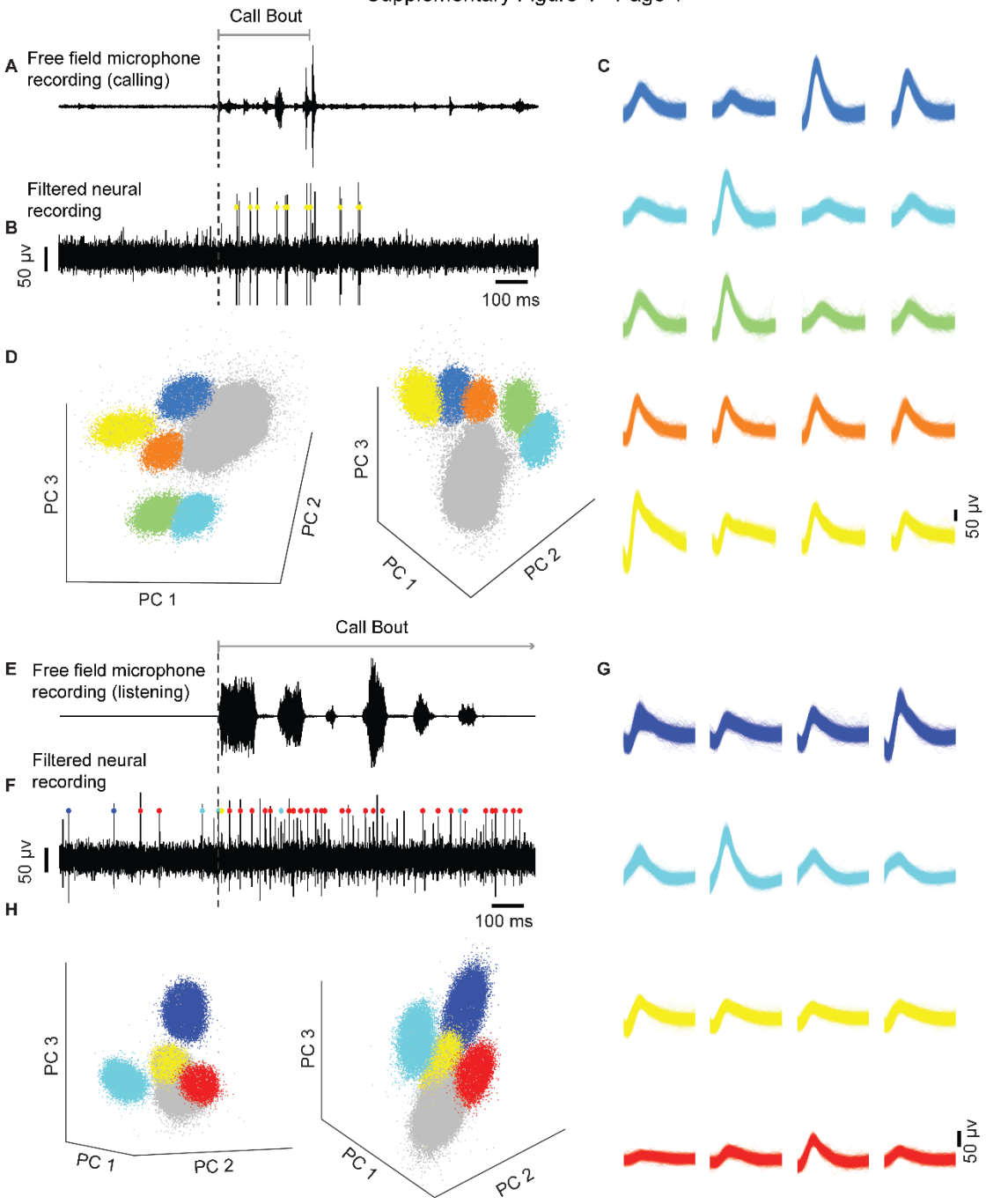

Fig. S4: Example audio and electrophysiological recordings during calling and listening and sorted spikes. **(A)** Audio recorded on the free field microphone of a vocalization bout during the free communication session. Dashed vertical line indicates start of vocalization bout and gray horizontal line indicates duration of call bout. Data in A and B are aligned and presented on the same time basis. **(B)** Electrophysiological recording from one channel of one tetrode from a bat producing the vocalization presented in (A). Recording bandpass filtered between 600 – 6,000Hz (frequency range used for spike detection). Spikes that were detected and sorted into clusters are highlighted with dots colored according to the clusters shown in C and D. **(C)** Spike waveforms from five well sorted clusters detected on the same tetrode. Each row represents a separate cluster, and each column represents one of the four tetrode channels. **(D)** All spikes detected on the same tetrode, presented at two different orientation angles as a 3D projection of the first principal components of spike waveforms detected on three channels. Spikes that were sorted into clusters are colored, as in B and C. **(E – H)** Panels as in Fig. 2. Neural activity in F is from the bat listening to the calls in E.

Supplementary Figure 5 - Page 1

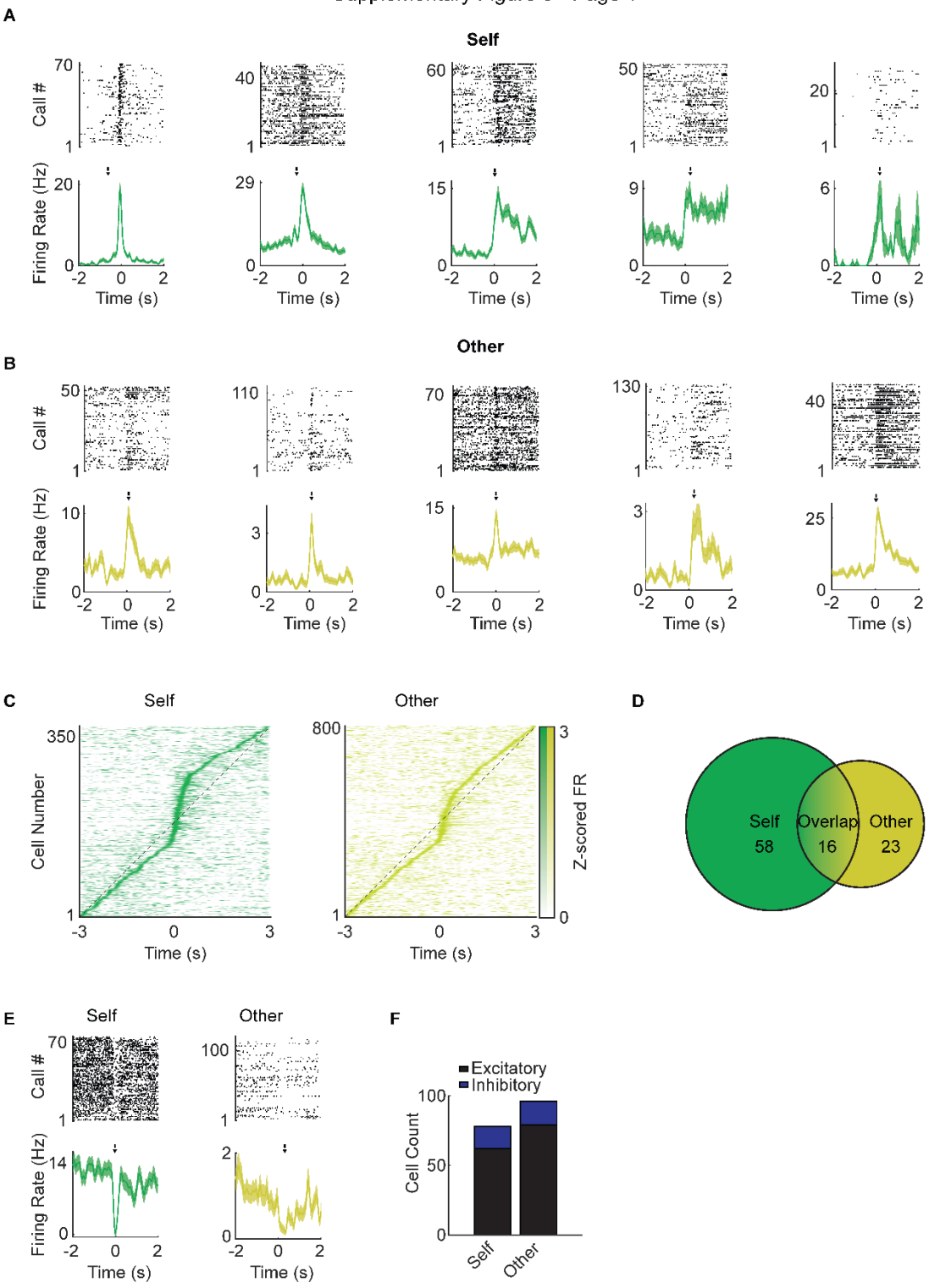

fig. S5. Example single units and population firing rate modulation during calling and listening. **(A)** Example self responsive cells: vocalization aligned raster (top) and PETHs (bottom). Arrows indicate detected response time (i.e. response latency). Shaded areas indicate SEM. **(B)** Example other responsive cells: raster and PETHs as in (A). **(C)** All usable cells' trial averaged firing rates, max normalized and sorted by time of maximum firing. **(D)** Venn diagram indicating the number of neurons (out of the population of neurons that could both be assessed as self- and other-responsive, n = 364) that were self-responsive, other-responsive, or both self- and other-responsive ("overlap"). **(E)** Example inhibitory responsive cells, self (left) and other right). **(F)** Proportion of self and other responsive cells that showed excitatory (black) and inhibitory (blue) firing rate modulation.

Supplementary Figure 6

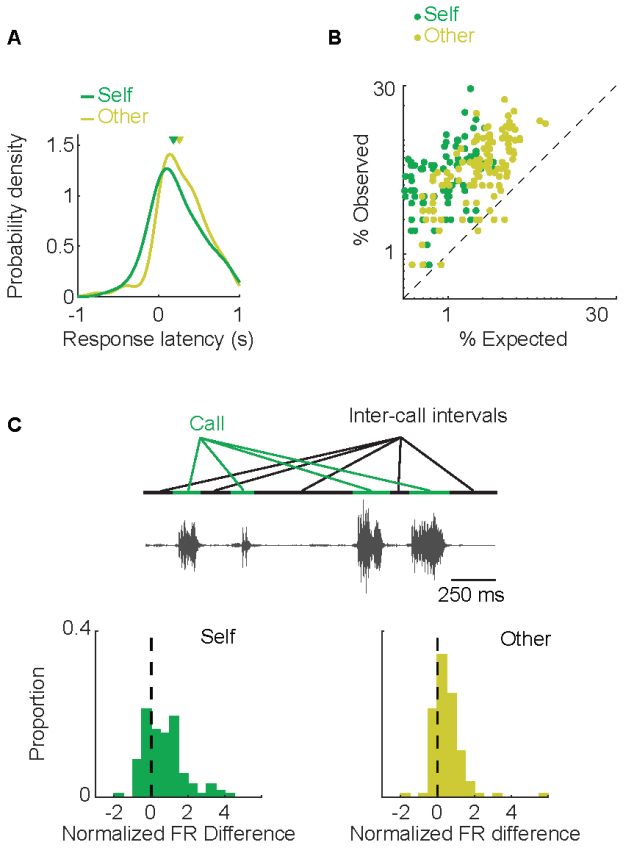

fig. S6. Specificity and precision of responsive neurons with respect to vocalizations. (A) Distribution of response latency for self and other responsive cells (green and yellow, respectively). Average response latency indicated by arrowheads (median values of 145ms and 245ms for self and other, respectively). 75% and 93% of responsive cells, self and other respectively, had a detected response latency after vocalization onset. **(B)** Percent of total session time containing vocalizations (expected by chance) vs. percent of high firing rate periods containing a vocalization (observed). Each point represents a responsive neuron and is shown on a logarithmic scale. Dashed black line represents the unity line predicted by chance. Note that nearly all neurons are above the unity line, suggesting a high degree of responsivity specifically around vocalization times. **(C)** Top, schematic illustrating call vs. inter-call intervals. Bottom, distributions of normalized differences in firing rates between time during calls and time immediately surrounding vocalizations for self (left) and other (right) responsive cells. 75/123 self-responsive and 65/108 other-responsive cells have significantly different firing rates during calls as compared to between call intervals ($p < 0.05$ Wilcoxon signed rank test).

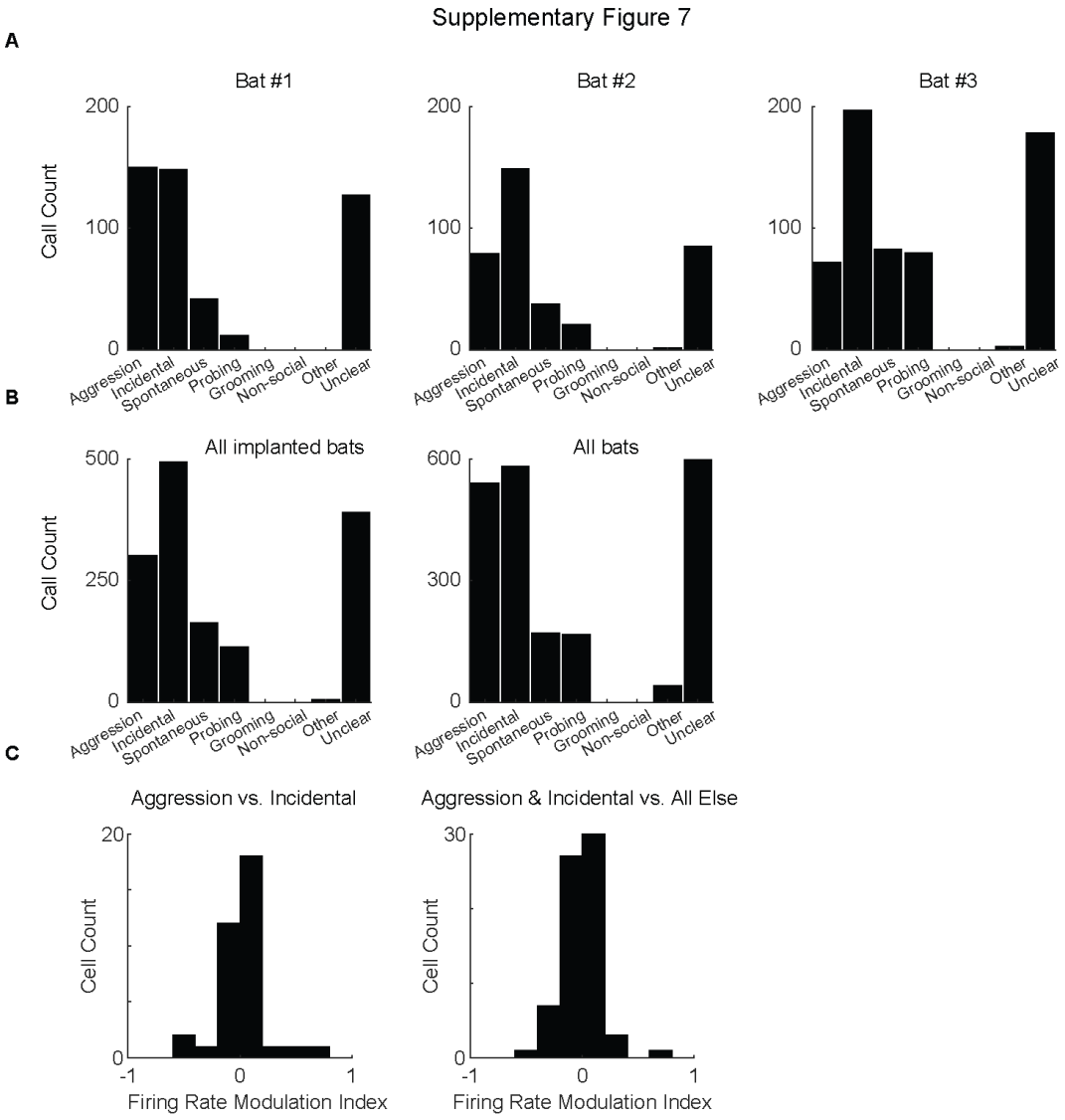

fig. S7. Vocalization related behavior annotation and impact on firing rates. (A) Distributions of manually annotated behaviors that bats engaged in during vocal interactions. Annotation is shown for each implanted bat where annotation was possible. Two main behavioral types, aggression and incidental contact, made up the majority of interactions that we were able to annotate. Behaviors occurring around vocalizations that could not be annotated (e.g., due to physical occlusions) were labeled as 'unclear'. **(B)** Distribution of vocal interaction behaviors summed across all implanted bats displayed in (A) (left), and across all bats that participated in the experiment (including 'interlocutor' bats; right). **(C)** Modulation index of responsive neurons' firing rates in the window ±500ms around vocalization onset comparing vocalization related activity across behaviors. Left, comparing the two main behavioral types (aggression vs. incidental contact; 1/36 significantly differentially modulated neurons). Right, comparing both main behaviors to all other behaviors (11/69 significantly differentially modulated neurons). $P < 0.05$, Wilcoxon rank sum test.

Supplementary Figure 8 - Page 1

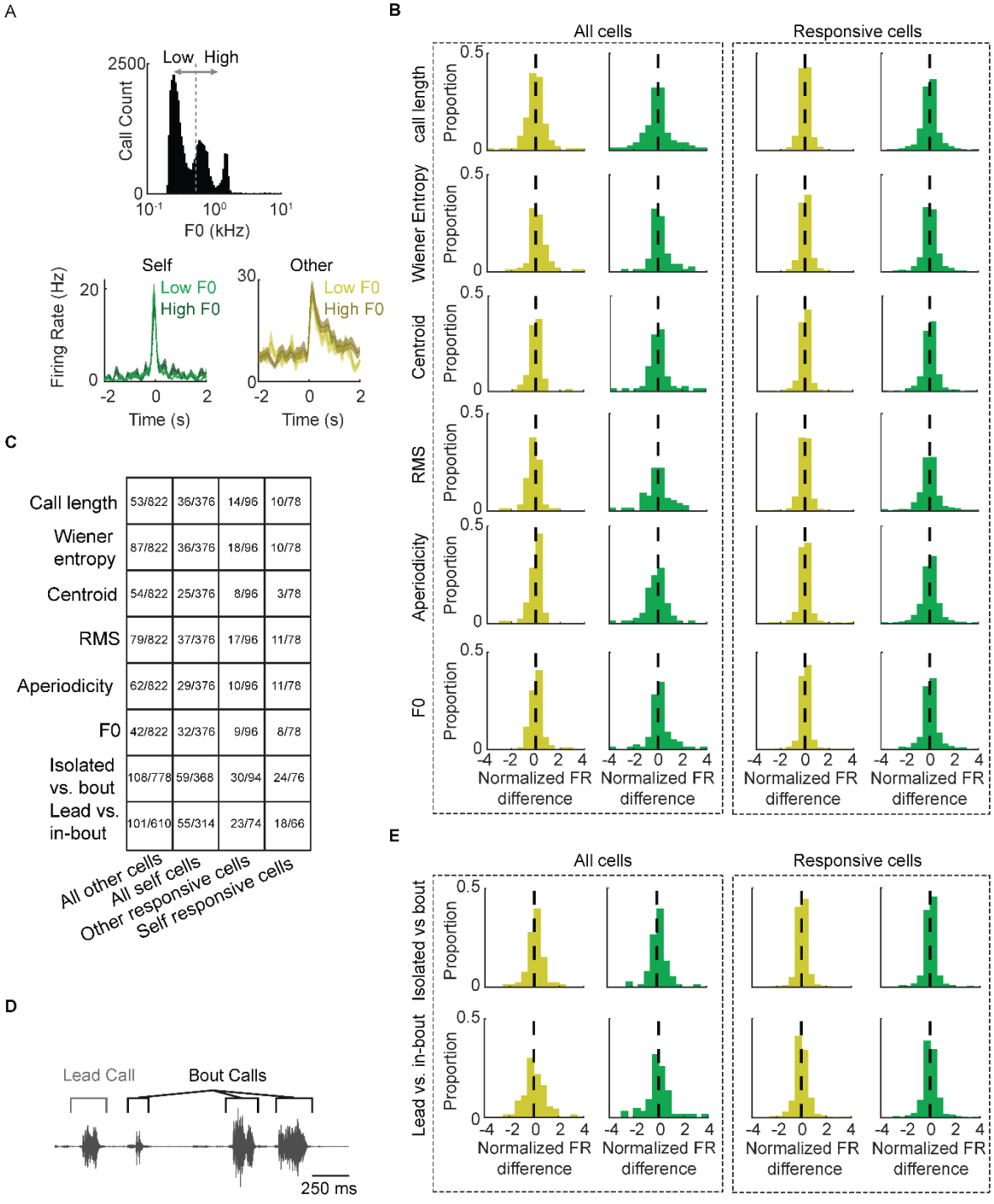

fig. S8. Single neurons are not modulated by call acoustic features or position within a call bout. **(A)** Top: distribution of call F0, gray dashed line indicates median. Bottom: PETHs from example responsive neurons split according to the median fundamental frequency (F0) value of the calls. **(B)** Comparisons of firing rates during vocalizations, split according to high and low values of various bio-acoustic features. For each plot, firing rates are calculated for all vocalizations (both self, green, and other, yellow) for a given usable neuron and split by the median value of the indicated feature. The average difference in firing rate is calculated. Histograms are the distribution of the average differences for either all neurons (left) or only responsive neurons (right). **(C)** Fraction of neurons that individually have significant differences in firing according to the indicated feature ($p < 0.05$, uncorrected Wilcoxon rank sum test). Note that the difference in the total number of neurons for each feature is due to imposing a minimum of 10 calls each within the high and low ranges for each feature separately. **(D)** Illustration of lead and bout calls. **(E)** As in (A), but calls are split by their relative position within a call bout. Top: isolated vs. in-bout call. Bottom: Lead call of the bout vs. in-bout call. Isolated calls are defined as single calls not included in any bout.

Supplementary Figure 9

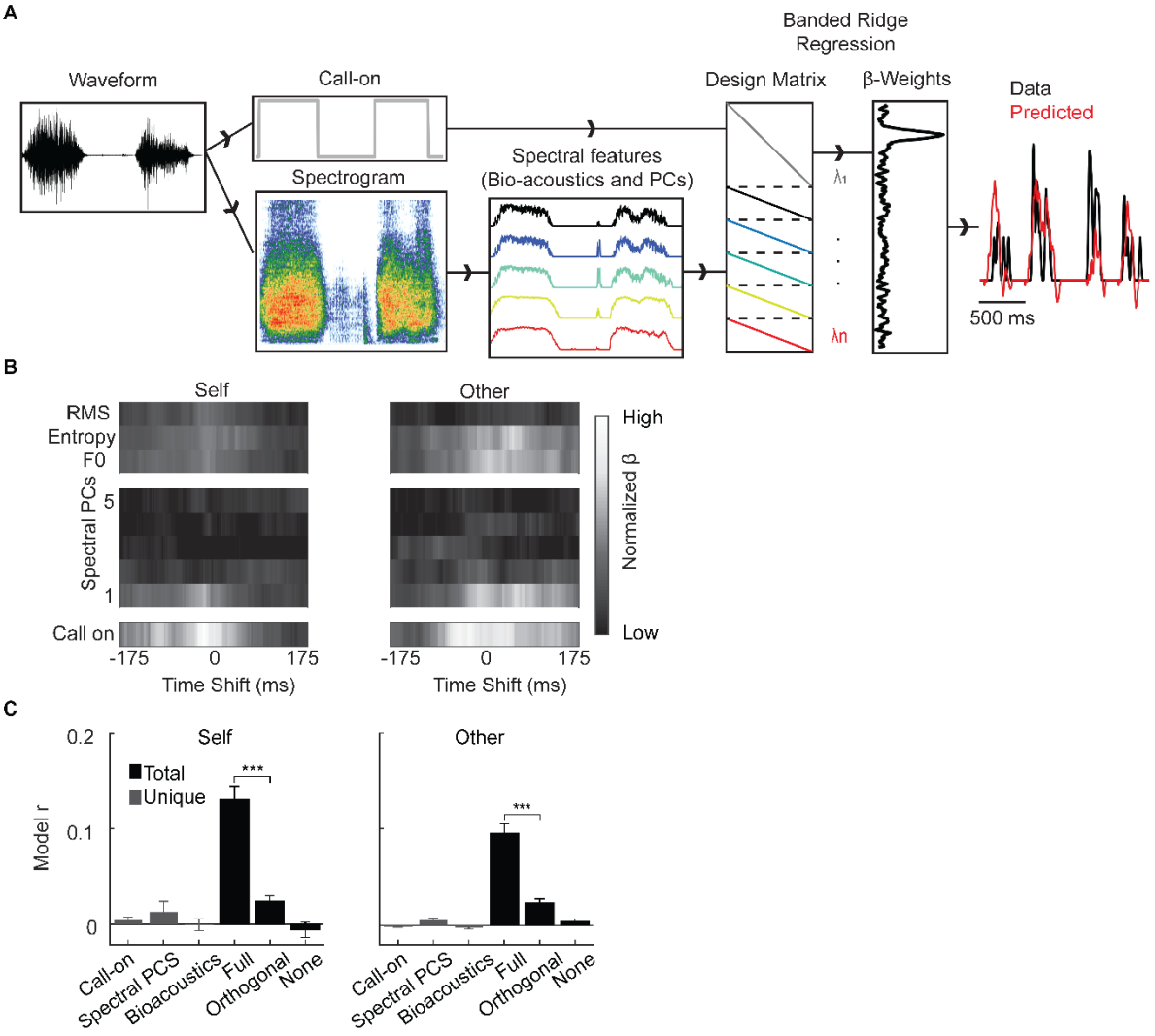

fig. S9. Encoding model testing the prediction of single neuron firing rates using acoustic call features. (A) Schematic of linear encoding model. Vocalizations are converted to bio-acoustic features and spectral principal components and shifted backward and forward in time to create a design matrix. We then regress the observed firing rate on that design matrix using banded ridge regularized regression. The fit is assessed as the cross-validated correlation of the predicted firing and the observed firing. **(B)** Normalized beta coefficients for all time shifted predictors averaged across self (left) and other (right) responsive cells. **(C)** Correlation between actual and predicted firing rates of responsive neurons using a linear model with acoustic feature predictors during calling ('Self', n = 78 neurons) and listening ('Other', n = 96). In gray are predictor unique contribution (decrease in correlation when a given predictor is removed). In black is the correlation using: all predictors ("full"), predictors orthogonalized with respect to "call-on" ("orthogonal"), and randomly shuffled predictors ("none"). *** $p < 10\text{-}10$, paired t-test. Note the near zero unique contribution of each individual feature combined with the marked reduction in "orthogonal" correlation indicates that, of these features, "call-on" is generally the exclusive driver of activity.

Supplementary Figure 10 - Page 1

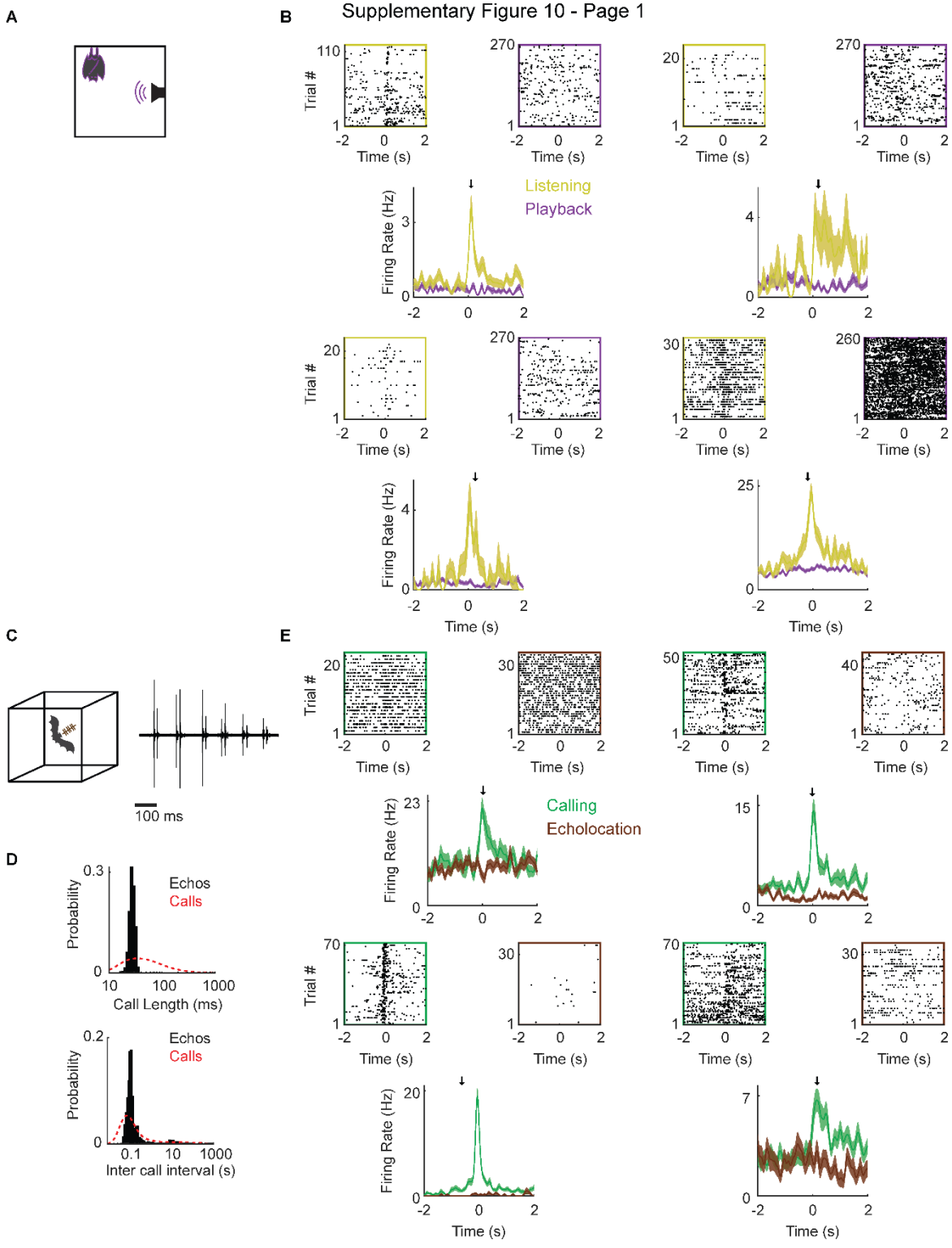

fig. S10. Call responsive neurons do not respond during audio playback or echolocation. (A) Playback experiment schematic. **(B)** Example raster and PETHs comparing responses to listening in the free communication experiment (yellow), to playback (purple). Rasters are shown side by side and PETHs are overlaid below for each individual neuron. Arrows indicate detected response time (i.e. response latency). Shaded areas indicate SEM. **(C)** Left: Echolocation experiment schematic. Right: example train of echolocation clicks. **(D)** Distributions of call length (top) and inter-call interval (bottom) for echolocation clicks (black) and social vocalizations (red). **(E)** Example raster and PETHs comparing calling in the free communication experiment (green), to echolocation (brown). Organization as in (B).

Supplementary Figure 11

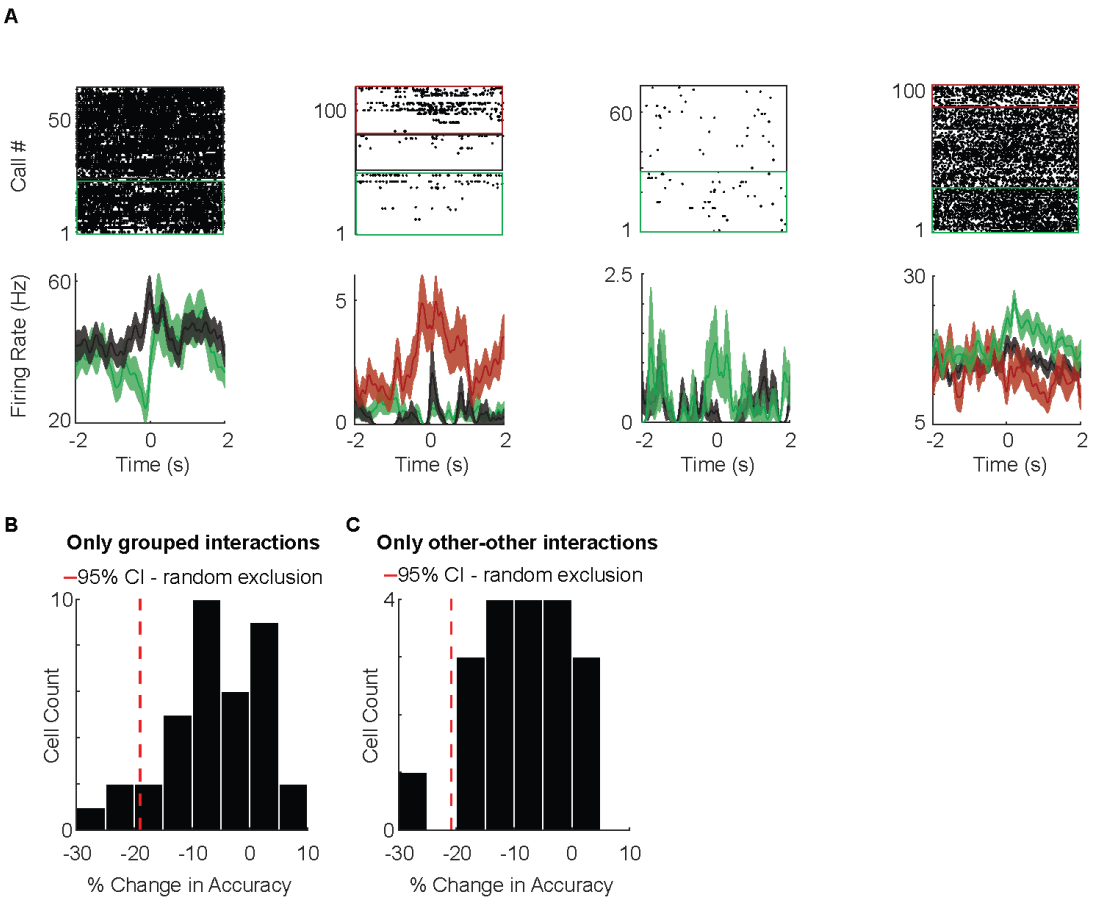

fig. S11. Identity selectivity of single neurons. (A) Example raster and PETHs of identity encoding cells that fire selectively when hearing a vocalization made by a particular bat (indicated by color of PETH and boxes over raster plots). Shaded areas indicate SEM. **(B)** Difference in identity decoding accuracy for identity selective neurons by physical proximity (n = 37 neurons). Plotted is the difference in accuracy when using all vocalizations compared to restricting analysis to interactions that were positively identified as "grouped" (i.e. all bats clearly in physical contact with one another). Also plotted is the average (across neurons) lower bound of the bootstrapped 95% confidence interval of expected decrease in accuracy due to randomly subsampling to the number of calls available for this analysis (red dashed line). **(C)** Difference in identity decoding accuracy for identity selective neurons according to participation in the vocal interaction (n = 19 neurons). Plotted is the difference in accuracy when using all vocalizations compared to restricting analysis to only other-other interactions (i.e. those interactions that did not involve the bat from which that neuron was recorded). Confidence interval also plotted, as in (B).

Supplementary Figure 12

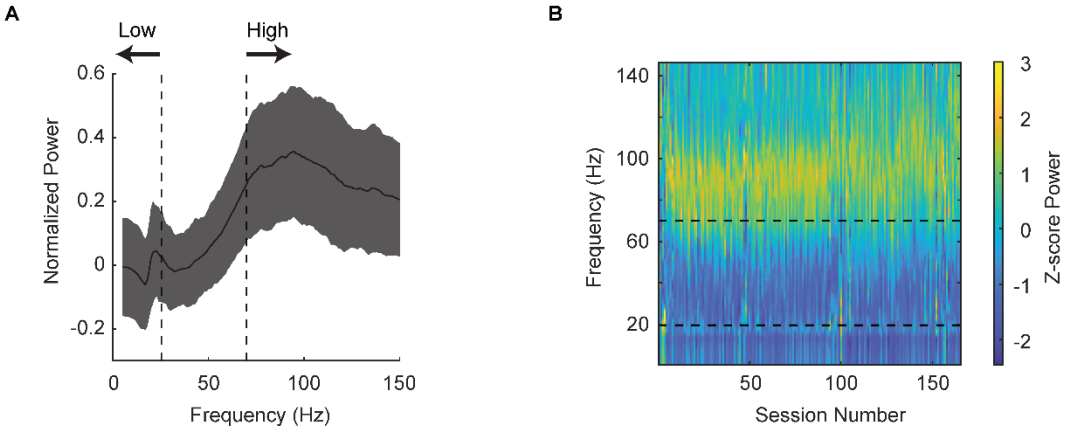

fig. S12. Average LFP response and frequency bands used for analysis. (A) Average LFP power spectrum across trials, channels and sessions in a window of ±250ms around vocalizations. Shaded region indicates ± one standard deviation. Black dashed lines indicate divisions for high and low frequency bands. Note the peaks in the low and high frequency bands. **(B)** LFP power spectra averaged across trials and channels for each session in the window of ±250ms around vocalizations. Black lines indicate division for high and low frequency bands that were used for subsequent analysis.

Supplementary Figure 13

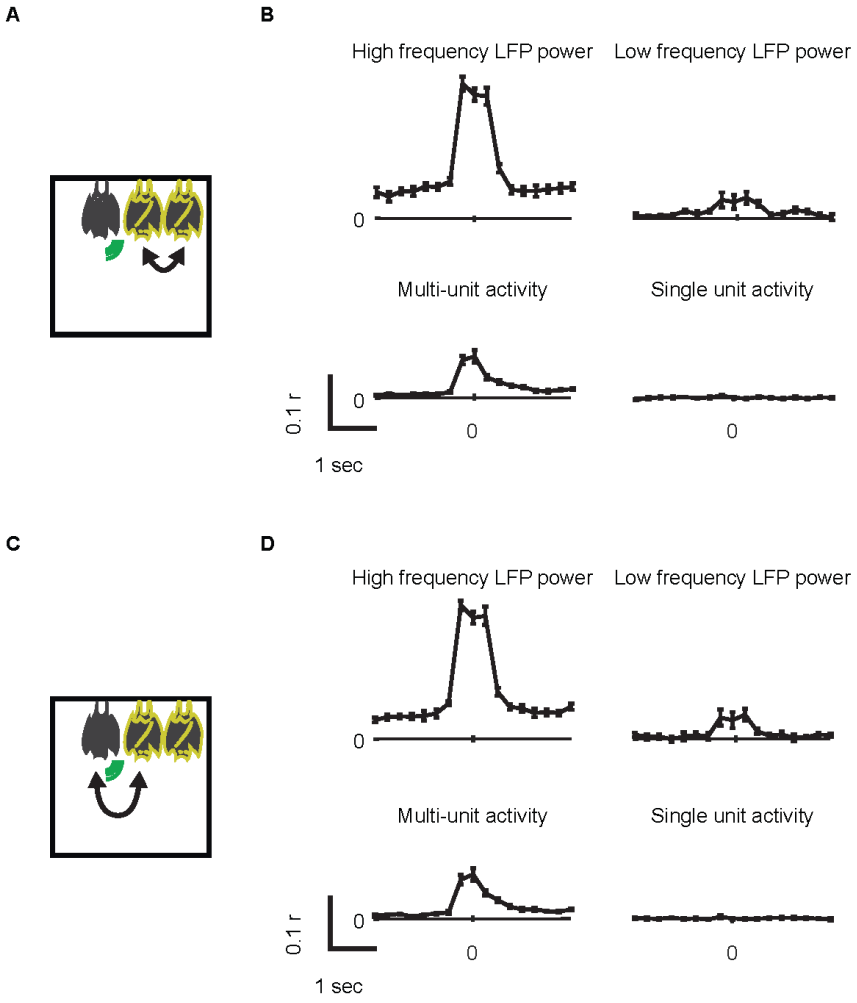

fig. S13. Pairwise interbrain correlation during vocal interactions. (**A**) Schematic of interbrain correlation between a pair of listening bats. (**B**) Call aligned interbrain Pearson correlation averaged across all vocalizations and bat pairs using high frequency (70-150Hz) LFP power, low frequency (5-20 Hz) LFP power, multi-unit firing rates, and single unit firing rates. Error bars represent SEM. (**C**-**D**) As in (A-B), for pairs of calling and listening bats. Scale bar indicated time (horizontal) and correlation value (vertical).

Supplementary Figure 14 - Page 1

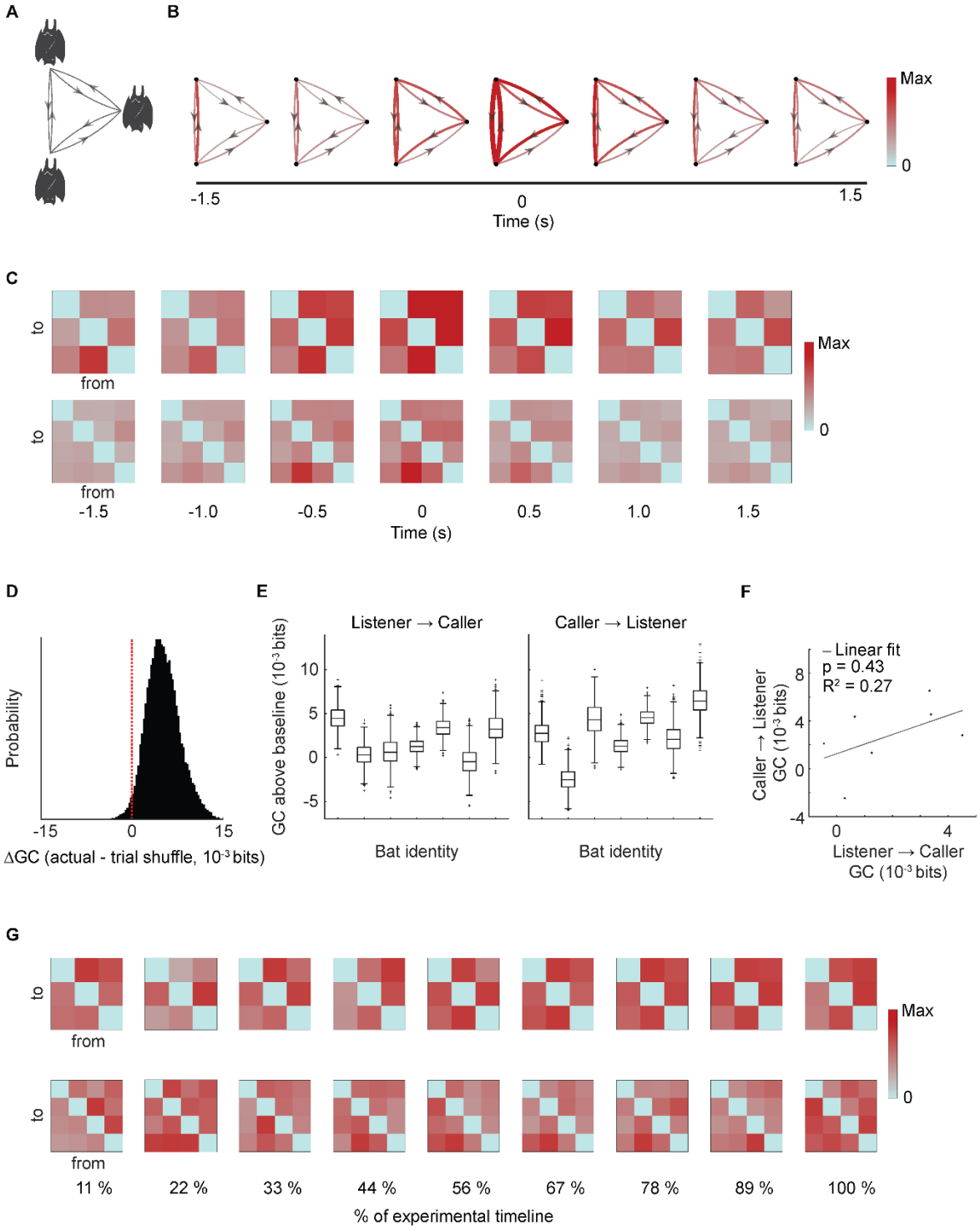

fig. S14. Group-wise interbrain connectivity networks during vocal interactions. (A) Network schematic illustrating all possible connections in a group of three bats. Nodes indicate bats, edges indicate connection weights, arrows indicate directionality. **(B)** Group interbrain Granger causal graphs using all vocalizations, calculated using a sliding window of 1s duration around call onset. GC magnitude are represented by both color and line width. **(C)** As in (B), for a group of three (top) and a group of four (bottom) bats, presented as connectivity matrices instead of graphs. **(D)** Distribution of difference in GC magnitude between actual data and trial-shuffled data, dashed red line indicates zero difference. Actual data has significantly higher GC values (permutation test, $p = 0.02$) indicating a specificity in activity to interactions, as opposed to generic co-activation. **(E)** Bootstrapped distributions of GC values for both listener to caller (left) and caller to listener (right) directions for each bat individually, normalized to pre-call GC values. Box plot display showing median, interquartile range and 1.5 STD. **(F)** Each dot represents GC values for a single bat, plotted as listener to caller vs. caller to listener and fit to a line. The p-value and R2 values for that fit are shown. **(G)** Group interbrain GC values presented as connectivity matrices for the group of three (top) and the group of four (bottom) bats, calculated in bins containing an equal distribution of all vocalizations across the duration of all experimental days.

Supplementary Figure 15

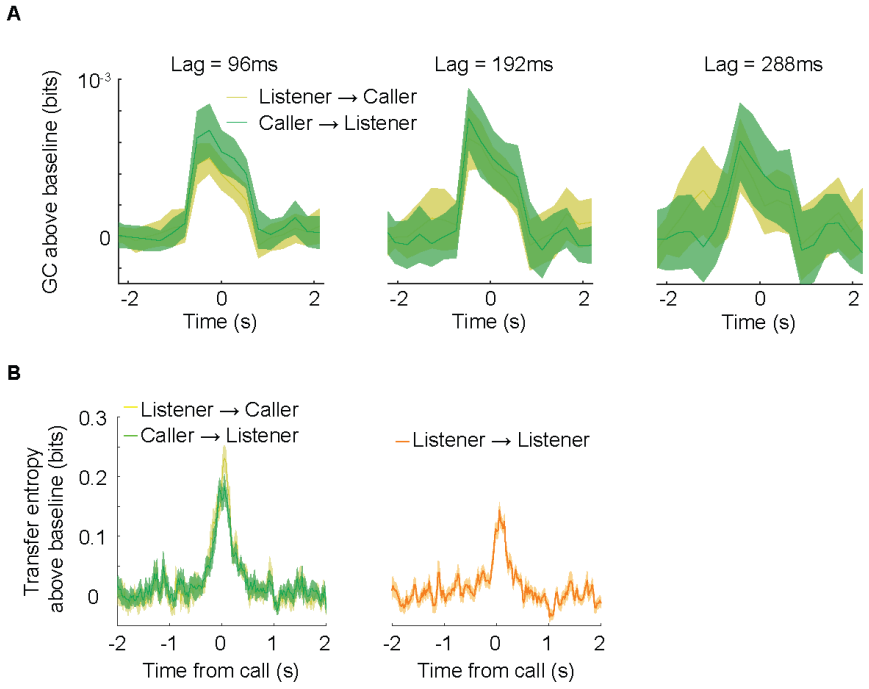

fig. S15. Interbrain connectivity patterns are robust across methodological choices. (A) Baseline-subtracted GC values aligned to call onset, calculated separately for vocalizations from each bat and averaged across bats. From left to right, GC calculated with different model order or lag. Shaded areas indicate SEM. **(B)** Baseline-subtracted transfer-entropy values aligned to call onset, calculated separately for vocalizations from each bat and averaged across bats pairs. Shaded areas indicate SEM.

Supplementary Figure 16 - Page 1

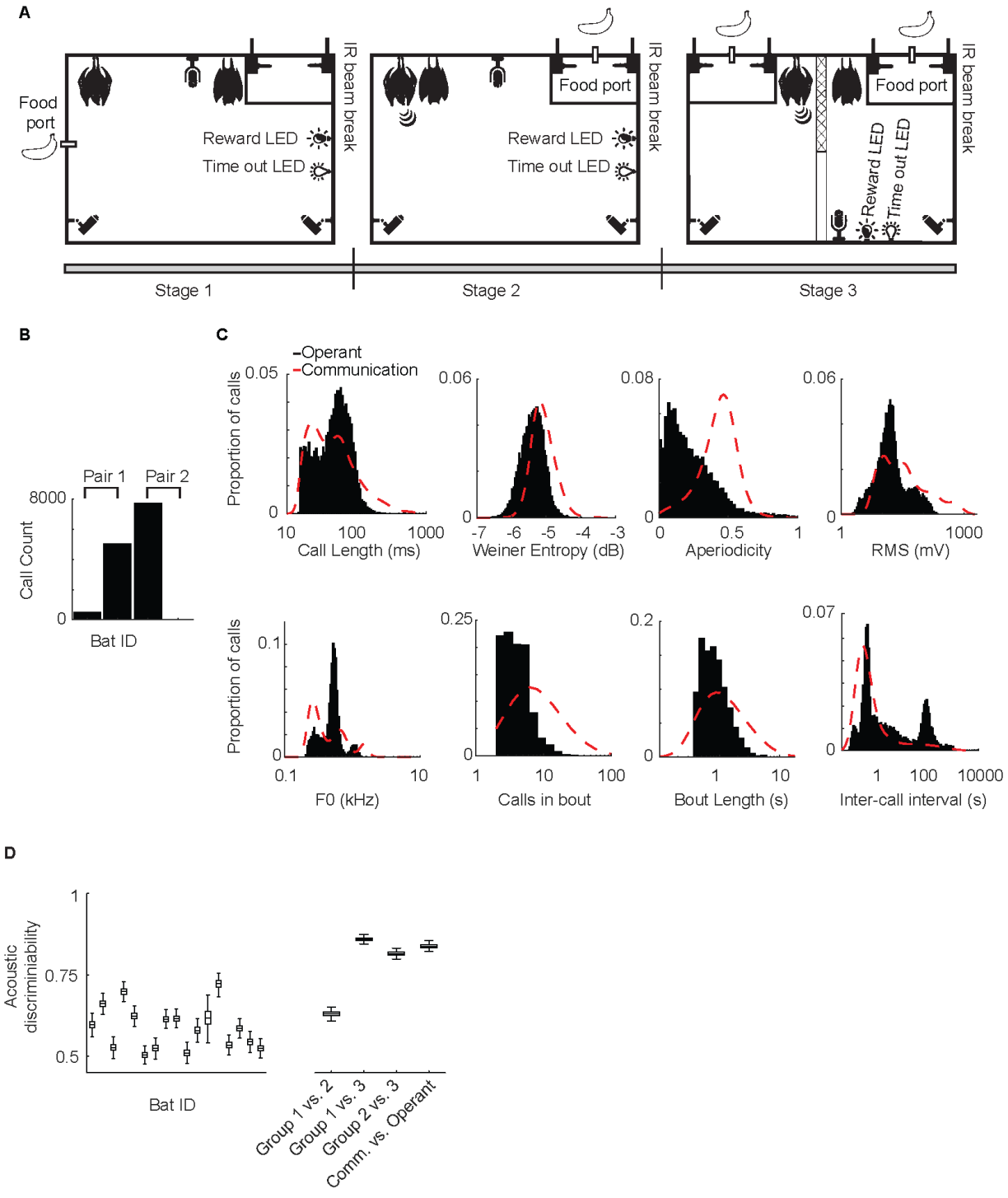

fig. S16. Operant task design and distribution of bio-acoustic features of operant vocalizations. (**A**) Schematic of training procedure for the operant conditioning task. In the first stage (left) two bats are initially placed in the chamber together and learn to associate breaking an IR beam and a reward LED with food reward. A timeout LED is also present to indicate a failure to retrieve reward in the allotted time. In the second stage (middle), bats learn to associate vocalization with food reward by spontaneously vocally interacting with each other. In the third stage (right) a divider is placed between the two bats and they learn to vocalize for food reward in this context that would normally preclude vocalizations. (**B**) Number of calls produced by each bat across all operant sessions. In each pair, one bat becomes the clear caller and the other the listener. (**C**) Distribution of various bio-acoustic measures averaged within calls during the operant session (black). Outline of the distributions for the same measures during the free communication session (shown in fig. S2) are overlaid (red). (**D**) Left, comparison of cross-validated linear discriminant analysis classification accuracy based on acoustic features of calls across different groups. While the calls made in the operant session can be distinguished from the free communication session with a mean accuracy of (84%), it is also true that calls from different groups can be distinguished with similar if not greater accuracy (e.g. average discriminability between group 1 and 3 is 86%). Right, Classification accuracy between calls made by a single bat and calls made by other bats in the same group (n = 17 bats that made at least 1,000 total calls). Discriminability accuracies range from 50-71%.

Supplementary Figure 17

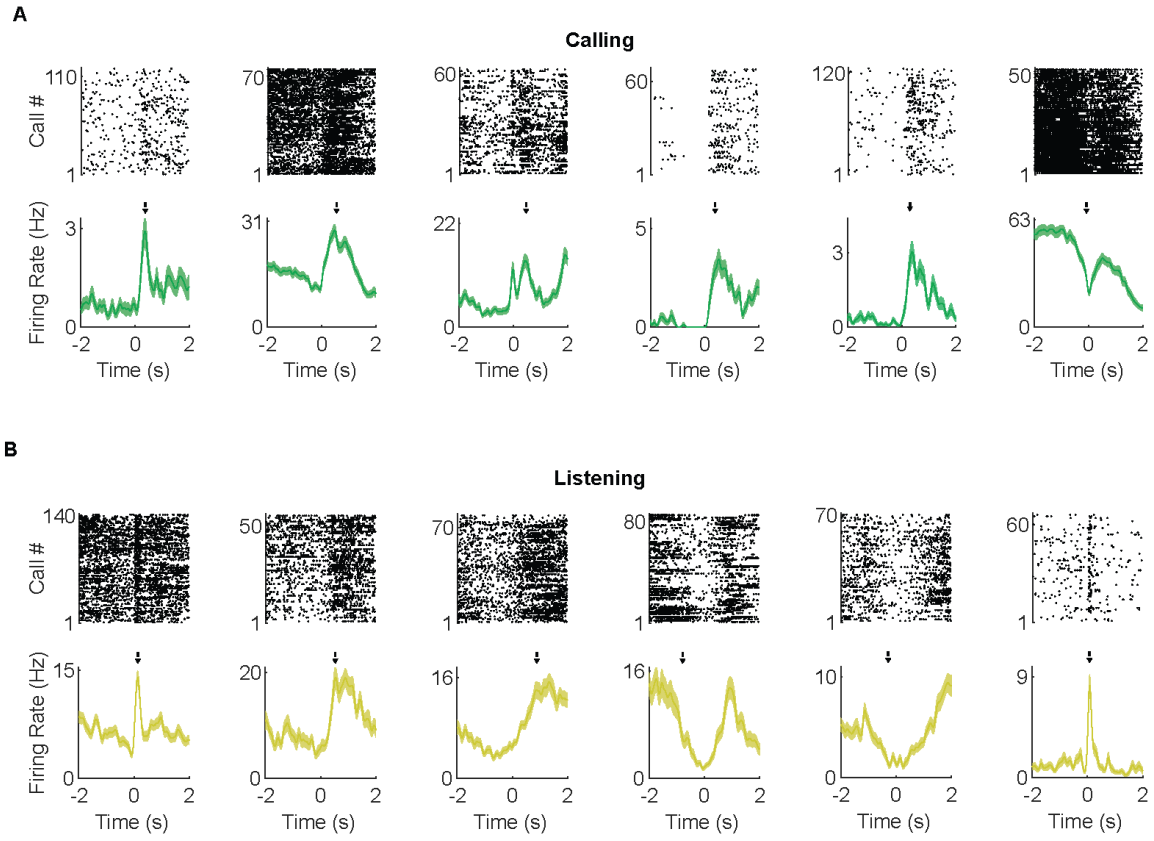

fig. S17. Example single unit firing rate modulation during operant vocalizations. (**A**) Example raster and PETHs of self responsive cells during the operant session. Shaded areas indicate SEM. (**B**) Example raster and PETHs of other responsive cells during the operant session. Note the presence of modulation of firing rates 1-2s after vocalization for some of the neurons, approximately at the time of reward delivery.

Supplementary Figure 18 - Page 1

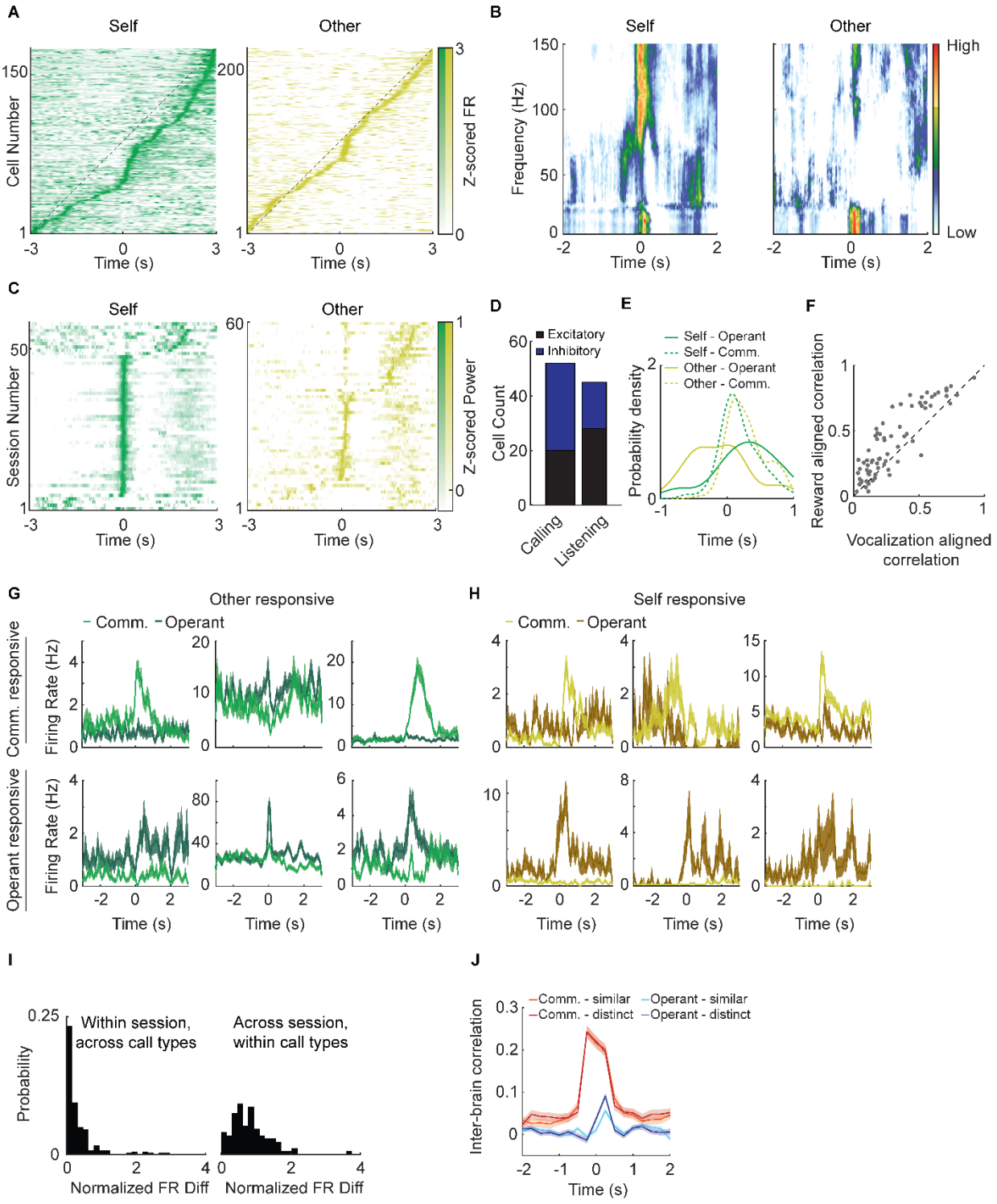

fig. S18. Restructuring of neural activity during operant vocalizations. (A) Max-normalized average firing rates of all cells during self (left) and other (right) vocalizations, sorted by time of max firing rate. Black dashed line indicates expected distribution of max firing rate times given a uniform distribution across cells. Note the time range extends to ± 3s to include the time of reward delivery approximately 2s after vocalization. **(B)** Example average frequency normalized LFP spectrograms for self and other vocalizations from one bat during one session. Note the lack of high frequency activity around vocalization during listening. **(C)** Power in high frequency LFP (70-150Hz) for all operant sessions, displayed as in (A). **(D)** Proportion of excitatory and inhibitory responsive cells in the operant session. **(E)** Distribution of response latency for self (green) and other (yellow) responsive cells during free communication (dashed) and operant (solid) session. Note the wider spread of response latencies during the operant session compared to the free communication session. **(F)** Within session firing rate correlation when activity is aligned to either reward or vocalization during the operant session. Correlation is significantly higher when aligned to reward ($p < 0.01$, Wilcoxon rank sum test). **(G)** Example PETHs of other responsive cells during calls in the operant and free communication sessions. Top row, cells responsive only in the free communication session, bottom row, operant session responsive. Shaded areas indicate SEM. **(H)** As in panel G, showing self responsive cells. **(I)** Absolute normalized single neuron firing rate differences during calls across call types ("similar" and "distinct") and sessions (free communication and operant). Left, firing rate differences within sessions between calls that are acoustically overlapping ("similar") across sessions and calls that are acoustically non-overlapping ("distinct") across sessions. Right, firing rate differences across sessions only during calls classified as similar. Differences are displayed for all self- and other-responsive cells for both free communication and operant sessions. **(J)** Average inter-brain correlation between calling and listening bat pairs during the free communication session and the operant session. Calls are classified as "similar" and "distinct" calls, as in panel I, and averaged within sessions. Note that inter-brain correlation instead of Granger causality is shown here in order to assess the effect of acoustic differences on a call-by-call basis.

Supplementary Figure 19

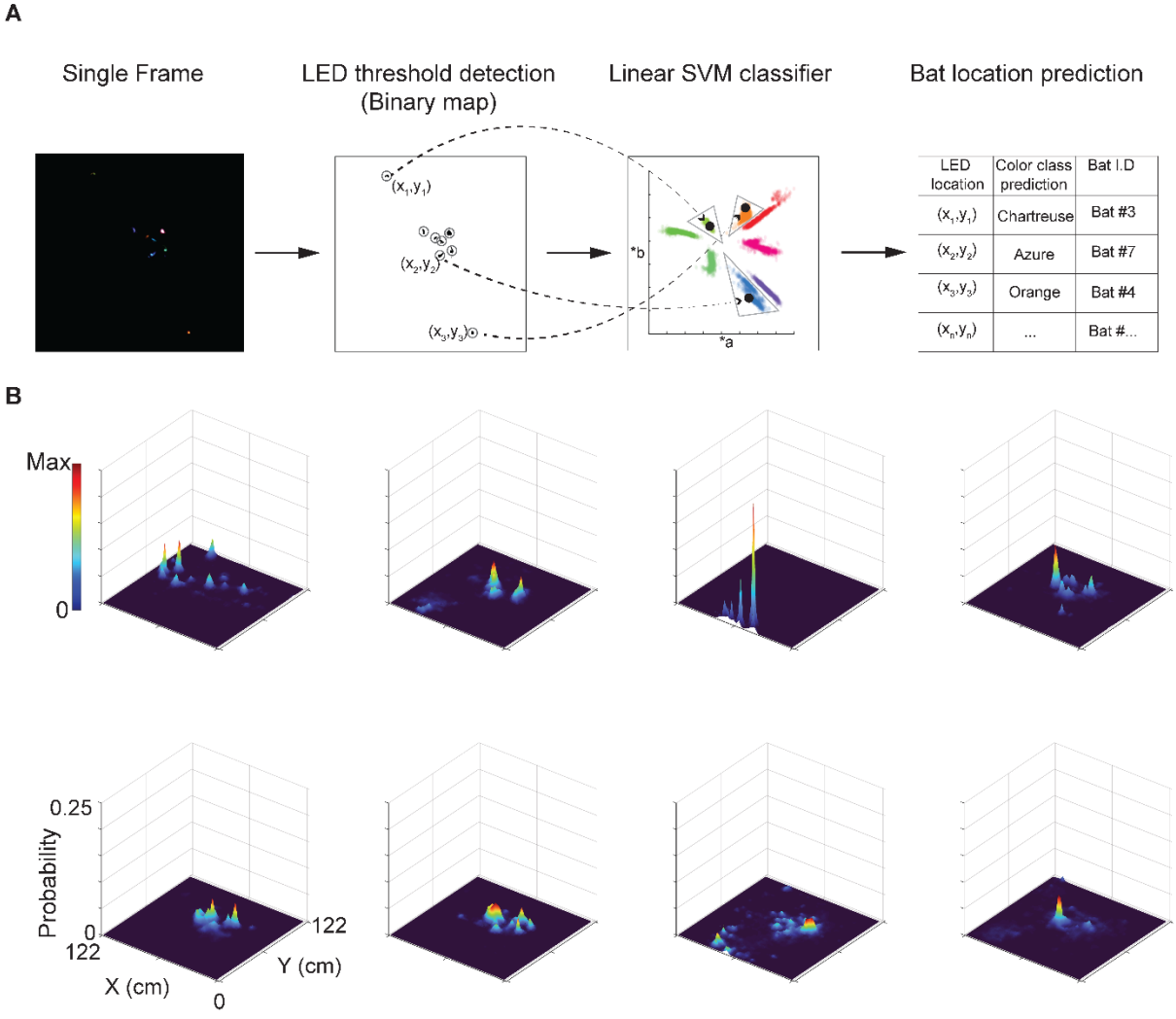

fig S19 Schematic of pipeline used for the prediction of bat locations and example posi tion distributions. (A) From left to right: An example of a single frame taken during the social-space session showing LED lights of different colors onboard the call-detection devices worn by each bat. Next, a binary map of the frame is produced by using a threshold for luminance. Bats' locations are collected after filtering for size and shape of LED area (Methods). Next, the median color for each detected area is projected in L*a*b color space (see arrows leading to black dots, only 3 locations are shown for clarity). A previously trained classifier is used to assign a color prediction according to previously annotated data. Color clusters shown are the labeled examples used to train the model (gray triangles show potential class boundaries for the 3 color classes). Next, the location of each LED area is matched to the bats' identity according to its known assigned color. **(B)** Example position distributions for a single session for each bat individually. Height (normalized across all bats) and color (separately scaled within each bat) correspond to more time spent in a given location. Distribution plots here correspond to data shown in Fig. 5B.

Supplementary Figure 20 - Page 1

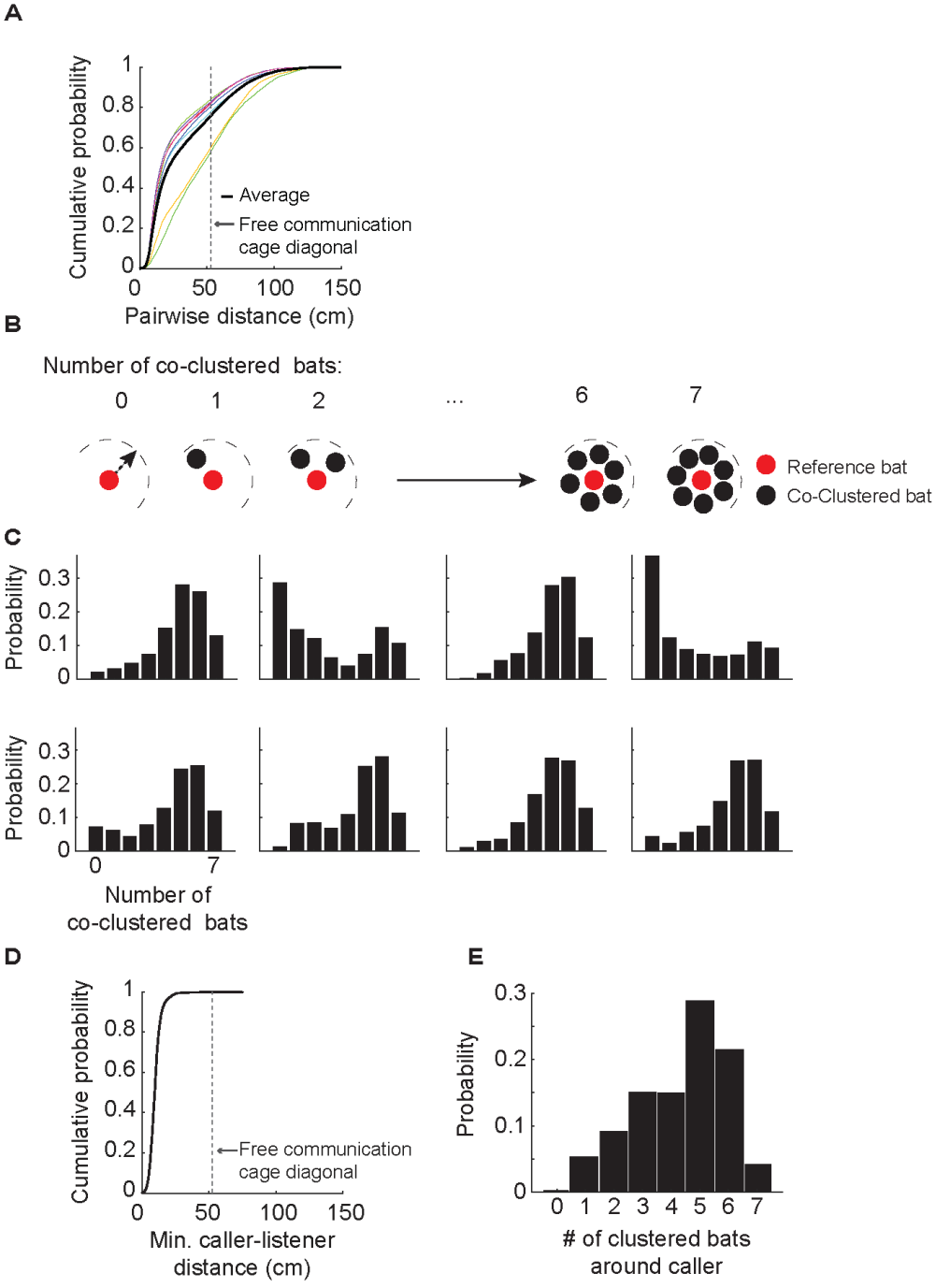

fig S20: Clustering behavior of bats in the social space session. (**A**) Cumulative probability of pairwise distances across all sessions for each pair of bats (colors indicate different bat pairs, black line shows the average across all pairs). Dotted line indicates the diagonal length of the free communication cage top. (**B**) A schematic illustration showing the different cluster states each bat can display for each time point, according to how many bats are less than the distance threshold (35.8cm) away. (**C**) Probability distribution for each bat of the number of bats that were "co-clustered" (less than the distance threshold away) calculated across all social space sessions. For each panel, a different bat was used as the reference bat. Zero indicates no bats were within the distance threshold of the reference bat. 7 indicates all bats in the group were within the distance threshold of the reference bat. (**D**) Cumulative probability distribution of the distances between the caller and the nearest bat during vocalizations in the social-space session (averaged distances over 2 seconds around the call time). (**E**) Probability distribution of the number of co-clustered bats using the caller as the reference bat.

Supplementary Figure 21

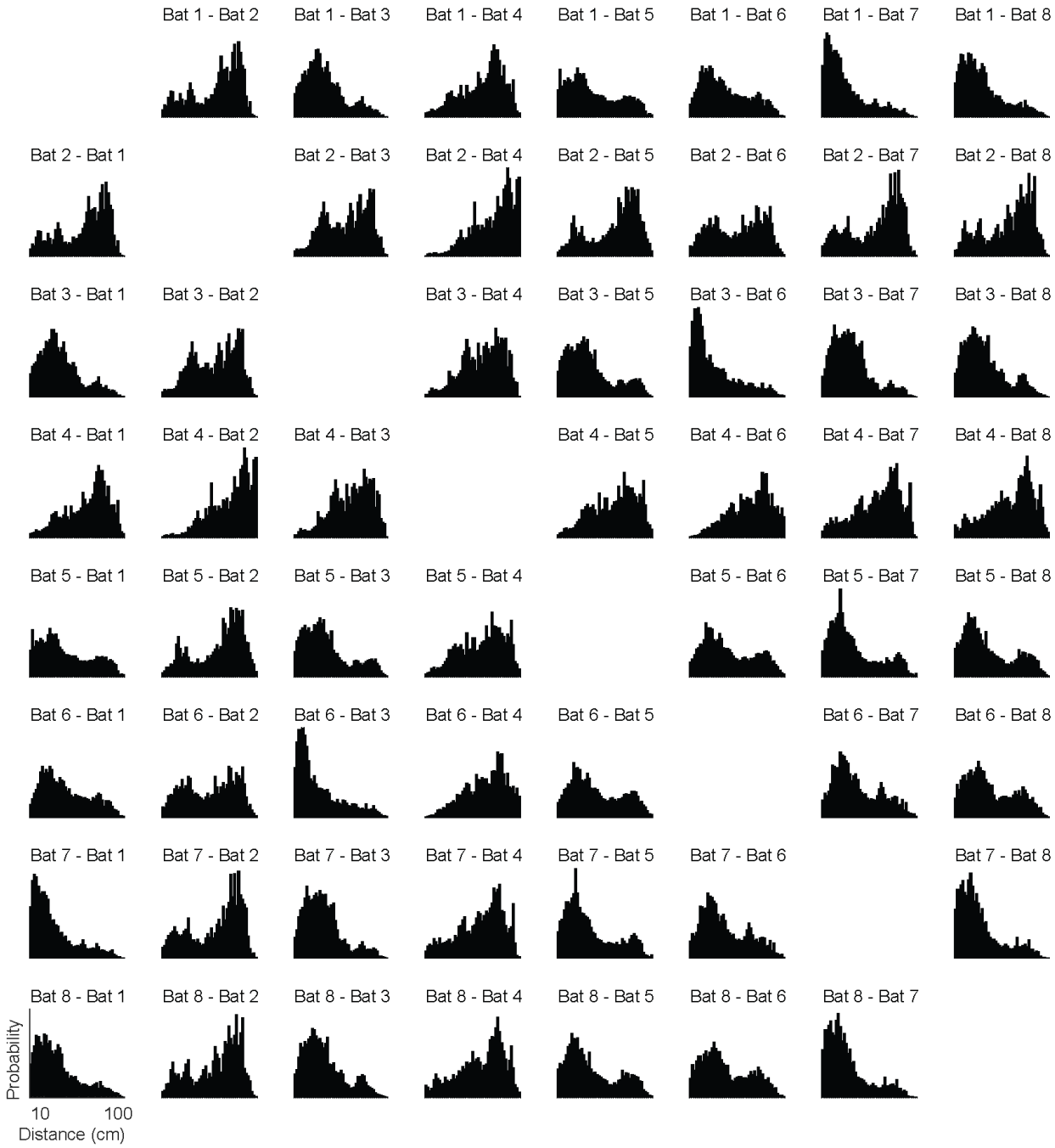

fig. S21: Pairwise distance distributions across all bats. Histograms of all measured instantaneous distances between each bat pair across all sessions displayed on a logarithmic scale. All plots share the same X and Y axes, labeled in the bottom left corner.

Supplementary Figure 22

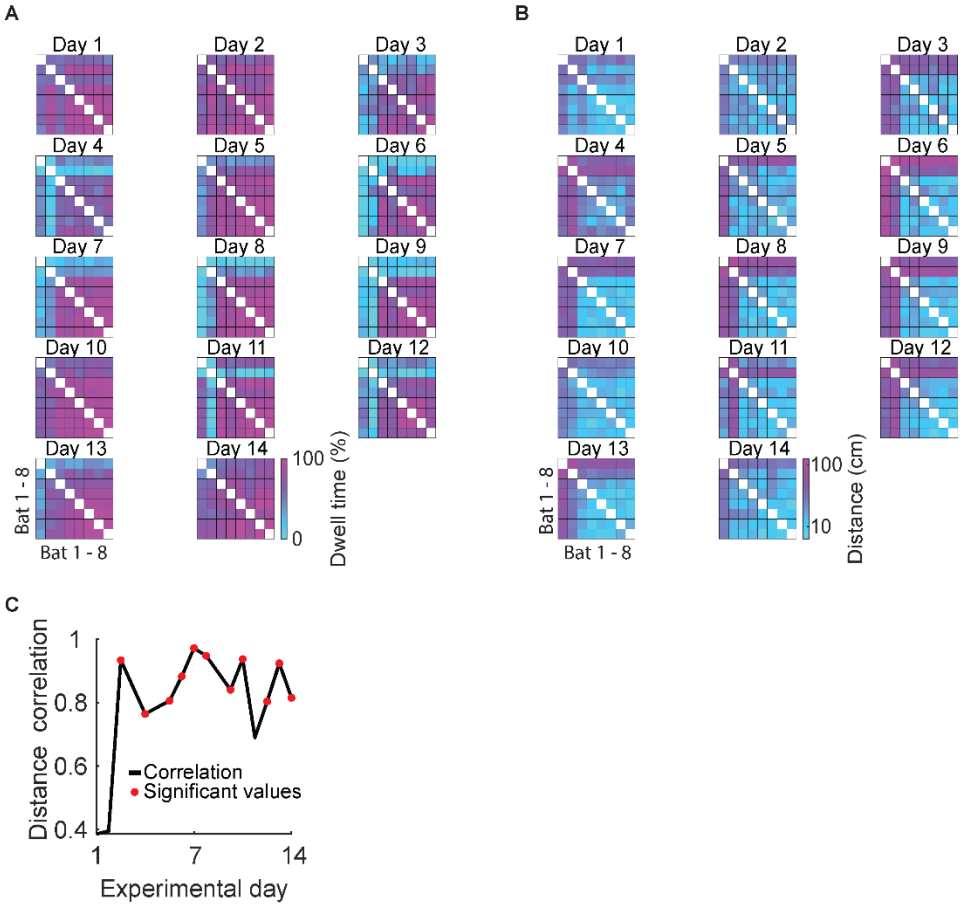

fig. S22: Inter-bat dwell time and distance stability over days. (A) Dwell time matrices showing the pair dwell time percentage between each pair of bats during each day's social space session. **(B)** Pairwise distance matrices as in A. Note that distances are displayed on a log scale. **(C)** Correlation between average distances for all bat pairs on a given day and the average pairwise distance across all other days. Statistically significant correlation values are indicated with red dots ($p < 0.05$; Mantel test).

Supplementary Figure 23

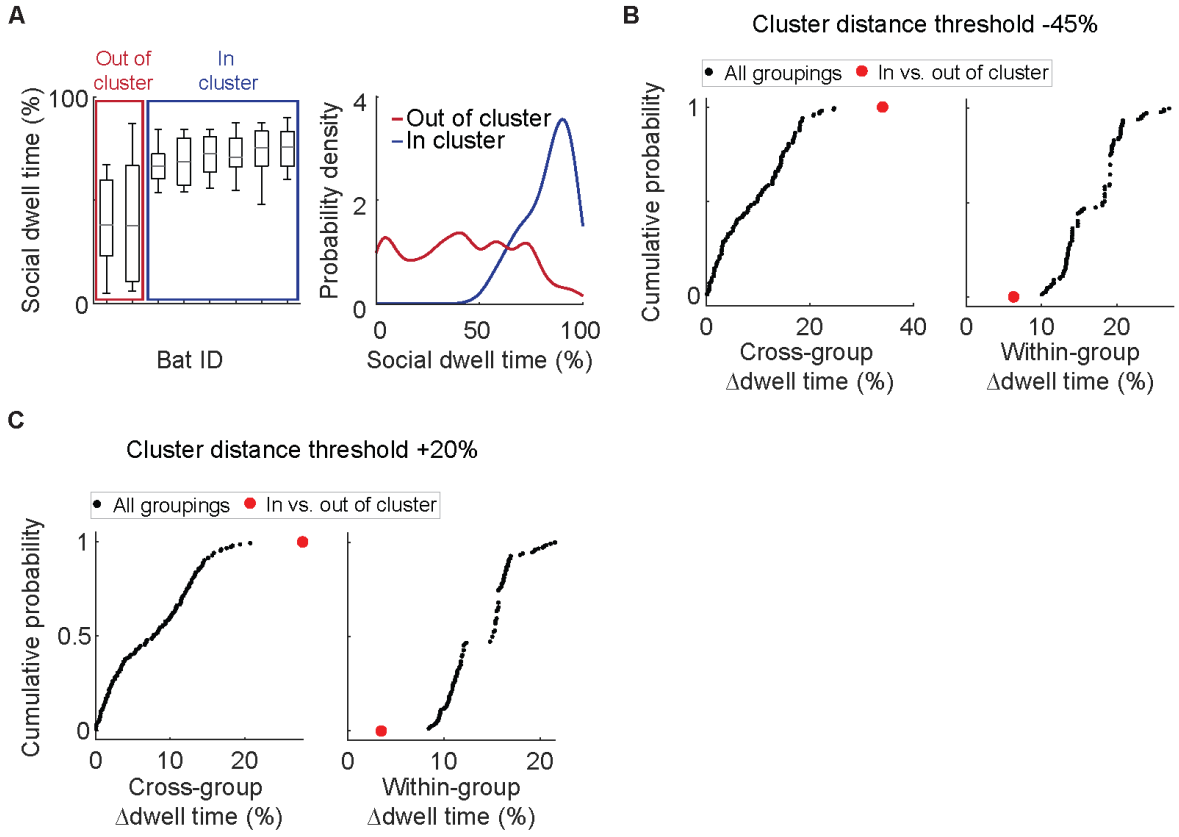

fig. S23: Two different patterns of individual spatial preferences. (A) Left, boxplot showing the distribution of each bat's social dwell time (fraction of session spent in proximity to other bats) across all social space sessions averaged over all pairs. In- and out-of-cluster bat groups defined by individual average dwell times are highlighted. Right, Probability density estimates of dwell times for all "in-cluster" bats and all "out-of-cluster" bats, estimated using dwell times across all sessions. **(B)** Cumulative probability distribution of the difference in mean dwell times across (left) and within (right) groupings for all possible subgroupings of bats into two groups using a cluster distance threshold 45% less than originally defined. Note that the in- and out-of-cluster subgroups still maximize and minimize these values, respectively, and still consist of the same bats using this decreased threshold. **(C)** As in panel B, using a cluster distance threshold 20% greater than originally defined.

Supplementary Figure 24

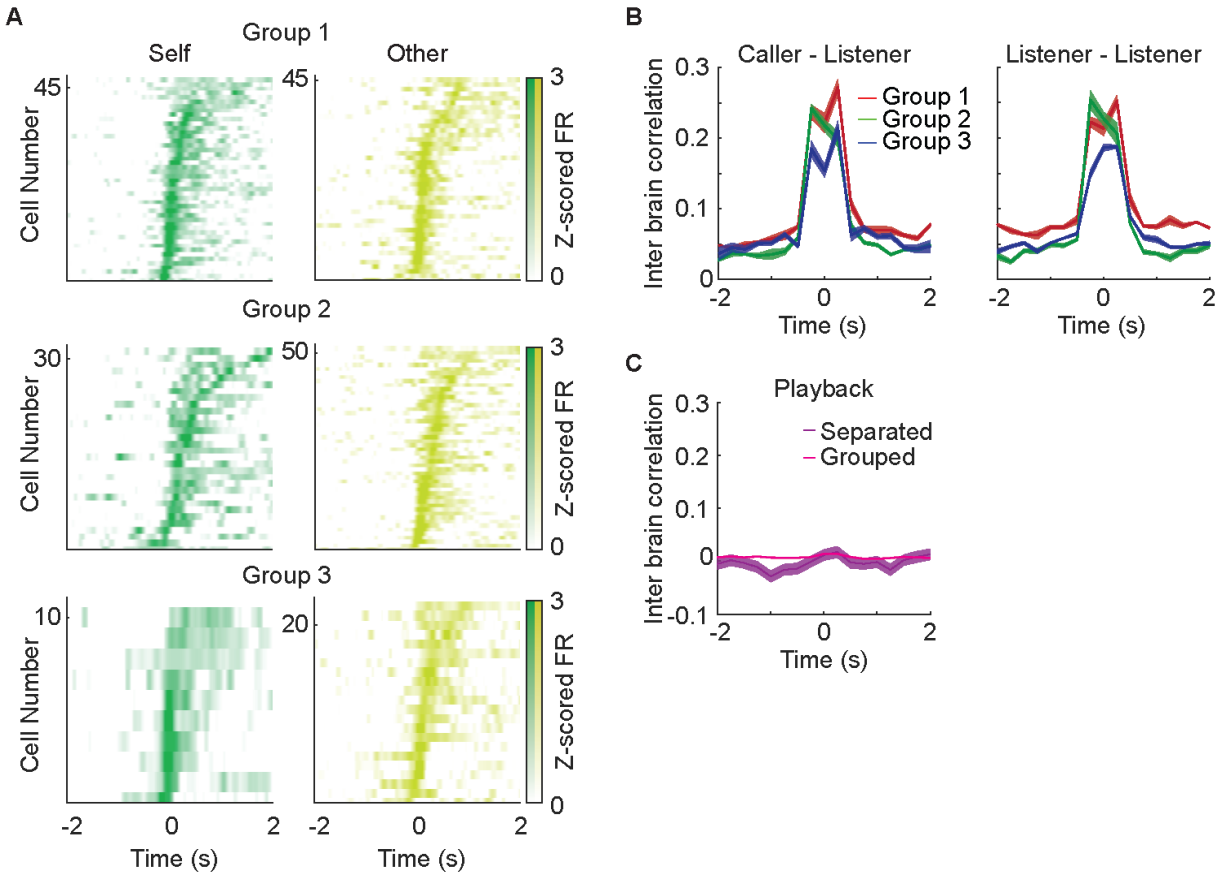

fig. S24: Neural results replicate over groups of different sizes. (A) normalized call-aligned firing rates for all self and other responsive cells for each of the three groups of bats. **(B)** Average IBC between all bat pairs around calls for all groups between caller-listener pairs (left) and listener-listener (right) vocalizations. Shaded areas indicated SEM across bats within a group. **(C)** Average IBC between all bat pairs around playback of vocalizations to separated bat pairs in different enclosures and to a group of bats in the same enclosure. Shaded areas indicated SEM across playback repetitions.

Supplementary Figure 25

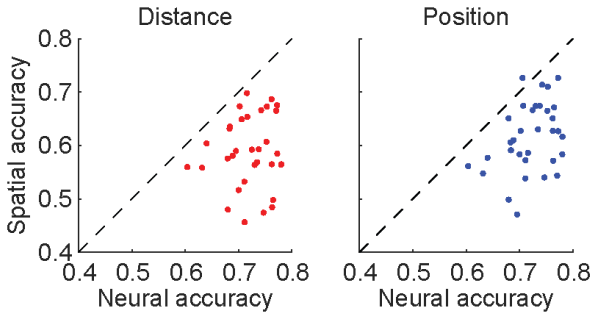

fig. S25: Neural identity decoding cannot be accounted for by position. Identity decoding accuracy using the firing rates of selective neurons during calls plotted against accuracy obtained using inter-bat distance between the self-bat and target-bat (left) and absolute spatial position of the target-bat (right) around calls. Dashed line represents unity line. Only 4 and 11 out of 31 ID selective neurons were recorded in sessions when identity could be significantly decoded by using distance and absolute spatial position, respectively.

Supplementary Figure 26

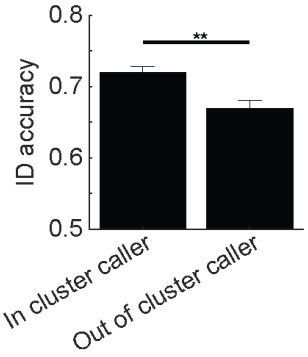

fig. S26: Controlling for implanted bat when comparing identity selectivity according to clustering behavior of caller. Average identity decoding accuracy of single neurons when representing in-cluster vs. out-of-cluster bats after accounting for variability due to the identity of the bat from which the neuron was recorded (n = 68 neuron - bat pairs; p = 0.006, likelihood-ratio test). Bars indicate mean and error bars indicate SEM.

Supplementary Figure 27

fig. S27: Robust difference in interbrain correlation according to clustering behavior of caller. **(A)** Average inter-brain correlation arising only from pairs of bats that were both listening during vocalizations produced by in-cluster vs. out-of-cluster bats ($p = 4.0 \times 10^{-7}$; likelihood-ratio test, controlling for bat pair and date of recording; n = 5,210 calls and bat pairs). **(B)** Inter-brain correlation arising only from pairs of bats that included one in-cluster bat and one out-of-cluster bat ($p = 1.6 \times 10^{-8}$; n = 2,998). **(C)** Inter-brain correlation arising only from pairs of bats composed only of in-cluster bats ($p = 4.3 \times 10^{-4}$; n = 2,760). **(D)** Inter-brain correlation after accounting for variability due to average distance between bat pairs during the FC session ($p = 1.7 \times 10^{-4}$; likelihood-ratio test, controlling for bat pair, date of recording and FC distance; n = 5,758).

Supplementary Table 1

Bat ID	Bat 1	Bat 2	Bat 3	Bat 4	Bat 5	Bat 6	Bat 7
Call Length (ms)	43.4	69.1	60.8	91.3	55.1	70.7	93.7
Call Length STD	46.3	95	58.3	90.9	81.2	76	162
F0 (Hz)	507	402	575	513	473	642	528
F0 STD	455	497	387	342	576	428	449
Wiener Entropy (dB)	-5	-5.25	-5.03	-5.17	-5.2	-5.03	-5.19
Wiener Entropy STD	0.32	0.29	0.33	0.3	1	0.29	0.3
Aperiodicity	0.45	0.43	0.42	0.44	0.29	0.41	0.45
Aperiodicity STD	0.12	0.1	0.14	0.11	0.48	0.14	0.13
RMS	0.03	0.11	0.05	0.24	0.12	0.05	0.21
RMS STD	0.05	0.18	0.06	0.23	0.11	0.06	0.29
Inter-bat Inter-call Interval (s)	116	157	339	133	0.17	190	323
Inter-bat Inter-call Interval STD	402	289	600	257	89.6	507	567
Calls in Bout	9.3	11	12.5	5.8	187 8	15.8	8.1
Calls in Bout STD	8.6	10.9	11.7	6.4	5.6	13.8	5.9
Bout Length (s)	1.4	1.6	1.8	1.4	1.1	2.2	1.3
Bout Length STD	1.2	1.5	1.5	1.4	0.9	1.9	1.3

Table S1. **Acoustic feature values by bat.** Acoustic variability of vocalizations across bats with the mean and standard deviation of each of the features plotted in fig. S2A-H reported for each implanted bat individually.

Supplementary Table 2

	Number of bats used	Usable single neurons	Responsive neurons	Notes
Total	7	1153	N/A	
Self (FC)	7	376	78	
Other (FC)	7	822	96	
Self and other (FC)	7	364	16	16/74 and 16/39 self and other responsive neurons exhibit mixed selectivity
Self vs. other selective (FC)	7	397	104	Responsive neurons determined by decoding analysis
Echolocation	3	201	12	
Self (FC) and Echolocation	3	68	0	15 self responsive neurons in this population
Playback (isolated)	3	257	0	
Other (FC) and playback	3	257	0	
Self (operant)	4	162	44	
Self (FC and Operant)	4	48	3	21 total self responsive cells in this population (3/21 functionally stable)
Other (operant)	4	211	52	
Other (FC and operant)	4	114	11	43 total other responsive cells in this population (11/43 functionally stable)
Playback (group)	4	265	1	

Table S2. Neuronal subpopulations for various analyses. Numbers of usable and responsive neurons recorded from all bats in groups 1 and 2 across conditions (self and other vocalizations) and experiments ('FC' = 'Free communication session', 'Operant' = 'Operant session'). Usable refers to the pool of neurons that met the criteria to perform a given analysis. Responsive refers to neurons that modulate their firing rates around calls (see Methods "Vocalization responsive neurons") except for "Self vs. other selective" where responsive neurons were found using a decoding analysis similar to identity selectivity (see Methods "Self vs. other selectivity"). Rows with multiple conditions (self and other) represent the number neurons that were usable under both of those conditions and the number of neurons that were jointly responsive (i.e. responsive under both conditions). Rows with multiple experiments (FC and Operant) represent the number of neurons that were stably recorded across both sessions, allowing us to evaluate the functional stability of responsive neurons (i.e. neurons that were similarly responsive across both sessions).

Supplementary Table 3

Group	**1**	**2**	**3**
Implanted bats	3	4	4
Group size	4	5	8
Sessions performed	FC, playback, echolocation	FC, operant	FC, group playback, social space
Other responsive	45 (436)	51 (361)	22 (229)
Self responsive	47 (194)	31 (164)	10 (32)
ID selective	36 (337)	26 (332)	31 (229)
ID selective (group playback)	N/A	N/A	0 (31)
Other responsive (group playback)	N/A	N/A	0 (22)

Table S3. Neuronal subpopulations for each experimental group. Numbers of bats included in each group, experimental session performed using each group, and numbers of responsive (number of usable neurons for each analysis indicated in parentheses) neurons recorded from all bats in each group. Other and self responsive and identity selective neurons were all recorded in the FC session. ID selective (playback) refers to identity selective cells for which pre-recorded calls from the specific bat which that neuron was selective for were played back in the group playback session. Note that not a single identity selective neuron was selective for the same bat when that bat's vocalizations were played back.

Supplementary Table 4

Bat ID	Other (FC)	Self (FC)	Identity	Other (Operant)	Self (Operant)	Group
1	31 (225)	19 (75)	26 (181)	N/A	N/A	1
2	7 (147)	25 (95)	8 (109)	N/A	N/A	1
3	7 (64)	3 (24)	2 (47)	N/A	N/A	1
4	10 (121)	11 (66)	6 (109)	31 (60)	0 (0)	2
5	13 (100)	7 (57)	9 (91)	0 (0)	36 (142)	2
6	2 (43)	2 (10)	2 (39)	0 (0)	8 (20)	2
7	26 (97)	11 (31)	9 (93)	21 (151)	0 (0)	2
8	9 (52)	0 (6)	5 (52)	N/A	N/A	3
9	2 (79)	10 (26)	12 (73)	N/A	N/A	3
10	11 (80)	0 (0)	12 (71)	N/A	N/A	3
11	0 (34)	0 (0)	2 (33)	N/A	N/A	3

Table S4. Neuronal subpopulations for each bat. Numbers of usable and responsive neurons recorded from each bat in each group across conditions (self and other vocalizations) and experiments ('FC' = 'Free communication session', 'Operant' = 'Operant session') and for identity selectivity. Group membership is also indicated.

Chapter 7: References

Chapters 1, 3, and 4

1. American Psychiatric Association, *Diagnostic and Statistical Manual of Mental Disorders* (American Psychiatric Association, 2013).
2. C. Segrin, *Clinical Psychology Review*. **20**, 379–403 (2000).
3. M. F. Green, *American Journal of Psychiatry*. **153**, 321–330 (1996).
4. J. Uekermann *et al.*, *Neuroscience & Biobehavioral Reviews*. **34**, 734–743 (2010).
5. C. Keysers, V. Gazzola, in *Social Behavior from Rodents to Humans: Neural Foundations and Clinical Implications*, S. Wöhr Markus and Krach, Ed. (Springer International Publishing, Cham, 2016; http://link.springer.com/10.1007/7854_2016_439), pp. 179–191.
6. E. J. Nestler, S. E. Hyman, *Nature Neuroscience*. **13**, 1161–1169 (2010).
7. J. L. Silverman, M. Yang, C. Lord, J. N. Crawley, *Nature Reviews Neuroscience*. **11**, 490–502 (2010).
8. J. N. Crawley, *Brain Pathology*. **17**, 448–459 (2007).
9. K. Kondrakiewicz, M. Kostecki, W. Szadzińska, E. Knapska, *Genes, Brain and Behavior*. **18**, e12525 (2019).
10. A. L. Juavinett, J. C. Erlich, A. K. Churchland, *Current Opinion in Neurobiology*. **49**, 42–50 (2018).
11. Y. Shemesh *et al.*, *eLife*. **2** (2013), doi:10.7554/eLife.00759.
12. G. Hoyle, *Behavioral and Brain Sciences*. **7**, 367–381 (1984).
13. A. Krogh, *American Journal of Physiology-Legacy Content*. **90**, 243–251 (1929).
14. A. J. Doupe, M. Konishi, *Proceedings of the National Academy of Sciences of the United States of America*. **88**, 11339–11343 (1991).
15. R. H. R. Hahnloser, A. a Kozhevnikov, M. S. Fee, *Nature*. **419**, 65–70 (2002).
16. F. Nottebohm, T. M. Stokes, C. M. Leonard, *Journal of Comparative Neurology*. **165**, 457–486 (1976).
17. F. E. Theunissen, J. E. Elie, *Nature reviews. Neuroscience*. **15**, 355–66 (2014).
18. D. E. Okobi, A. Banerjee, A. M. M. Matheson, S. M. Phelps, M. A. Long, *Science (New York, N.Y.)*. **363**, 983–988 (2019).
19. P. Znamenskiy, A. M. Zador, *Nature*. **497**, 482–5 (2013).

20. T. Hromádka, M. R. Deweese, A. M. Zador, S. Figs, **6**, 4–5 (2008).

21. L. M. Romanski, B. B. Averbeck, *Annual Review of Neuroscience*. **32**, 315–346 (2009).

22. A. J. Doupe, P. K. Kuhl, *Annu. Rev. Neurosci.* **22**, 567–631 (1999).

23. M. S. Brainard, A. J. Doupe, *Annu. Rev. Neurosci*. **36**, 489–517 (2013).

24. C. F. Moss, S. R. Sinha, *Current Opinion in Neurobiology*. **13**, 751–758 (2003).

25. G. Schuller, S. Radtke-Schuller, *Experimental Brain Research*. **79**, 192–206 (1990).

26. W. Metzner, *Journal of Comparative Neurology*. **368**, 252–269 (1996).

27. N. Suga, W. O'Neill, *Science*. **206**, 351–353 (1979).

28. G. G. Kwiecinski, T. A. Griffiths, *Mammalian Species*. **95**, 1–9 (1999).

29. E. Kulzer, *Zeitschrift fur Morphologie und Okologie der Tiere*. **47**, 374–402 (1958).

30. K. R. Moreno *et al.*, *Annals of the New York Academy of Sciences* (2021), doi:10.1111/nyas.14600.

31. L. Harten *et al.*, *Science Advances*. **4**, e1603293 (2018).

32. L. Harten, Y. Prat, S. ben Cohen, R. Dor, Y. Yovel, *Current Biology*. **29**, 1895-1900.e3 (2019).

33. O. Mann *et al.*, *Acta Chiropterologica*. **13**, 411–417 (2011).

34. E. Bachorec *et al.*, *PLOS ONE*. **15**, e0229110 (2020).

35. E. Bachorec *et al.*, *Journal of Zoology*. **312**, 111–121 (2020).

36. Y. Prat, M. Taub, Y. Yovel, *Scientific Reports*. **6**, 39419 (2016).

37. D. Genzel, J. Desai, E. Paras, M. M. Yartsev, *Nature Communications*. **10**, 3372 (2019).

38. Y. Prat, M. Taub, Y. Yovel, *Science Advances*. **1**, e1500019 (2015).

39. H. Herbert, *Zeitschrift für Säugetierkunde*. **48**, 187–189 (1983).

40. Y. Prat, L. Azoulay, R. Dor, Y. Yovel, *PLOS Biology*. **15**, e2002556 (2017).

41. V. M. Janik, P. J. B. Slater, *Vocal Learning in Mammals* (Elsevier Masson SAS, 1997; http://dx.doi.org/10.1016/S0065-3454(08)60377-0), vol. 26.

42. E. Z. Lattenkamp, S. C. Vernes, L. Wiegrebe, *The Journal of Experimental Biology*. **221**, jeb180729 (2018).

43. M. Knörnschild, *Current Opinion in Neurobiology*. **28**, 80–85 (2014).

44. A. S. Stoeger, P. Manger, *Current Opinion in Neurobiology*. **28**, 101–107 (2014).

45. B. McCowan, D. Reiss, *Social influences on vocal development*, 178–207 (1997).

46. J. G. Miller *et al.*, *Neuropsychologia*. **124**, 117–124 (2019).

47. A. Goldshtein, L. Harten, Y. Yovel, *Current Biology* (2021), doi:10.1016/j.cub.2021.11.010.

48. R. Báez-Mendoza, E. P. Mastrobattista, A. J. Wang, Z. M. Williams, *Science*. **374** (2021), doi:10.1126/science.abb4149.

49. W. Zhang, M. M. Yartsev, *Cell*. **178**, 413–428 (2019).

50. P. R. Montague *et al.*, *NeuroImage*. **16**, 1159–1164 (2002).

51. F. Babiloni, L. Astolfi, *Neuroscience and Biobehavioral Reviews*. **44**, 76–93 (2014).

52. D. Liu *et al.*, *Frontiers in Psychology*. **9**, 1–11 (2018).

53. S. Dikker *et al.*, *Current Biology*. **27**, 1375–1380 (2017).

54. J. Yang, H. Zhang, J. Ni, C. K. W. de Dreu, Y. Ma, *Nature Neuroscience*. **23**, 754–760 (2020).

55. P.-H. Tseng, S. Rajangam, G. Lehew, M. A. Lebedev, M. A. L. Nicolelis, *Scientific Reports*. **8**, 4699 (2018).

56. L. Kingsbury *et al.*, *Cell*. **178**, 429-446.e16 (2019).

57. Y. Mu, C. Guo, S. Han, *Social Cognitive and Affective Neuroscience*. **11**, 1882–1893 (2016).

58. Q. Wang *et al.*, *Brain Topography*. **33**, 112–122 (2020).

59. J. A. Kruppa *et al.*, *Social Cognitive and Affective Neuroscience*. **16**, 103–116 (2021).

Chapter 2

1. R. M. Seyfarth, D. L. Cheney, P. Marler, *Anim. Behav.* **28**, 1070–1094 (1980).

2. J. E. Elie, F. E. Theunissen, *Anim. Cogn.* **19**, 285–315 (2016).

3. Y. Prat, M. Taub, Y. Yovel, *Sci. Rep.* **6**, 39419 (2016).

4. S. R. Hage, A. Nieder, *Nat. Commun.* **4**, 2409 (2013).

5. S. D. Washington, J. S. Kanwal, *J. Neurophysiol.* **100**, 3285–304 (2008).

6. I. M. Carruthers, R. G. Natan, M. N. Geffen, *J. Neurophysiol.* **109**, 1912–1927 (2013).

7. D. E. Okobi, A. Banerjee, A. M. M. Matheson, S. M. Phelps, M. A. Long, *Science*. **363**, 983–988 (2019).

8. N. M. Adreani, P. B. D'Amelio, M. Gahr, A. ter Maat, *Front. Neurosci.* **14**, 1–15 (2020).

9. S. Hoffmann *et al.*, *Nat. Commun.* **10**, 2577 (2019).

10. C. Fichtel, M. Manser, in *Animal Behaviour: Evolution and Mechanisms* (Springer Berlin Heidelberg, Berlin, Heidelberg), 2010 , pp. 29–54.

11. G. Kerth, *Bioscience*. **58**, 737–746 (2008).

12. G. G. Kwiecinski, T. A. Griffiths, *Mamm. Species*. **95**, 1–9 (1999).

13. L. Harten *et al.*, *Sci. Adv.* **4**, e1603293 (2018).

14. L. Harten, Y. Prat, S. Ben Cohen, R. Dor, Y. Yovel, *Curr. Biol.* **29**, 1895-1900.e3 (2019).

15. Y. Prat, M. Taub, Y. Yovel, *Sci. Adv.* **1**, e1500019 (2015).

16. D. Genzel, J. Desai, E. Paras, M. M. Yartsev, *Nat. Commun.* **10**, 3372 (2019).

17. S. U. Nummela, V. Jovanovic, L. De La Mothe, C. T. Miller, *J. Neurosci.* **37**, 7036–7047 (2017).

18. L. M. Romanski, B. B. Averbeck, M. Diltz, *J. Neurophysiol.* **93**, 734–747 (2005).

19. A. K. Kuhlen, C. Bogler, S. E. Brennan, J. D. Haynes, *Soc. Cogn. Affect. Neurosci.* **12**, 871–880 (2017).

20. L. Kingsbury *et al.*, *Cell*. **178**, 429-446.e16 (2019).

21. S. W. C. Chang, J. F. Gariépy, M. L. Platt, *Nat. Neurosci.* **16**, 243–250 (2013).

22. W. Zhang, M. M. Yartsev, *Cell*. **178**, 413–428 (2019).

23. S. R. Hage, A. Nieder, *J. Neurosci.* **35**, 7030–7040 (2015).

24. L. J. Silbert, C. J. Honey, E. Simony, D. Poeppel, U. Hasson, *Proc. Natl. Acad. Sci. U. S. A.* **111**, E4687–E4696 (2014).

25. C. T. Miller, A. W. Thomas, S. U. Nummela, L. A. de la Mothe, *J. Neurophysiol.* **114**, 1158–1171 (2015).

26. K. Weineck, F. García-Rosales, J. C. Hechavarría, *PLoS Biol.* **18**, 1–29 (2020).

27. F. P. Möhres, E. Kulzer, *Z. Vgl. Physiol.* **38**, 1–29 (1956).

28. W. J. Lee *et al.*, *PLOS Biol.* **15**, e2003148 (2017).

29. T. Sugihara, M. D. Diltz, B. B. Averbeck, L. M. Romanski, *J. Neurosci.* **26**, 11138–11147 (2006).

30. F. Babiloni, L. Astolfi, *Neurosci. Biobehav. Rev.* **44**, 76–93 (2014).

31. A. Pérez, M. Carreiras, J. A. Duñabeitia, *Sci. Rep.* **7**, 4190 (2017).

32. G. J. Stephens, L. J. Silbert, U. Hasson, *Proc. Natl. Acad. Sci. U. S. A.* **107**, 14425–14430 (2010).

33. A. Stolk *et al.*, *Proc. Natl. Acad. Sci. U. S. A.* **111**, 18183–18188 (2014).

34. S. Dikker *et al.*, *Curr. Biol.* **27**, 1375–1380 (2017).

35. O. Mann *et al.*, *Acta Chiropterologica*. **13**, 411–417 (2011).

36. R. Schmälzle, F. E. K. Häcker, C. J. Honey, U. Hasson, *Soc. Cogn. Affect. Neurosci.* **10**, 1137–1143 (2015).

37. R. Hyon *et al.*, *Proc. Natl. Acad. Sci.* **117**, 33149–33160 (2020).

38. J. Yang, H. Zhang, J. Ni, C. K. W. De Dreu, Y. Ma, *Nat. Neurosci.* **23**, 754–760 (2020).

39. J. Kobler, S. Isbey, J. Casseday, *Science.* **236**, 824–826 (1987).

40. J. S. Kanwal, M. Gordon, J. P. Peng, K. Heinz-Esser, *Neuroreport*. **11**, 367–372 (2000).

41. A. Eiermann, K. H. Esser, *Neuroreport*. **11**, 421–425 (2000).

42. L. López-Jury, A. Mannel, F. García-Rosales, J. C. Hechavarria, *Eur. J. Neurosci.* **51**, 1011–1025 (2020).

43. J. D. Pettigrew, B. C. Maseko, P. R. Manger, *Neuroscience*. **153**, 226–231 (2008).

44. A. Thiele, R. Rübsamen, K. P. Hoffmann, *Exp. Brain Res.* **112**, 223–236 (1996).

45. K. Hu, Y. Li, X. Gu, H. Lei, S. Zhang, *Neuroreport*. **17**, 1743–1746 (2006).

46. M. Nikaido *et al.*, *DNA Res.* **27**, 1–12 (2020).

47. E. Covey, Anat. Rec. - Part A Discov. Mol. Cell. Evol. Biol. **287**, 1103–1116 (2005).

48. T. Ito *et al.*, *Neurosci. Lett.* **712**, 134481 (2019).

49. M. Kössl, J. Hechavarria, C. Voss, M. Schaefer, M. Vater, *Eur. J. Neurosci.* **41**, 518–532 (2015).

50. M. Medalla, H. Barbas, *Front. Neurosci.* **8**, 1–15 (2014).

51. B. Plakke, L. M. Romanski, *Front. Neurosci.* **8**, 1–13 (2014).

52. J. B. Fritz, S. V. David, S. Radtke-Schuller, P. Yin, S. A. Shamma, *Nat. Neurosci.* **13**, 1011–1019 (2010).

53. Y. E. Cohen, F. Theunissen, B. E. Russ, P. Gill, *J. Neurophysiol.* **97**, 1470–1484 (2007).

54. U. Hasson, A. A. Ghazanfar, B. Galantucci, S. Garrod, C. Keysers, *Trends Cogn. Sci.* **16**, 114–121 (2012).

55. P. Barraza, A. Pérez, E. Rodríguez, *Front. Hum. Neurosci.* **14**, 1–11 (2020).

56. J. W. Krakauer, A. A. Ghazanfar, A. Gomez-Marin, M. A. MacIver, D. Poeppel, *Neuron*. **93**, 480–490 (2017).

57. M. M. Yartsev, *Science*. **358**, 466–469 (2017).

58. M. C. Rose, B. Styr, T. A. Schmid, J. E. Elie, M. M. Yartsev, *Zenodo* (2021). doi: 10.5281/zenodo.5152173

59. G. Neuweiler, *Z. Vgl. Physiol.* **46**, 13–56 (1962).

60. H. Q. Liu *et al.*, *Sci. Rep.* **5**, 1–13 (2015).

61. E. Z. Lattenkamp, S. C. Vernes, L. Wiegrebe, *J. Exp. Biol.* **221**, jeb180729 (2018).

62. M. M. Yartsev, N. Ulanovsky, *Science*. **340**, 367–372 (2013).

63. A. Finkelstein *et al.*, *Nature*. **517**, 159–164 (2015).

64. M. Fukushima, D. Margoliash, *Sci. Rep.* **5**, 8800 (2015).

65. A. de Cheveigné, H. Kawahara*, J. Acoust. Soc. Am*. **111**, 1917–1930 (2002).

66. E. Glerean et al., *Hum. Brain Mapp.* **37**, 1066–1079 (2016).

67. R. Q. Quiroga, Z. Nadasdy, Y. Ben-Shaul, *Neural Comput.* **16**, 1661–1687 (2004).

68. E. S. Page, *Biometrika*. **41**, 100 (1954).

69. L. Koepcke, G. Ashida, J. Kretzberg, *Front. Syst. Neurosci*. **10**, 51 (2016).

70. A. O. Nunez-Elizalde, A. G. Huth, J. L. Gallant, *Neuroimage*. **197**, 482–492 (2019).

71. S. Musall, M. T. Kaufman, A. L. Juavinett, S. Gluf, A. K. Churchland, *Nat. Neurosci*. **22**, 1677–1686 (2019).

72. L. Barnett, A. K. Seth, *J. Neurosci. Methods*. **223**, 50–68 (2014).

73. L. Barnett, A. B. Barrett, A. K. Seth, *Phys. Rev. Lett*. **103**, 238701 (2009).

74. N. M. Timme, C. Lapish, *eNeuro*. **5,** 1–40 (2018).